A STUDY OF THE IMPLICATIONS OF SOIL-STRUCTURE INTERACTION EFFECTS ON THE SEISMIC RESPONSE OF HIGH-RISE REINFORCED CONCRETE BUILDINGS

A STUDY OF THE IMPLICATIONS OF SOIL-STRUCTURE INTERACTION EFFECTS ON THE SEISMIC RESPONSE OF HIGH-RISE REINFORCED CONCRETE BUILDINGS

By

SHAMEL HOSNI, M.Sc.

A Thesis

Submitted to the School of Graduate Studies

in Partial Fulfilment of the Requirements

for the Degree

Doctor of Philosophy

McMaster University

DOCTOR OF PHILOSOPHY (1992)
(Civil Engineering and
Engineering Mechanics)

McMASTER UNIVERSITY
Hamilton, Ontario

TITLE: A Study of the Implications of Soil-Structure Interaction Effects on the Seismic Response of High-Rise Reinforced Concrete Buildings

AUTHOR: Shamel Hosni, B.Sc. (Cairo University)
M.Sc. (Cairo University)

SUPERVISOR: Professor A.C. Heidebrecht

NUMBER OF PAGES: xv, 187

ABSTRACT

In spite of significant improvements in the quantification of site effects in the NBCC (National Building Code of Canada) since the introduction of the foundation factor (F) in 1965, recent parametric studies have shown the 1990 NBCC provisions for site effects to be inadequate. In addition, soil-structure interaction effects are neglected in the current NBCC provisions. The current study, aimed at investigating the implications of these soil-structure interaction effects on the seismic response of high-rise reinforced concrete buildings, is carried out for three cities in Canada, namely Ottawa, Vancouver and Prince Rupert.

Soil models are developed to correspond to the soil classifications used to define F in the 1990 NBCC. For each of the three cities, structural models are developed to represent both 20-storey reinforced concrete ductile moment-resisting frames and ductile flexural walls. Three sets of ground motion records are developed to represent the postulated bedrock motions at each of the three cities, based on the magnitude and source-distance combinations dominating the seismic hazard at the respective sites. The computer program FLUSH is used to perform the analyses of the various soil-structure systems.

Results from the current study indicate that the code F values generally underestimate the site effects associated with the respective soil deposits, but appear to be reasonably adequate, in most cases, when

soil-structure interaction effects are taken into consideration. In spite of some apparent deficiencies in the code F values, the 1990 NBCC design base shear is shown to be conservative for regular high-rise reinforced concrete buildings. Conventional uncoupled analyses are shown to provide estimates of the coupled base shear demand that are too conservative. A simple measure to account for the inertial interaction effects in uncoupled analyses is proven to provide a significant improvement in the prediction of the coupled base shear demand. A simplified approach to estimate the coupled system period is shown to provide a satisfactory estimate of values based on the rigorous, but time-consuming coupled analyses.

ACKNOWLEDGEMENTS

I wish to express my gratitude and appreciation to Professor A.C. Heidebrecht, my research supervisor, for his guidance and invaluable contributions throughout the course of this research work. It has been a privilege to have Dr. Heidebrecht as my supervisor. His dedication to academic excellence is quite inspiring.

I wish to extend my appreciation to Dr. J.C. Wilson and Dr. M. Dokainish, members of my supervisory committee, for their constant encouragement and valuable suggestions.

I wish to thank Dr. A. Ghobarah, the department chair, for his encouragement and support. I also wish to thank Dr. N. Naumoski for the many valuable discussions we had during the course of this research work.

I gratefully acknowledge the financial support of McMaster University, in the form of scholarships and teaching assistantships offered through the department.

Finally, I would like to express my sincere gratitude to my parents for their encouragement and support during the various stages of my education. I hope that my achievements are worthy of the love and care they have always shown me.

This thesis is dedicated to my dear wife Jun and my dear daughter Nada. Their love and support were indispensable in bringing four years of research work to this fruitful conclusion.

TABLE OF CONTENTS

Table of Contents (cont'd) PAGE

Table of Contents (cont'd) PAGE

LIST OF TABLES

List of Tables (cont'd) PAGE

LIST OF FIGURES

List of Figures (cont'd) PAGE

List of Figures (cont'd) PAGE

List of Figures (cont'd) PAGE

CHAPTER 1

INTRODUCTION

1.1 BACKGROUND AND MOTIVATION.

Past observations of structural damage patterns during earthquakes have helped draw attention to and underscore the influence of local soil conditions on the seismic response of engineering structures. In general, a soil deposit tends to focus the seismic energy, associated with the bedrock motions, within a narrow band of frequencies in the neighbourhood of the natural frequency of the deposit. As a result, the ground motions at the surface of the deposit (free field motions) will have a higher content of low frequencies and thus may pose a higher seismic hazard to engineering structures as compared to the corresponding bedrock motions. This behaviour of soil deposits is termed site effects. Site effects are customarily incorporated in the development of various aseismic codes, with the first such attempt dating back to the 1932 Chilean code (Seed, 1986).

NBCC 90 (Associate Committee on the National Building Code, 1990) provisions incorporate site effects in the specification of the design base shear through the use of the foundation factor (F). This factor is defined in NBCC 90 as a function of both soil type and depth. NBCC 90 provides values for this factor that range from F=1 for structures situated directly on bedrock to a maximum value of F=2 for structures underlain by deep deposits of soft clay. This factor is provided in NBCC

to simulate the effects of soil amplification on seismic base shear demand in regular buildings.

In spite of significant improvements in the quantification of site effects since the introduction of the foundation factor to the NBCC in 1965, a parametric study (Elhmadi et al., 1990) has shown the current NBCC provisions for site effects to be inadequate, especially for structures having fundamental periods (T) in the neighbourhood of the natural period for the soil deposit (T_s). In that study, four artificial soil models were developed to be representative of homogeneous deposits of normally to lightly overconsolidated clay, heavily overconsolidated clay, alluvial sand with silt and dense sand. These soil models were based on properties of four sites in Canada and the United Kingdom. For each soil model, four depths were studied, namely 5, 15, 40 and 100 m. Three sets of ground motion records were used in that study to represent three different ranges of the PHA/PHV ratio, namely high (>1.2), intermediate (0.8-1.2) and very low (<0.6). PHA and PHV are the peak horizontal ground acceleration, in g, and velocity, in m/s, for the bedrock motions. These records were also scaled to four different ground motion intensity levels, measured in terms of PHV.

The PHA/PHV ratio serves as an indicator of the frequency content of the ground motions. The higher ratios are associated with ground motions recorded during small earthquakes at short distances from the fault, while the lower values are associated with ground motions recorded during large earthquakes at long distances from the fault. High PHA/PHV ratios usually indicate ground motions rich in high frequencies, while low values usually indicate ground motions rich in low frequencies.

The influence of the PHA/PHV ratio on the seismic response of structures (Lu, 1984; Zhu, 1989) and soil deposits (Henderson et al., 1989b; Elhmadi et al., 1990) has long been recognized. It is, therefore, important to take this parameter into account in the selection of ground motion records for use in studies of the seismic response of structures situated on soil deposits. The influence of this ratio on seismic base shear demand has been accounted for in the NBCC provisions since 1985. In 1985, seismic zoning maps of PHA and PHV, based on the seismological model for Canada proposed by Basham et al. (1982), and corresponding to a probability of exceedence of 10 percent in 50 years were introduced to the NBCC provisions. The seismic zoning map of peak horizontal ground acceleration divides Canada into 7 zones (Z_a=0-6) based on PHA. Similarly, the seismic zoning map of peak horizontal ground velocity divides Canada into 7 zones (Z_v=0-6) based on PHV. Sites corresponding to $Z_a>Z_v$ are associated with earthquake ground motions having PHA/PHV ratios usually greater than 1. On the other hand, sites corresponding to $Z_a<Z_v$ are associated with ground motions having PHA/PHV ratios usually lower than 1.

Current NBCC provisions for design base shear are based on the premise that lateral seismic forces in long period structures (T>.5 sec) are proportional to PHV while those in short period structures (T<.25 sec) are proportional to PHA, with the intermediate period range being transitional (Heidebrecht and Tso, 1983). For this reason, design base shear in NBCC is defined as an explicit function of PHV for structural periods greater than .5 sec. For periods shorter than .25 sec, the design base shear becomes an implicit function of PHA through the use of three different base shear levels corresponding to $Z_a>Z_v$, $Z_a=Z_v$ and $Z_a<Z_v$.

In their study, Elhmadi et al. (1990) used simple linear continuum models of frame and wall structures to compute the base shear demand. Computations for the nonlinear soil models were carried out using a one-dimensional shear body-wave propagation algorithm. Based on their study, new foundation factors were proposed (Elhmadi and Heidebrecht, 1991) that are significantly higher, especially for low intensity ground motions, than those provided in NBCC 90. The proposed factors recognize that the level of soil amplification of the structural response is usually higher for lower intensity ground motions. Soil deposits usually show higher levels of amplification for low intensity bedrock motions due to the lower levels of hysteretic soil damping involved. These proposed factors were also defined as a function of the three different ranges of the PHA/PHV ratio used in that study. The proposed foundation factors, presented as a function of the ratio of T to T_s, have a trapezoidal shape with peak values associated with T being in the neighbourhood of T_s. This is believed to be the most promising approach towards an economical design since the penalty of designing a structure to a base shear level higher than that associated with an identical structure situated on bedrock is only exacted upon structures having fundamental periods in the neighbourhood of T_s (soil-structure resonance). The broad-band F factor spectra that are defined in NBCC 90 without due consideration of the soil-structure resonance effects are less desirable for two main reasons. First, these are usually too conservative for structural periods sufficiently removed from T_s. Second, these usually underestimate the amplification level for the soil-structure resonance case. It is important to note that the variation of the soil amplification level with the PHA/PHV ratio and the ground motion intensity

is not yet recognized in the NBCC provisions for site effects.

Results from a similar parametric study were presented for three deep soft clay sites (Heidebrecht et al., 1990) and four sand sites (Henderson et al., 1990). These results established the influence of the frequency content of the bedrock motions (indicated by the PHA/PHV ratio) on the soil amplification level. This amplification was found to be highest when a substantial portion of the seismic energy at bedrock is associated with frequencies in the neighbourhood of the natural frequency of the soil deposit. Results for the soft clay sites indicated that the code provisions for site effects are inadequate for structures located on deep soft clay sites in regions of low seismicity. Results for the sand sites indicated that the amplification levels, associated with sand sites, are significantly underestimated by the NBCC provisions for site effects.

Hosni and Heidebrecht (1991) studied the amplification potential of deep soft clay deposits. Their results were based on bedrock and free field ground motions recorded in Mexico City during the 1985 earthquake (main shock). Bilinear sdof (single-degree-of-freedom) systems were used to model the nonlinear response of structures subjected to these ground motion records. Their results indicated that the value of F=2, provided in NBCC 90 for deep soft clay deposits, is not adequate to account for soil amplification levels similar to those recorded in the Lake Zone of Mexico City during the 1985 Mexican earthquake. This should cause some concern because of the potential for large subduction earthquakes near Vancouver that could induce soil amplifications in the thick recent sediments in the Fraser River delta that are of the order of those recorded in the Lake Zone (Mitchell et al., 1986).

All the above-mentioned studies of the NBCC provisions for site effects are based on uncoupled analyses of the combined structural and soil models (soil-structure systems). In uncoupled analyses, the soil model is subjected to some bedrock ground motions and the corresponding free field motions are computed. These free field motions are then used as base motions for the structural model. In engineering practice, uncoupled analyses are preferred to the more rigorous and time-consuming coupled analyses. Coupled analyses allow for modelling soil-structure interaction effects, whereas these effects are neglected in the corresponding uncoupled analyses.

Soil-structure interaction refers to the combined effects of both kinematic and inertial interactions. Kinematic interaction refers to the integration of the temporal and spatial variations of the ground motions at different points of the foundation into a common average motion by virtue of the relatively stiff foundation. The resulting average motion is expected to be of lower amplitude than the corresponding free field motions due to the common observation that seismic ground motion amplitudes decay with depth below the ground surface. As a result, accounting for kinematic interaction will invariably result in a lower base shear demand, as compared to that based on uncoupled analyses, for structures situated on soil deposits. This reduction, in base shear demand, is obviously a function of the foundation embedment depth. Seed (1986) has demonstrated that even shallow embedments of the order of 5 m can result in foundation motions that are 20 percent lower than the corresponding free field motions.

Inertial interaction, on the other hand, refers to the soil

deformations resulting from the inertial forces in the structure during the seismic response. These soil deformations, being a function of soil flexibility, introduce a rocking component to the response of the structure which will invariably increase the relative displacements of the flexibly supported structure. This rocking component has no counterpart in the widely used uncoupled analyses and results in an observed increase in the fundamental period of the flexibly supported structure as compared to an identical structure situated on bedrock.

Merritt and Housner (1954) used the Electric Analog Computer to investigate the effect of soil flexibility on seismic base shear demand in multi-storey buildings and the corresponding increase in their fundamental periods of vibration. Since their model makes no allowance for kinematic interaction or soil amplification effects, their results provide a direct measure of inertial interaction effects. Their results for a 15-storey building indicated that inertial interaction effects, in most but not all cases, result in a lower base shear demand as compared with an identical structure situated on a rigid surface. This reduction in base shear demand was shown to be, in general, an increasing function of the ratio of soil to building compliancies. That is, inertial interaction effects are more profound for softer soils. Merritt and Housner concluded that for the range of soil compliancies that can be expected in standard building practice, the increase in the fundamental period of the structure associated with inertial interaction effects is within 10 percent. It must be noted, however, that their analytical model does not account for soil nonlinearity. In fact, Seed (1986) has shown that for soft soils, the fundamental period of the flexibly supported structure (system period, $\bar{T}$)

can be as much as 50 percent higher than that for the structure assumed to be directly situated on a rigid base (structural period, T).

Consequently, in the case of T being very close to T_s, this inertial interaction is expected to bring about a reduction in the induced base shear because of the shift in $\bar{T}$ away from T_s. In some other cases, as was observed in Mexico City during the 1985 Mexican earthquake, this shift in $\bar{T}$ resulted in significant increases in the inertial forces and consequent damage in structures having fundamental periods less than 2 sec. In this case, inertial interaction effects resulted in a shift of $\bar{T}$ closer to the predominant period of the free field motions, which was about 2 sec., thus accounting for the increased damage observed for such structures.

Seed (1986) was able to associate the change in base shear demand, associated with inertial interaction effects, with the change in the fundamental period of structures situated on soil deposits during the seismic response. He has shown that if $\bar{T}$, rather than T, is used in an uncoupled analysis, the computed base shear demand would more closely match results based on the corresponding coupled analysis. In lieu of rigorous coupled analyses to determine $\bar{T}$, the Applied Technology Council (1978) provides a simple formula to estimate $\bar{T}$ based on knowledge of some properties of the structure, its foundation and the soil deposit. This formula is based on extensive analytical studies of idealized coupled soil-structure systems (Veletsos and Nair, 1975).

Soil-structure interaction effects are neglected in the current NBCC provisions on the premise that these, for most of the buildings addressed in the code, lead to a reduction in base shear demand and thus

a more conservative design. However, soil-structure interaction effects, being a function of the properties of the structure as well as the properties of the local soil deposit, may increase, decrease or have no effect on the lateral forces induced in the structure during seismic response. Seed (1986) presented a case where accounting for these interaction effects using a coupled analysis was shown to result in a seismic base shear demand that is as much as 50 percent lower than that based on the corresponding uncoupled analysis. He also presented another case where the coupled analysis resulted in a base shear demand that is as much as 60 percent higher than that based on the corresponding uncoupled analysis.

Based on the above, the possible reduction in seismic base shear demand due to soil-structure interaction effects provides a strong argument against the recommendation, based on previous studies involving uncoupled analyses of soil-structure systems, for an increase in the F values specified in NBCC 90. On the other hand, the possible increase in base shear demand due to inertial interaction effects casts a doubt on the level of protection, based on neglecting these interaction effects, provided in NBCC 90. The current study is motivated by both the lack of appropriate provisions to account for soil-structure interaction effects in NBCC and the substantiated recommendations for an increase in code provisions for site effects. The study attempts to provide a rational assessment of the current NBCC provisions for structures situated on soil deposits and a better understanding of the individual and combined roles of site effects and soil-structure interaction during the seismic response of these structures.

1.2 SCOPE.

In the current study, soil models are developed to represent the soil classifications used to define F in NBCC 90. Three models are developed to represent loose, compact and dense sand deposits. Three other models are developed to represent soft, firm and stiff clay deposits. For each soil model, two depths are chosen for analysis, namely 15 and 40 m to represent shallow and deep deposits respectively.

In the previously mentioned parametric studies relating to the NBCC 90 provisions for site effects, three different sets of ground motion records were used to represent the high, intermediate and very low ranges of PHA/PHV. These sets were then scaled to four different intensity levels, measured in terms of PHV. The resulting ground motion simulations were then used to represent expected variations in ground motion characteristics across Canada. There are obvious drawbacks to following a similar approach in developing ground motion simulations for use in the current study involving the more rigorous and time-consuming coupled analyses. First, simply scaling a set of ground motion records to different PHV values corresponds to the erroneous assumption that all recorded ground motions are similar in frequency content and strong motion duration. To alleviate this drawback, a scheme is proposed to explicitly account for the frequency content and implicitly account for the strong motion duration in scaling of the ground motion records. Second, large areas of Canada are sparsely populated. Seismic hazard in these areas is not associated with any appreciable risk. Consequently, to ensure that the current study is both practical and feasible, it is considered essential to restrict computations to urban parts of Canada.

Atkinson (1988) has demonstrated that earthquake ground motions in ENA (Eastern North America) attenuate more slowly with distance from the fault (source-distance) than those in WNA (Western North America). Consequently, corresponding to some specified earthquake magnitude and source-distance, ENA ground motions would impose a higher level of seismic hazard for most engineering structures, especially at longer source-distances, as compared to their WNA counterparts. Atkinson attributed this to the relatively stable and unfractured crust characterizing the regional geological conditions in ENA. This difference in attenuation rates was recognized by Hasegawa et al. (1981) in the development of their attenuation relations for Canada. These attenuation relations were used in the mapping of PHA and PHV for the purpose of developing the seismic zoning maps currently incorporated in the NBCC provisions. Moreover, Somerville et al. (1987) have demonstrated some differences in source characteristics between earthquakes in ENA and WNA. Therefore, it is important to differentiate, in the development of site-specific ground motion simulations, between sites in ENA and those in WNA.

Seismic hazard in Eastern Canada is associated with intraplate faulting within the American plate (Weichert, 1990). However, seismic hazard in Western Canada is dominated by either interplate faulting between the Pacific and American plates along the Queen Charlotte Transform or the subduction of the Juan de Fuca plate beneath the American plate (Milne et al., 1978). Due to significant differences in strain release patterns, and consequently to the maximum earthquake magnitudes that can be sustained, it is important to distinguish between these two sources of seismic hazard in the development of ground motion simulations

for sites in Western Canada.

Since the ground motion scaling scheme used in the current study is based on the earthquake magnitude and source-distance combinations dominating seismic hazard at the site for which ground motion simulations are needed, it is necessary to carry out the computations on a site-specific basis. To acknowledge the differences between the three major sources of seismic hazard in Canada, the study is carried out for three cities in Canada. These cities are selected such that the seismic hazard for each city is associated with a different one of these three sources. In view of the significance of the PHA/PHV ratio on the response of structures and soil deposits, the chosen three cities also represent three combinations of Z_a and Z_v, namely $Z_a>Z_v$, $Z_a=Z_v$ and $Z_a<Z_v$.

While it is commonly observed that sites in Western Canada are usually associated with $Z_a \leq Z_v$, sites in Eastern Canada are usually associated with $Z_a \geq Z_v$ (Heidebrecht et al., 1983). Consequently, Ottawa ($Z_a=4, Z_v=2$, PHA/PHV=2) is chosen from Eastern Canada to represent sites where seismic hazard is associated with intraplate faulting within the American plate and for which $Z_a>Z_v$. Vancouver ($Z_a=4, Z_v=4$, PHA/PHV=1) is chosen from Western Canada to represent sites where seismic hazard is associated with subduction earthquakes and for which $Z_a=Z_v$. Finally, Prince Rupert ($Z_a=3, Z_v=5$, PHA/PHV$\approx$.5) is chosen from Western Canada to represent sites where seismic hazard is associated with interplate faulting along the Queen Charlotte Transform and for which $Z_a<Z_v$.

Both Ottawa and Vancouver are metropolitan centres with populations of over 100,000. Prince Rupert, on the other hand, has a relatively small population but yet is chosen in the current study

because, unlike densely populated cities in Canada, it is representative of sites where seismic hazard is associated with the seismically active Queen Charlotte Transform.

Although the ground motion intensity is not a deciding factor in the selection of the sites included in the current study, the three chosen sites correspond to three different levels of the ground motion intensity, measured in term of PHV. While Ottawa is associated with the lowest intensity among the three sites, Prince Rupert is associated with the highest intensity. Consequently, the three selected sites also represent the variation of the ground motion intensity across Canada. The extensive computations involved in the current study have made it impractical to include more sites to represent other possible combinations of Z_a and Z_v for other urban parts of Canada. The computational approach adopted in the current study is versatile enough to be readily extended to other sites in Canada. For such cases, ground motion simulations could be developed for the particular source of seismic hazard associated with these sites by following the procedure adopted in the current study. However, it is believed that engineering judgement of the results from the current study in light of the previous parametric studies of site effects could help extend these results to other sites in Canada.

There are definite advantages to carrying out computations on a site-specific basis. First, this allows for due consideration of significant parameters, other than PHA and PHV, defining the seismological model of Canada underlying the NBCC 90 provisions (Basham et al., 1982), such as the regional geological conditions, the sources of seismic hazard and the associated magnitude recurrence relations. Second, it becomes

possible to use a site-specific scheme for ground motion scaling. This allows for a more accurate representation of PHV, frequency content and strong motion duration of the postulated seismic ground motions at the specified site.

For each of the three sites included in the current study, an ensemble of 5 strong ground motion records (10 time histories) are selected from the available ground motion data base. The selected records are then scaled to be compatible with the seismological model of Canada underlying the current NBCC provisions. The scaled set of records for each site are then used as the ground motion excitations for all computations specific to that site.

For each site, the structural models consist of a 20-storey reinforced concrete frame and a 20-storey reinforced concrete wall, both designed according to CAN3-A23.3-M84 (Canadian Standards Association, 1984). In this study, distinction is made between frame and wall structural systems. A reason for this is that differences in dynamic properties between both systems entail differences in the significance of the soil-structure interaction effects, even for the same soil model and ground motion excitation. Another reason is that both systems constitute the extremes of the dynamic response of regular multi-storey buildings (Fenves and Newmark, 1969).

Numerical models are set up for each of the possible combinations of the structural and soil models. The pseudo 3-D finite element program FLUSH (Lysmer et al., 1975) is used to perform both coupled and uncoupled analyses of the various soil-structure systems, subjected to the appropriate ground motion ensembles.

1.3 OBJECTIVES.

Objectives of the current study are to:

First. Evaluate the NBCC 90 provisions for site effects, for 20-storey reinforced concrete structures. The foundation factor, as specified in NBCC 90, is compared to base shear ratio results based on uncoupled analyses of the soil-structure systems. The base shear ratio is the ratio of computed base shear for the structure situated on a soil deposit to the corresponding base shear for an identical structure assumed to be directly situated on bedrock and subjected to the same bedrock motions.

Second. Assess the common practice of neglecting soil-structure interaction in aseismic design. Base shear results, based on uncoupled analyses, are compared to corresponding results based on the more rigorous coupled analyses. Linear regression analyses are performed using both sets of results. The regression analysis results are used to discuss the potential for using the widely adopted uncoupled analyses in making reasonable predictions of the base shear computed using the more rigorous coupled analyses.

Third. Study the implications of soil-structure interaction effects on the NBCC 90 provisions, for 20-storey reinforced concrete structures. The foundation factor, as specified in NBCC 90, is compared to base shear ratio results based on coupled analyses of the soil-structure systems. In addition, the code design base shear is directly compared to the base shear demand, based on these coupled analyses.

Fourth. Investigate a simplified approach, proposed by Seed (1986), to

account for the inertial interaction effects in uncoupled analyses of soil-structure systems. Base shear results, based on this simplified approach, are compared to the corresponding results based on coupled analyses. Linear regression analyses are performed using both sets of results. The regression analysis results are used to assess the improvements in base shear predictions when this modified, rather than the conventional, approach for uncoupled analyses is adopted.

Fifth. Evaluate a simplified approach, presented by the Applied Technology Council (1978), to estimate the coupled system period ($\bar{T}$) without resorting to the time-consuming coupled analyses. The potential for incorporating this simplified approach in future NBCC provisions is discussed.

1.4 ORGANIZATION.

In this introductory chapter, the significance of site effects and soil-structure interaction, on the seismic response of structures situated on soil deposits, is emphasized. The current NBCC provisions, for soil-structure systems, are critically reviewed with reference to related previous studies. The rationale and scope of the current study are outlined. The objectives of the study are then clearly stated.

In Chapter 2, soil models are developed to correspond to the soil classifications used to define the foundation factor in NBCC 90. Both the static and dynamic properties for these soil models are then specified.

In Chapter 3, structural models are developed to represent both 20-storey reinforced concrete ductile moment-resisting frames and ductile

flexural walls, for each of the three sites included in the current study. Foundation models that are consistent with the desired hierarchy for energy dissipation in the superstructure during the seismic excitations are also developed.

In Chapter 4, a set of 5 records (10 horizontal ground motion components) are developed to represent the postulated bedrock motions at each of the three sites, based on the magnitude and source-distance combination dominating the seismic hazard at the respective site.

In Chapter 5, the choice of the computer program FLUSH, to perform the analyses of the soil-structure systems, is justified. In addition, the main characteristics of the adopted analytical models are described.

In Chapter 6, the base shear results, from the current study, are statistically analyzed. These results are then discussed with reference to the objectives of the study.

Finally, Chapter 7 provides a brief summary of the current study. In addition, the main conclusions, based on results from this study, are clearly stated.

CHAPTER 2

REPRESENTATIVE SOIL MODELS

2.1 INTRODUCTION

Numerical modelling of soil deposits for seismic analyses requires the specification of some static and dynamic properties of the modelled soil. Since the current study aims at evaluating the NBCC 90 provisions for soil-structure systems, it is more relevant to develop soil models that correspond to the soil classifications used to define F in NBCC 90. For this purpose, artificial soil models are developed to represent homogeneous deposits of loose, compact and dense sands. Artificial soil models are also developed to represent homogeneous deposits of soft, firm and stiff clays. This selection is based on the interpretation of the term 'coarse-grained soils' in the categorization of F in NBCC 90 as mainly referring to sand and the term 'fine-grained soils' as mainly referring to clay. For each of the soil models, developed in the current study, two depths are included to represent shallow and deep soil deposits.

In the parametric study of Elhmadi et al. (1990), the base shear ratio was used as a measure of the soil amplification of the structural response. They developed soil models to represent four different types of soil deposits. For each soil model, four possible depths were studied, namely 5, 15, 40 and 100 m. Mean base shear ratio results, from their study, for the normally to lightly overconsolidated clay and the dense sand soil models are shown in Figures 2.1 and 2.2 respectively, as these

models represent the extremes of both static and dynamic soil properties for the four models included in their study. Results are shown for both the 40 and 100 m soil models corresponding to a ground motion intensity, measured in terms of PHV, of .2 m/s. Elhmadi et al. presented results corresponding to four levels of the ground motion intensity at bedrock, namely .05, .1, .2 and .4 m/s. Herein, the intensity level of .2 m/s is specifically chosen for demonstration as it represents, approximately, an average of the ground motion intensities included in the current study. Results are presented in Figures 2.1 and 2.2 for the three ranges of the PHA/PHV ratio included in their study, namely high, intermediate and very low. Both figures indicate no appreciable differences in the levels of the soil amplification of the structural response for the 40 and 100 m models. In other words, it appears that the level of site effects is independent of the soil model depth beyond a depth of 40 m. This is mainly due to the fact that as bedrock motions are propagated upwards through the soil deposit, they are mainly influenced by the low shear wave velocity upper layers of the deposit.

Wallace and Moehle (1990) have developed a soil model for a relatively uniform soil deposit in Viña del Mar, Chile. Since the actual depth of the deposit was not precisely known, they carried out site response analyses for assumed depths of 50, 75 and 100 m and found no significant difference in the dynamic response of the soil model in the three cases. Based on both these studies, a depth of 40 m appears to be quite appropriate for representing deep soil deposits in the current study as it maintains a reasonable bound on the size of the numerical model while providing a reliable representation of site effects for much deeper

deposits.

In the categorization of F in NBCC 90, 15 m is the depth used to distinguish between shallow and deep soil deposits. In addition, the structural models developed in the current study have foundations that are embedded in the soil deposits to a depth of 5 m. Consequently, 15 m is the soil depth chosen for representing shallow soil deposits in the current study. This is based on the belief that shallower depths of the soil models would not allow for the full development of soil-structure interaction effects due to the proximity of the foundation and the underlying rigid base (bedrock).

For simplicity, four character codes are used hereafter to denote the different soil models included in the current study. The first two characters denote the soil type and the other two characters denote the depth of the respective model in metres. The two character codes used to represent the different soil types are S1, S2 and S3 for the loose, compact and dense sand deposits respectively. Similarly, C1, C2 and C3 are used to represent the soft, firm and stiff clay deposits respectively.

With reference to the soil classifications used to define F in NBCC 90, Table 2.1 provides the F values associated with the different soil models in this study.

2.2 REPRESENTATIVE SAND SOIL MODELS.

Following is an outline of the development of both the static and dynamic soil properties characterizing the S1, S2 and S3 soil models.

2.2.1 Static Soil Properties.

Three static soil properties are required to define the numerical soil models in FLUSH (Lysmer et al., 1975). These are the soil unit weight (γ_s), Poisson's ratio (ν) and the low strain shear modulus (G_o) profile. Low shear strain refers to shear strains smaller than .0001 percent and represents almost linear response of the deposit.

γ_s values, in kN/m^3, are listed in Table 2.2 for the different sand soil models as average values of the respective typical ranges given in Bowles (1988). ν values are also listed in Table 2.2. In this case, ν values are identical for the three soil models and represent the average value of the commonly used range of values given in Bowles (1988).

Seed et al. (1984) provided a guide for the selection of soil properties for cohesionless soil deposits, based on a review of related previous studies. They provided the following relation to derive the shear modulus for cohesionless soils:

$$G = 220K_2(\sigma_m)^{.5} \qquad (2.1)$$

G = soil shear modulus (kPa)

σ_m = mean principal effective stress (kPa)

K_2 = soil modulus coefficient

This relation is based on the premise that, for cohesionless soils, the factors most strongly influencing G are the confining pressures (represented by σ_m), the shear strain amplitude (γ) and the relative density (D_r). The influences of both γ and D_r are incorporated in the specification of K_2 in Equation 2.1. K_2 is a decreasing function of γ, but an increasing function of D_r. Based on Equation 2.1, G_o is derived using the maximum value of K_2, corresponding to low shear strain (γ=.0001

percent). This maximum value, $(K_2)_{max}$, is independent of γ. Consequently, G_o becomes a function of D_r and σ_m and is derived using the appropriate form of Equation 2.1:

$$G_o = 220(K_2)_{max}(\sigma_m)^{.5} \qquad (2.2)$$

D_r values, in percent, are listed in Table 2.2 based on interpolation of the values given in Bowles (1988). Corresponding $(K_2)_{max}$ values are obtained from Seed et al. (1984) and listed in Table 2.2. The following relation is used to derive σ_m (Moriwaki et al., 1981):

$$\sigma_m = \frac{(1+2K_o)}{3}\sigma_v \qquad (2.3)$$

K_o = coefficient of earth pressure at rest

σ_v = effective vertical overburden pressure (kPa)

= $\gamma_s Z$ for non-submerged soil deposits

Z = depth below ground surface (m)

For natural soil deposits, K_o represents the ratio of the lateral soil pressure to σ_v at any point within the soil mass. K_o values depend on the process of formation of the soil deposits. For sand deposits, these also depend on the relative density. K_o values, corresponding to the S1 and S3 soil models, are obtained from Prakash (1981). The K_o value, corresponding to the S2 soil model, is taken as the mean of these two values. These values are listed in Table 2.2 along with the corresponding ratios of σ_m to σ_v derived using Equation 2.3.

Using information from Table 2.2, Equation 2.2 is used to develop the G_o profiles for the different sand soil models. These are shown, to a depth of 40 m below the ground surface, in Figure 2.3.

2.2.2 Dynamic Soil Properties.

Two dynamic soil properties are required in the development of the numerical models of the soil deposits in FLUSH. These are the shear modulus ratio (G/G_o) and the hysteretic damping ratio (λ). Based on Equations 2.1 and 2.2, the shear modulus ratio, for sand soils, can be expressed as:

$$\frac{G}{G_o} = \frac{K_2}{(K_2)_{max}} \qquad (2.4)$$

For dynamic soil response involving no residual displacements, the response can be evaluated using G/G_o and λ characteristics determined under reasonably symmetric cyclic loading conditions (Seed et al., 1984). Figure 2.4 illustrates the hysteresis loops for such loading conditions at two different shear strain levels. It also shows how the corresponding G and λ are determined. G_o is usually determined using field shear wave velocity measurements at low strain levels.

Based on Equation 2.4, G/G_o is a decreasing function of γ. Seed et al. (1984) discounted the influence of soil parameters, other than γ and D_r, on K_2. Based on Equation 2.4, Figure 2.5 shows the G/G_o curves determined for the different sand soil models using the respective D_r and $(K_2)_{max}$ values, obtained from Table 2.2, and the K_2 curves presented in Seed et al. (1984). The three curves fall within a relatively narrow band, in agreement with results from many investigators (Seed et al., 1984).

Seed et al. (1984) found that λ is mainly influenced by γ and σ_v. They also found that with the exception of the top few feet of soil, the influence of σ_v is very small compared to that of γ. Based on this, they concluded that an average relationship between λ and γ, determined for σ_v

in the range of 96 to 144 kPa, could be considered adequate for practical purposes. This relationship, obtained from Seed et al. (1984), is shown in Figure 2.6.

2.3 REPRESENTATIVE CLAY SOIL MODELS.

Following is an outline of the development of both the static and dynamic soil properties characterizing the C1, C2 and C3 soil models.

2.3.1 Static Soil Properties.

ν values, for the clay soil models, are listed in Table 2.3. Similar to the case of the sand soil models, ν values are identical for the three clay soil models and represent the average value of the commonly used range for saturated clays as given in Bowles (1988).

Hardin and Drnevich (1972) have provided a relation to derive the G_o profile for undisturbed cohesive soils. For normally consolidated clay deposits, this relation takes the form:

$$G_o = 3270 \frac{(2.97-e)^2}{(1+e)} (\sigma_m)^{.5} \qquad (2.5)$$

e = void ratio

σ_m is derived using Equation 2.3. In the case of clay soils, however, K_o is related to the plasticity index (I_p) as given by Alpan (Bowles, 1988):

$$K_o = .19+.233\log_{10}(I_p) \qquad (2.6)$$

I_p = plasticity index (in percent)

As a result, the G_o profile becomes a function of both e and I_p. For natural clay deposits, e and I_p are essentially independent parameters

that can occur in various combinations. Classification of the consistency of the clay deposit (i.e. soft, firm or stiff) depends on the values of both these parameters. To ensure that the soil models, developed herein, are representative of the clay soil consistencies included in the current study, these models are developed based on measured properties for three clay deposits located in Ontario (Kim and Novak, 1981). The soft clay soil model (C1) is based on a very soft silty clay deposit in the west side of Windsor. The firm clay soil model (C2) is based on a firm clayey silt deposit in south central Chatham. The stiff clay soil model (C3) is based on a stiff-hard clayey silt deposit in St. Catharines.

γ_s and I_p corresponding to the clay soil models are obtained from Kim and Novak (1981) for the respective soil deposits and are listed in Table 2.3. Corresponding K_o and σ_m/σ_v values, derived according to Equations 2.6 and 2.3 respectively, are also listed in Table 2.3.

The solid curve in Figure 2.7 illustrates a typical e versus $\log_{10}(\sigma_v)$ curve for a laboratory tested, undisturbed soil sample obtained from a preconsolidated soil deposit. Based on this curve, the dashed curve represents the expected variation of e with $\log_{10}(\sigma_v)$ in the field (Das, 1985). It is obvious, from this figure, that e is expected to decrease almost linearly with the increase of $\log_{10}(\sigma_v)$ for virgin compression. The virgin compression branch of the field curve corresponds to the primary consolidation of the soil under pressures in excess of σ_c, the maximum effective vertical pressure to which this soil has ever been subjected. For normally consolidated deposits, σ_c is equal to σ_o, the existing in-situ effective vertical pressure. Since the three soil deposits used to develop the clay soil models were preconsolidated (i.e. $\sigma_c > \sigma_o$), the measured void

ratio (e_o) corresponding to σ_o needs to be modified to yield the void ratio (e_c) corresponding to σ_c. This is achieved using the recompression index (C_r), shown in Figure 2.7, as follows:

$$e_c = e_o - C_r[\log_{10}(\sigma_c) - \log_{10}(\sigma_o)]$$

$$= e_o - C_r \log_{10}(\sigma_c/\sigma_o) \qquad (2.7)$$

Nagaraj and Murthy (1985) developed the following generalized relation for C_r based on the normally consolidated e versus $\log_{10}(\sigma_v)$ curves for different fine-grained soils:

$$C_r = .0463e_L \qquad (2.8)$$

e_L = void ratio at the liquid limit

$$e_L = .01w_L G_s \qquad (2.9)$$

w_L = water content at the liquid limit (in percent)

G_s = specific gravity of the soil

G_s and w_L values for the soil deposits, obtained from Kim and Novak (1981), are listed in Table 2.3. The corresponding e_L values, computed according to Equation 2.9, and the C_r values, computed according to Equation 2.8, are listed in Table 2.3. The values of σ_o, σ_c and e_o, obtained from Kim and Novak (1981), along with the corresponding e_c values, derived according to Equation 2.7, are also listed in Table 2.3. For each of the clay soil models, these values correspond to the soil sample taken from the soil deposit used in the development of this specific soil model.

σ_c and e_c represent a single point on the virgin compression branch of the field consolidation curve in Figure 2.7. This branch is shown in Figure 2.7 to have a constant slope, referred to as the compression index (C_c). If the value of C_c is determined, the variation of e with $\log_{10}(\sigma_v)$ for virgin compression of the soil becomes well defined. Nakase et al.

(1988), who found strong correlation between many clay soil parameters and I_p, provide the following relation to derive C_c:

$$C_c = \frac{.02+.0045I_p}{.434} \tag{2.10}$$

C_c values, derived according to Equation 2.10, are listed in Table 2.3 for the three clay soil models. Since the soil models developed in the current study are assumed to represent normally consolidated deposits, the variation of e with depth below the ground surface, due to the variation of σ_v, can be determined using the virgin compression branch of the field consolidation curve. σ_v, corresponding to some specified depth within the soil, is used to derive the corresponding e using the virgin compression branch of the field consolidation curve as follows:

$$e = e_c - C_c \log_{10}(\sigma_v/\sigma_c) \tag{2.11}$$

The e profile, computed using Equation 2.11, along with the corresponding σ_m profile are used to derive the G_o profile for the respective clay soil model according to Equation 2.5. The G_o profiles for the three clay soil models are shown, to a depth of 40 m below the ground surface, in Figure 2.8.

2.3.2 Dynamic Soil Properties.

Sun et al. (1988) compiled available data on the dynamic shear moduli and damping for mostly clay soils under cyclic loading conditions. Based on examining the influence of different factors on the variation of G/G_o with γ, they found the influence of I_p to be the most dominant and consistent. Dobry and Vucetic (1987) carried out a study of the behaviour of saturated clays subjected to cyclic loading. Based on laboratory and

field measurements, they concluded that for normally consolidated clays, I_p is the main soil parameter influencing the dynamic soil response. Both studies show that higher plasticity indices are associated with a more linear soil response.

Vucetic and Dobry (1991) presented curves for G/G_0 versus γ and for λ versus γ as a function of I_p. These curves are based on quantifying and refining the trend observed in their earlier work (Dobry and Vucetic, 1987). Their curves for G/G_0 versus γ are fully supported by the results of Sun et al. (1988). Their curves for λ versus γ establish a trend that has been observed by others but not quantified until then. Based on the I_p values listed in Table 2.3, the G/G_0 and λ curves presented in Vucetic and Dobry (1991) for I_p=30 are selected for the C1 soil model. Meanwhile, the curves based on I_p=15 are selected for both the C2 and C3 soil models. The selected G/G_0 and λ curves are shown in Figures 2.9 and 2.10 respectively.

Table 2.1 NBCC 90 foundation factors for the soil models

Soil model	Foundation factor			
	F=1.0	F=1.3	F=1.5	F=2.0
Sand soil				
S115		X		
S140			X	
S215	X			
S240		X		
S315	X			
S340	X			
Clay soil				
C115		X		
C140				X
C215	X			
C240		X		
C315	X			
C340		X		

Table 2.2 Soil properties for the sand soil models

Soil model	γ_s	ν	D_r	$(K_2)_{max}$	K_o	σ_m/σ_v
S1	16.0	0.35	25	30	0.4	0.60
S2	18.5	0.35	50	45	0.5	0.67
S3	19.5	0.35	75	60	0.6	0.73

Table 2.3 Soil properties for the clay soil models

Soil model	γ_s	ν	I_p	K_o	σ_m/σ_v	G_s	w_L
C1	17.5	0.45	30	0.53	0.69	2.75	51.3
C2	20.0	0.45	14	0.46	0.64	2.74	29.0
C3	22.0	0.45	12	0.44	0.63	2.75	25.0

Table 2.3 (cont'd) Soil properties for the clay soil models

Soil model	e_L	C_r	σ_o	σ_c	e_o	e_c	C_c
C1	1.41	.0653	52.7	140	1.36	1.33	.3571
C2	0.79	.0368	79.6	170	0.75	0.74	.1912
C3	0.69	.0318	88.6	510	0.48	0.46	.1705

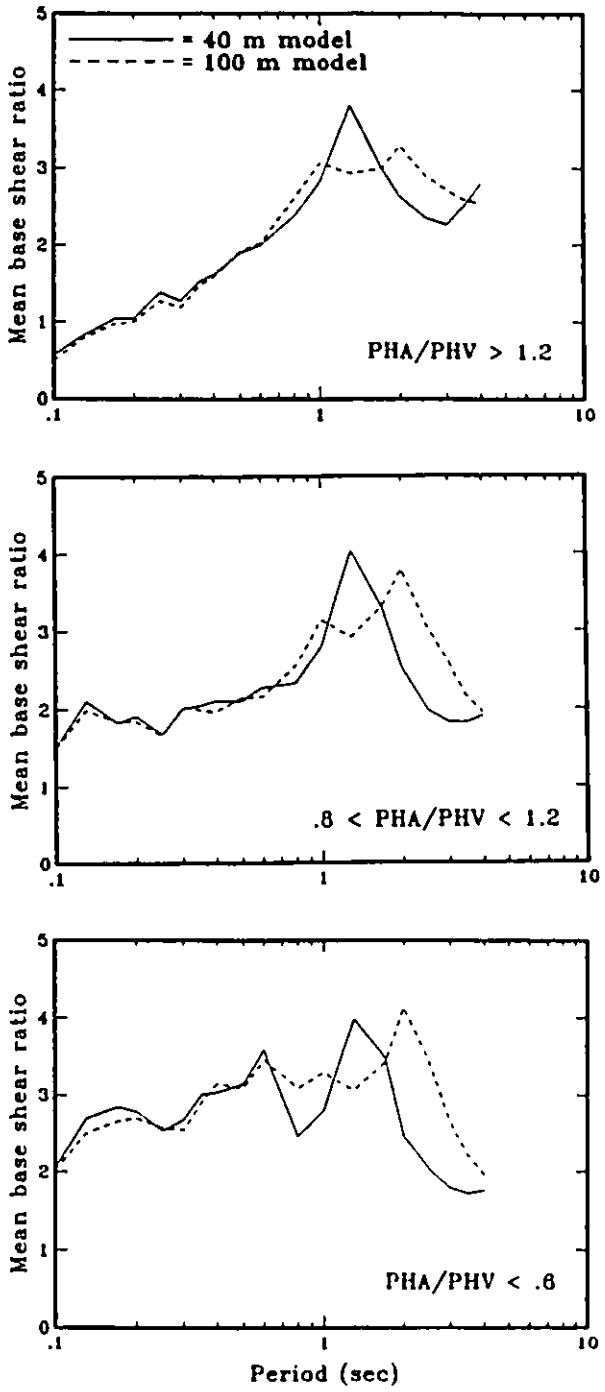

Figure 2.1 Mean base shear ratio results for the normally to lightly overconsolidated clay soil model

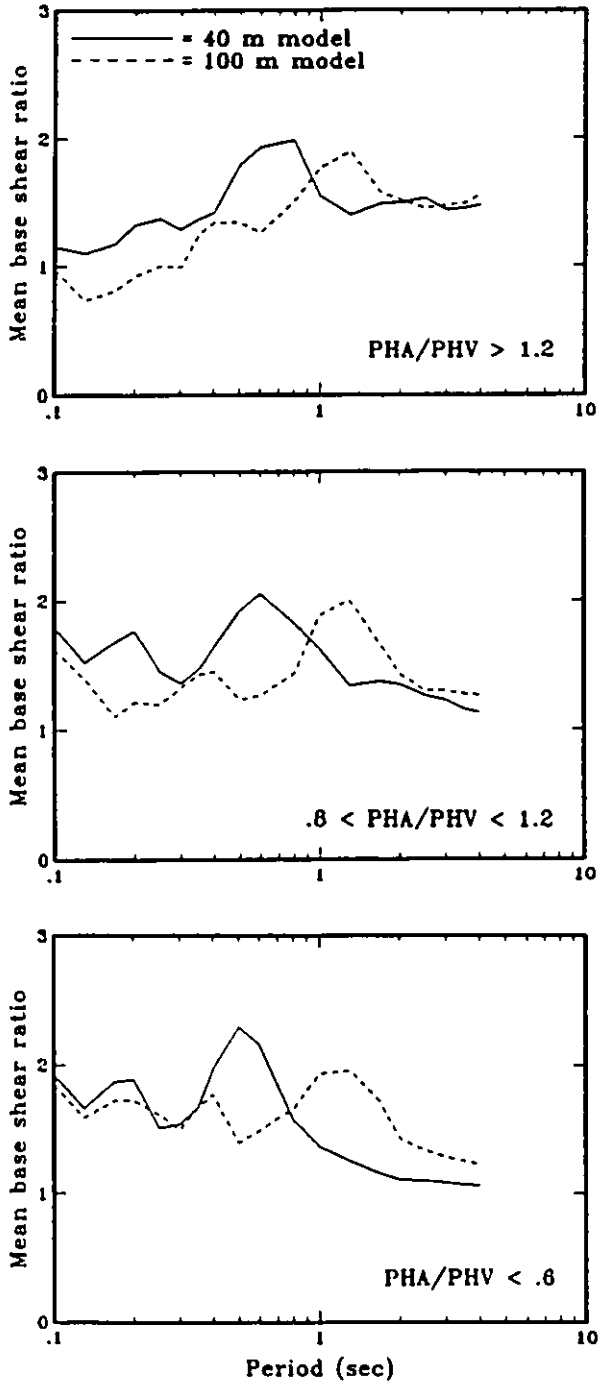

Figure 2.2 Mean base shear ratio results for the dense sand soil model

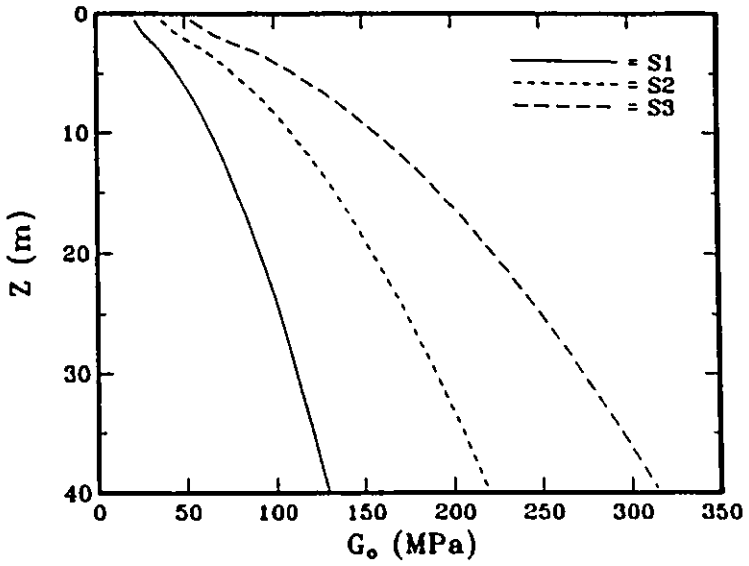

Figure 2.3 Low strain shear modulus profiles for the sand soil models

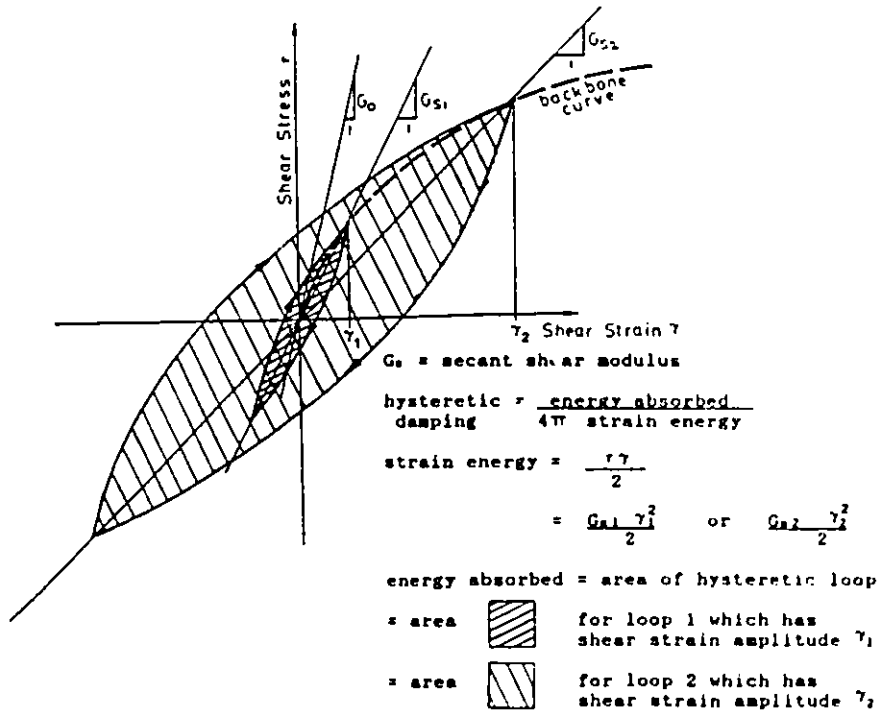

Figure 2.4 Stress-strain soil behaviour under cyclic loading conditions (after Pappin et al., 1989)

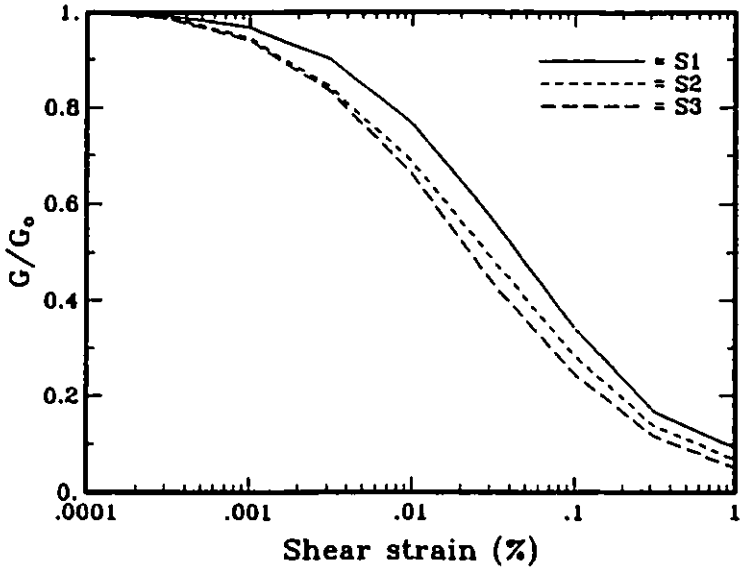

Figure 2.5 Shear modulus ratio curves for the sand soil models

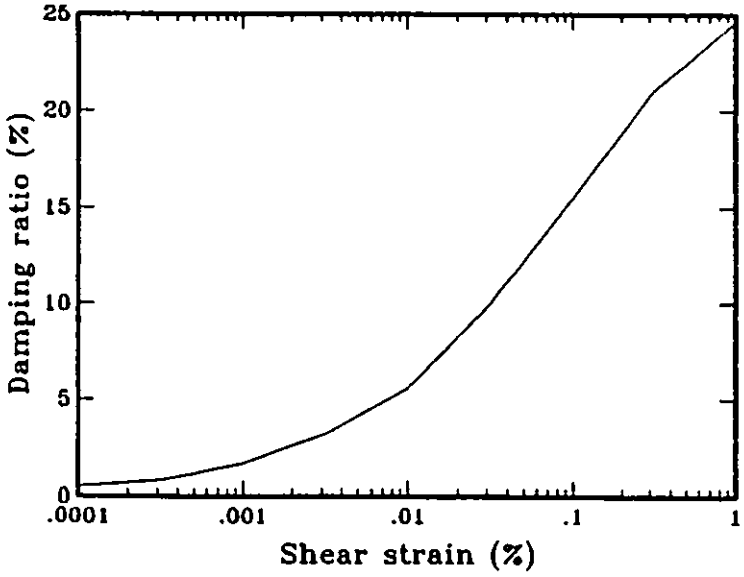

Figure 2.6 Hysteretic damping ratio curve for the sand soil models

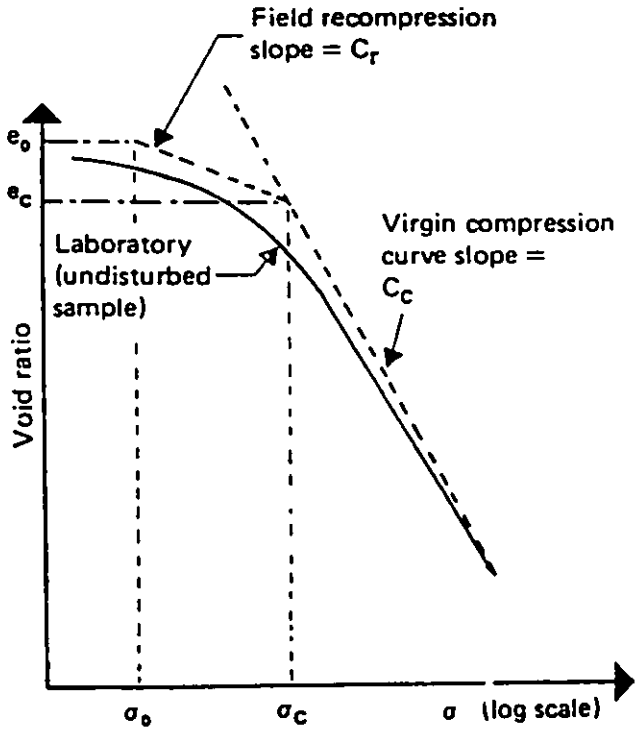

Figure 2.7 Typical consolidation curves for a preconsolidated clay soil (after Das, 1985)

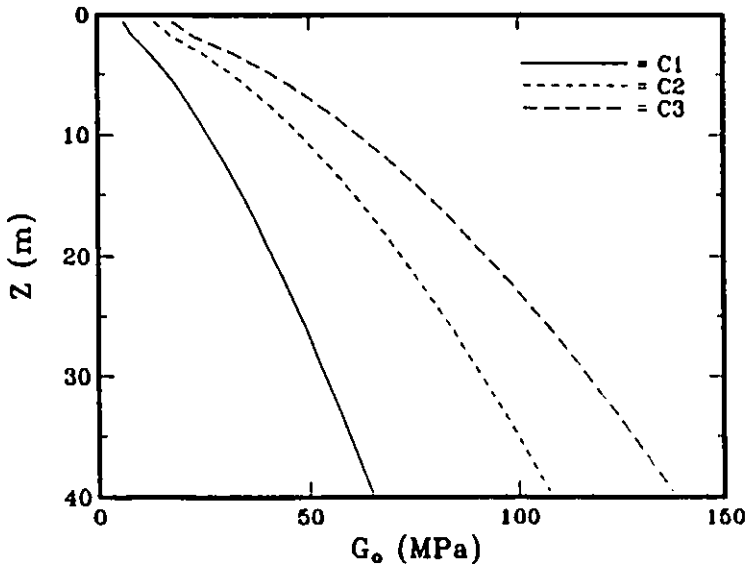

Figure 2.8 Low strain shear modulus profiles for the clay soil models

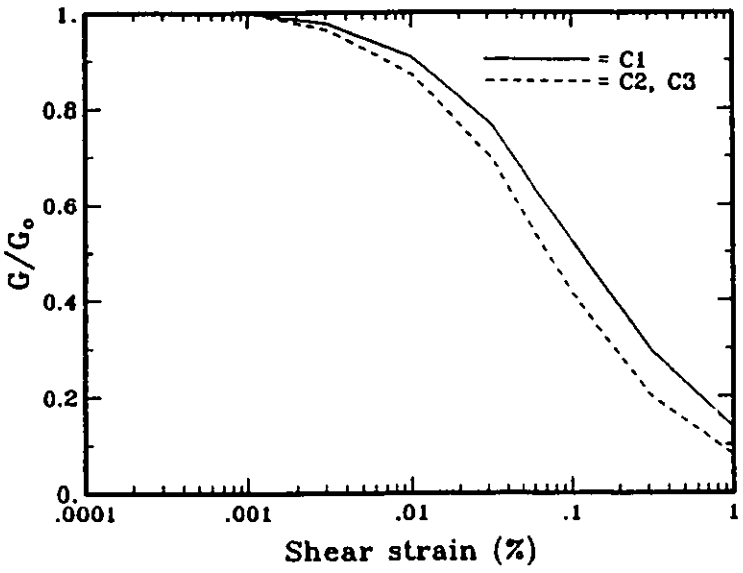

Figure 2.9 Shear modulus ratio curves for the clay soil models

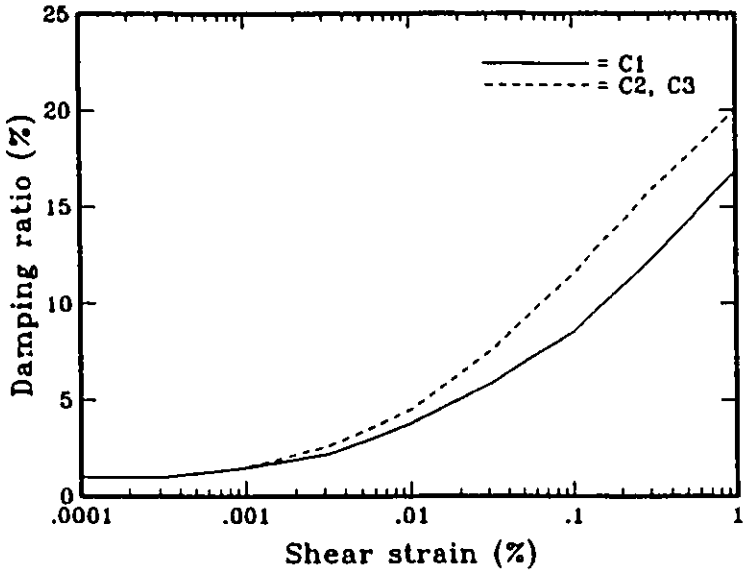

Figure 2.10 Hysteretic damping ratio curves for the clay soil models

CHAPTER 3

REPRESENTATIVE STRUCTURAL MODELS

3.1 INTRODUCTION.

It is recognized that there may be deficiencies in the NBCC 90 provisions for structures situated on soil deposits. However, it is possible that the overstrength, inherent in most engineering structures, may outweigh these deficiencies. The ratio of the actual strength of the structure to its design strength is the factor commonly used to measure this overstrength. Overstrength is the term used to describe the common observation that a structure designed to the code base shear will, in most cases, be capable of sustaining larger loads while maintaining the desired performance of the structure.

Fischinger and Fajfar (1990a) compiled a list of possible causes for this observed overstrength. They reported overstrength factors in the range of 3-4 for a full-scale 7-storey reinforced concrete frame-wall structure tested in Japan. Fischinger and Fajfar (1990b) carried out an analytical study of 10-storey reinforced concrete structures. Three different structural systems were considered in their study, namely ductile frame, frame-wall and bearing shear wall. They computed overstrength factors of about 2 for the frame and frame-wall structures, but only about 1.2 for the shear wall structure. Fischinger and Fajfar (1990a) expect short period structures to possess large overstrength because, for these structures, the minimum code requirements regarding

dimensions and reinforcement govern the design. As an example, they expect typical five-storey shear wall apartment buildings in Yugoslavia to have overstrength factors in excess of 5.

Osteraas and Krawinkler (1989) analyzed steel moment-resisting frames, designed according to the 1966 Mexico City code. The computed overstrength factors were observed to be larger for short period structures, as high as 13 for structures having fundamental periods of about .2 sec. For structures having fundamental periods in excess of 2 sec, the computed overstrength factors were only about 2.

Miranda and Bertero (1989) analyzed two-storey and four-storey reinforced concrete moment-resisting frames, designed according to the 1976 Mexico City code. For the two-storey frames, the computed overstrength factors were in the range of 4.5-7.5. For the four-storey frames, the overstrength factors were in the range of 2-2.5.

Zhu (1989) analyzed 4, 10 and 18-storey reinforced concrete moment-resisting frames, designed according to the 1985 NBCC provisions. He reported overstrength factors, corresponding to an overall drift of .5 percent, of 1.8 for the four-storey frame, but as low as 1.13 for the 18-storey frame.

Based on the above studies, it appears practical to give priority to long period structures in the current study, as these are associated with the lowest overstrength factors and would consequently be most affected by possible deficiencies in the NBCC 90 provisions for soil-structure systems. Consequently, computations in the current study are restricted to 20-storey reinforced concrete structures, selected to represent regular long period structures.

Fenves and Newmark (1969) stated that the type of framing and the relative contribution of the higher modes of vibration are primary factors influencing the seismic response of structures. On this basis, they believe that sufficiently reliable results, representative of the response of actual structures, can be obtained by studying the response of two simplified extremal models, namely the shear beam and the flexural beam.

Heidebrecht and Stafford Smith (1973) presented a method for simplified static or dynamic analyses of frame-wall structures. The method was based on assuming the structure to consist of vertical interacting shear and flexural beams. Results, based on this simplified model, compared satisfactorily with the corresponding results, based on a more rigorous method of analysis. Similarly, Fajfar and Strojnik (1980) presented charts to determine the shear forces and overturning moments, corresponding to elastic response, for regular multi-storey structures, that are based on a linear combination of the response of the two simplified extremal models, the shear beam and the flexural beam.

The shear beam represents a simplified model for moment-resisting frames, while the flexural beam represents a simplified model for uncoupled flexural walls. Based on the foregoing, moment-resisting frames and uncoupled flexural walls are expected to represent the extremes of the dynamic response of regular multi-storey buildings. For this reason, distinction is made between both structural systems in the current study. Another reason is that the inherent differences in stiffness characteristics, between both structural systems, entail differences in the levels of soil-structure interaction, even under the same ground motion excitation. Consequently, structural models are developed, in the

current study, to represent 20-storey moment-resisting frames and 20-storey uncoupled flexural walls.

3.2 SPECIFIED MATERIAL PROPERTIES.

Table 3.1 provides a summary of both the concrete and reinforcement material properties used in the development of the structural models. The unit weight of the reinforced concrete (γ_c) is taken as an average value for normal density concrete. The specified concrete compressive strength (f_c') is a typical value commonly used in engineering practice. The corresponding modulus of elasticity is derived using the relation provided in CAN3-A23.3-M84 (Canadian Standards Asscciation, 1984) for normal density concrete:

$$E_c = 5000(f_c')^{.5} \qquad (3.1)$$

E_c = modulus of elasticity for concrete (MPa)

f_c' = concrete compressive strength (MPa)

Poisson's ratio for the concrete (ν_c) is taken as the design value from Pillai and Kirk (1988). According to the theory of elasticity, the shear modulus for the concrete can be derived from E_c according to:

$$G_c = \frac{E_c}{2(1+\nu_c)} \qquad (3.2)$$

G_c = shear modulus for concrete (MPa)

For the reinforcement, a typical value for the yield strength (f_y) is specified. The modulus of elasticity (E_s) is taken as specified in CAN3-A23.3-M84 for nonprestressed reinforcement.

3.3 DESIGN LOADS FOR THE STRUCTURAL MODELS.

For the development of the structural models, the frames (or walls) are assumed to be spaced at 6 m centre-to-centre in plan. The storey heights are assumed to be 3.6 m, with a total height of 72 m, above the ground surface, for the 20-storey structures.

3.3.1 GRAVITY LOADS.

The dead loads, specified for the design, are described in Table 3.2. In this table, the specified dead load for the floor beams is basically the distributed dead load that is equivalent to the dead weight of these beams. The self-weight of the frame (or wall) is not included in Table 3.2. However, it is taken into consideration in the design as outlined in Subsection 3.4.2. The live load, listed in Table 3.2, is taken as specified in NBCC 90 for residential buildings. In the design, this value is reduced, according to NBCC 90, to account for the fact that the tributary areas associated with the structural members of the frame (or wall) models are in excess of 20 m^2. In view of the small differences between the gravity loads for the roof and other floors of the building, the gravity loads for the roof are assumed to be identical to those for the other floors.

3.3.2 EARTHQUAKE LOADS.

The dead and live loads, listed in Table 3.2, are identical for the three sites, included in the current study. Loads due to earthquakes, on the other hand, are specified in NBCC 90 as an increasing function of the ground motion intensity. Since the current study is carried out on a site-specific basis, this implies that the design of the structural model

varies according to the site at which it is located. For this reason, structural models are developed for each of the three sites. This is a realistic approach as in this case these structural models represent the expected variations in stiffness characteristics between actual structures located at these three sites.

In NBCC 90, the seismic design base shear is specified as follows:

$$V = \frac{V_e}{R} U \tag{3.3}$$

$$V_e = vSIFW \tag{3.4}$$

V_e = base shear corresponding to elastic response

R = force modification factor

U = calibration factor based on experience = .6

v = zonal velocity ratio

S = seismic response factor

I = importance factor = 1 for structures of normal importance

F = foundation factor

W = dead weight of the structure

The factor R accounts for the energy dissipation capacity of different structural systems as these undergo excursions into the inelastic response range under the seismic ground motion excitations. While R=1 corresponds to structural systems exhibiting little or no ductility, systems that have performed well in previous earthquakes are assigned higher values of R. For high-rise (long period) buildings, structural systems associated with large R values are customarily used in order to reduce the large seismic lateral forces, arising from the large dead weight (W) of these buildings.

In the current study, the structural models are designed to represent ductile moment-resisting frames, associated with the largest value of R=4, and ductile flexural walls, associated with R=3.5 (Associate Committee on the National Building Code, 1990). The design and detailing of these ductile structural systems is addressed in the special provisions for seismic design in CAN3-A23.3-M84 and is discussed in detail in subsequent sections of this chapter.

The seismic zoning map of peak horizontal ground acceleration divides Canada into seven acceleration-related seismic zones (Z_a=0-6) based on PHA. Each of these zones is associated with a zonal acceleration ratio (a) to be applied uniformly throughout this zone. For a specific zone, *a* represents an intermediate value of the range of PHA values corresponding to that zone. Similarly, the seismic zoning map of peak horizontal ground velocity divides Canada into seven velocity-related seismic zones (Z_v=0-6) based on PHV. Each of these zones is associated with a zonal velocity ratio (v) which represents an intermediate value of the range of PHV values corresponding to that zone. The definition of these seismic zones as well as the associated zonal acceleration or velocity ratios are summarized in Table 3.3.

The seismic response factor (S) represents the idealized elastic response of 5 percent damped mdof (multi-degree-of-freedom) systems, corresponding to a unit value for the zonal velocity ratio. The S curves for the three combinations of seismic zones ($Z_a > Z_v$, $Z_a = Z_v$ and $Z_a < Z_v$) are shown in Figure 3.1.

The implication of using both S and v in Equation 3.4 is that the design base shear (V) is defined explicitly in terms of v for structures

having fundamental periods in excess of .5 sec. On the other hand, V is defined implicitly in terms of a for fundamental periods shorter than .25 sec, with the intermediate period range being transitional.

Since the structural models are used in combination with the different soil models developed in the current study, the value of F to be used in deriving the design base shear for these structural models appears to be variable (see Table 2.1). However, only one value (F=2) is considered in the current study. This value of F=2 is applied consistently for the design of the structural models for the three sites. In the derivation of V, according to Equations 3.3 and 3.4, it is important to note that, as specified in NBCC 90, the product FS need not exceed 3 when Z_a does not exceed Z_v and need not exceed 4.2 when Z_a exceeds Z_v. The computed design base shear (V) is distributed along the height of the structure in accordance with the equivalent static load approach adopted in NBCC 90.

3.3.3 Cases of Loading.

Since the computed gravity and earthquake loads are to be used within the framework of a limit states design, appropriate load factors need to be applied to these loads. Load factors are specified in NBCC 90 to take into account the variability of the load magnitude and load patterns and, to some extent, inaccuracies in the structural analysis. The specified load factors are 1.25, 1.5 and 1.0 for the dead, live and earthquake loads respectively. However, in cases where the dead load acts to resist overturning, uplift or reversal of load effects, an alternative load factor of .85 should also be considered for the dead load. The load

factor of 1.0 for earthquake loads was introduced in NBCC 90 to replace the previous value of 1.5 in earlier editions of NBCC. This is in recognition of the fact that earthquake loads are accidental loads of very short duration.

NBCC provisions do not require wind loads and earthquake loads to be considered simultaneously in design because the probability of their simultaneous occurrence is extremely small. The earthquake loads, for the three sites included in the current study, are larger than the corresponding wind loads. Consequently, the wind loads are not considered in the design. The NBCC 90 provisions also specify a load combination factor of .7 to reduce the specified live and earthquake loads whenever these are considered simultaneously in the design. Based on the above, the following five cases of loading represent the possible ultimate design loads that need to be considered in the design of the structural systems:

1. 1.25DL+1.5LL
2. 1.25DL+QL
3. 0.85DL+QL
4. 1.25DL+1.05LL+.7QL
5. 0.85DL+1.05LL+.7QL

DL, LL and QL refer to the specified dead, live and earthquake loads prior to the application of the load factors or the load combination factor. In other words, DL, LL and QL are the unfactored design loads.

3.4 DUCTILE MOMENT-RESISTING FRAMES.

3.4.1 Symmetrical One-Bay Frames.

The response of symmetrical one-bay frames is considered a

satisfactory approximation to the response of actual multi-bay frames subjected to dynamic or static loads (Council on Tall Buildings and Urban Habitat, 1979). In view of the fact that computer time and space are a function of the frame size, it is considered appropriate to use one-bay frame models in the current study. These models are assumed to have a span of 10 m.

The computed unfactored dead and live loads from a single storey for a typical frame are shown in Figure 3.2. The distributed loads represent the portion of the floor loads transmitted to the frame girder, while the concentrated loads represent the remaining floor loads that are transmitted to the frame columns through the floor beams. These loads do not include the self-weight of the frame. A typical frame refers to an intermediate frame in the building. Computed design loads for this frame are based on a 6 m strip of the building, which is the assumed spacing of the frames.

For the purpose of calculating the earthquake loads used for the design of the frame models, the fundamental period of vibration (T) of the building should be estimated. When the lateral force-resisting system consists of moment-resisting frames, NBCC 90 provides the following relation to derive T:

$$T = .1N \qquad (3.5)$$

N = number of storeys

For 20-storey frames, Equation 3.5 results in a value of T=2 sec. According to Figure 3.1, the corresponding S value is 1.06. It is worth noting that for F=2, the product FS in this case is well below the aforementioned limits set in NBCC 90. The base shear is conveniently

described using the non-dimensional base shear coefficient (BSC), which is basically the base shear normalized to the dead weight (W) of the structure.

Using Equations 3.3 and 3.4, the BSC values are now determined for the three frames designed in the current study. Table 3.4 lists the values of v, W, BSC and V for the typical frames, corresponding to the three sites. The V values are approximated to the nearest 10 kN. Since the value of W is influenced by the cross-section dimensions for the girders and columns of the frame which in turn depend on the specified value of V, a process of iterations is used to arrive at the final values of W listed in Table 3.4. Based on an initial assumption for the cross-section dimensions of the frame girders and columns, an initial value of V is determined and used in the design. Based on the modified cross-section dimensions, a new value for W and consequently V are determined. The process is repeated until there is no change in these dimensions with further iterations. The distribution of the lateral earthquake load (V) along the height is given in Table 3.5 for the three frame models. In this table, the storeys are numbered sequentially from the ground surface upwards.

3.4.2 Static Analyses of the Frames.

The computer program SAP IV (Bathe et al., 1973) is used to perform the structural analyses necessary to design the frame models.

Shear deformations are incorporated in the analysis through the specification of the effective shear area (A_r). To take into account the non-uniform distribution of shear stresses, A_r is usually taken smaller than the cross-sectional area (A_g) used in the computation of the axial

deformations. Park and Paulay (1975) provide relations between A_r and A_g for different shapes of concrete sections. For T-sections (frame girders):

$$A_r = A_g \tag{3.6a}$$

Whereas for rectangular sections (frame columns):

$$A_r = \frac{A_g}{1.2} \tag{3.6b}$$

For the girders, both A_r and A_g are specified based on the web area only. This is necessary in the case of A_r while being reasonably accurate in the case of A_g. It is important to note that in frame structures, the axial forces and deformations induced in the horizontal girders are insignificant and such an assumption, in the case of A_g, is not expected to affect the results of the analyses.

The moments of inertia specified for the reinforced concrete sections are usually based on either the gross concrete section or the cracked section. Since it is difficult to accurately account for the influence of the state of cracking and the amount of reinforcement along the concrete member, the moments of inertia are commonly based on the gross concrete section (Pillai and Kirk, 1988). The provisions of CAN3-A23.3-M84 allow for any reasonable assumption in the specification of the flexural stiffness for the concrete sections as long as it is consistently applied throughout the structure.

In the specification of the moment of inertia for frame girders, the effect of the flange should be taken into consideration. Even at sections where the flange is in tension, CAN3-A23.3-M84 provisions allow for distribution of the tension reinforcement within the effective flange width resulting in a contribution of the flange to the flexural stiffness

of the concrete member. It is thus quite appropriate to use the effective flange width in the computation of the moments of inertia along the whole length of the girder (Pillai and Kirk, 1988). To avoid lengthy computations of the moments of inertia using the exact effective flange dimensions, an expedient and effective method, adopted herein, is to specify the moment of inertia for the frame girder as being twice the corresponding value based on the web area alone (Pillai and Kirk, 1988).

The self-weight of the frame, which is a function of the dimensions of the girders and columns, must be taken into account in the specification of the design loads. This is conveniently achieved using SAP IV. Once the unit weight of the reinforced concrete is specified in the input data file, the program progresses to compute the dead weight of the different members of the structural frame using the respective A_g values. After applying the appropriate load factor, the program combines these with the other factored loads specified for the design. Using the above information on design loads and cross-section properties for the frame members, static analyses are performed for the five cases of loading previously mentioned. The computed straining actions (axial and shear forces and bending moments) are consequently used for the design of the different reinforced concrete members. Each member is designed for the case of loading producing the most unfavourable effects in that member.

3.4.3 Design of the Reinforced Concrete Frames.

The design of the frame members conforms to the special provisions for the seismic design of ductile moment-resisting frames in CAN3-A23.3-M84. These provisions are based on the assumption that energy dissipation,

during the seismic response, mainly occurs by the formation of plastic hinges in the frame girders. The amount of reinforcement in a reinforced concrete section is conveniently expressed using the non-dimensional reinforcement ratio which is defined in Equations 3.7a and 3.7b for the frame girders and columns respectively:

$$\rho = \frac{A_s}{b_w d} \tag{3.7a}$$

ρ = reinforcement ratio for girders

A_s = area of tension reinforcement (mm^2)

b_w = width of the web (mm)

d = depth to the centroid of the tension reinforcement (mm)

$$\rho_g = \frac{A_{st}}{bh} \tag{3.7b}$$

ρ_g = reinforcement ratio for columns

A_{st} = total area of longitudinal reinforcement (mm^2)

h = dimension of the column in the direction of analysis (mm)

b = dimension of the column in the transverse direction (mm)

As outlined earlier, the axial, shear and flexural stiffnesses for the frame members are all specified in terms of the gross, rather than cracked, concrete section. As a result, variations in the reinforcement content, for a fixed cross-section, are not reflected in the calculation of the member stiffnesses. Therefore, it is important that the member cross-section dimensions reflect the variations in load demand throughout the structure. This is achieved by maintaining ρ and ρ_g at almost constant values throughout the structure. ρ_g is specified larger than ρ in accordance with common engineering practice.

CAN3-A23.3-M84 provisions for ductile moment-resisting frames specify the following limits on the reinforcement ratios:

For girders: $.0035<\rho<.025$ based on f_y=400 MPa

For columns: $.01<\rho_g<.06$

Based on these limits, it is decided to maintain ρ at approximately .02 for the girders and ρ_g at approximately .04 for the columns. The Canadian Portland Cement Association (1985) provides design charts, for reinforced concrete sections, which are expedient tools for design. For the frame girders, the cross-section dimensions are based on the computed bending moments from the static analyses. For the frame columns, the cross-section dimensions are based on both the computed axial forces and bending moments. In each case, however, a check is made to ensure that the selected cross-section can sustain the computed shear forces. Table 3.6 cites the specific tables and diagrams, from the Canadian Portland Cement Association (1985), that are used for the design of the different frame members.

As mentioned earlier, the design process is approached iteratively until there are no further changes in the cross-section dimensions with further iterations. Figure 3.3 shows the final cross-section dimensions for the girders and columns of the frames designed for Ottawa, Vancouver and Prince Rupert. For the girders shown in this figure, h refers to the overall depth of the concrete section. For practical purposes, the member cross-section dimensions are changed, if necessary, only every other storey.

3.4.4 Dynamic Analyses of the Frames.

The computer program FLUSH (Lysmer et al., 1975) is used to determine the fundamental periods of vibration (T) for the frames, shown in Figure 3.3. A viscous damping of 5 percent is assumed for the frame members, which is the typical value for cracked concrete members. The cross-section dimensions and material properties used in the static analyses are maintained in the dynamic analyses. The dynamic analyses are carried out using the unfactored dead loads only. The computed fundamental periods, for the three frames, are listed in Table 3.7. The Prince Rupert frame is associated with the largest cross-section dimensions, as shown in Figure 3.3, and consequently the lowest T as shown in Table 3.7. This is expected given the fact that Prince Rupert is associated with the highest ground motion intensity, measured in terms of v, among the three sites included in the current study.

The significant differences in the values of T for the different frame models lend credibility to the decision to carry out the design of the structural systems on a site-specific basis. The observation that the computed T values exceed the value estimated using Equation 3.5 is not surprising given the fact that the code usually provides a conservative estimate of T. In fact, NBCC 90 acknowledges that variations of the order of 50 percent have been observed when the relations provided in the code to estimate T are used. Since the NBCC design base shear does not increase with increasing value of T, a lower estimate of T corresponds to a more conservative design.

3.5 DUCTILE FLEXURAL WALLS.

3.5.1 Uncoupled Flexural Walls.

Structural models are developed to represent uncoupled ductile flexural walls. The wall length is taken as 10 m, identical to the span length assumed for the moment-resisting frames. The computed unfactored dead and live loads from a single storey for a typical wall are identical to those obtained earlier for a typical frame, and are shown in Figure 3.2. Similar to the case for the frame models, these unfactored loads do not include the self-weight of the wall. NBCC 90 provides the following relation to estimate T for buildings where the lateral force-resisting system consists of flexural walls:

$$T = \frac{.09H}{(L)^{.5}} \qquad (3.8)$$

H = total height of the wall above the ground surface (m)

L = length of the wall (m)

For 20-storey walls, Equation 3.8 results in a value of T=2 sec, similar to the value obtained earlier for the 20-storey moment-resisting frames. Ductile flexural walls are associated with an R value of 3.5, lower than that for moment-resisting frames. Consequently, the BSC values derived according to Equations 3.3 and 3.4 are slightly higher in the case of the ductile flexural walls. Table 3.8 lists the values of v, W, BSC and V for the typical walls, corresponding to the three sites, with W being the final values based on an iterative design approach. The distribution of the lateral earthquake load (V) along the height is given in Table 3.9 for the three walls.

3.5.2 Static Analyses of the Walls.

Since uncoupled walls are statically determinate structures,

structural analyses can be performed irrespective of any assumptions regarding the modelling of the reinforced concrete sections. Analyses are carried out for the five cases of loading stipulated earlier. Although hand calculations suffice for analyses of these statically determinate wall models, SAP IV is used as it allows for easy manipulation of the cases of loading and is less time-consuming. The self-weight of the wall is taken into account in the analyses. The computed straining actions are consequently used for the design of the wall sections.

3.5.3 Design of the Reinforced Concrete Walls.

Design of the wall models conforms to the special provisions for the seismic design of ductile flexural walls in CAN3-A23.3-M84. In the current study, walls with boundary elements, as that shown in Figure 3.4, are preferred to simple rectangular wall cross-sections for three main reasons. First, the increased thickness at the boundaries helps provide the required stability to these highly stressed regions of the wall. In this case, CAN3-A23.3-M84 stipulates that these boundary elements should extend over the region where both yielding of the reinforcement and compressive strains in excess of .0015 are expected. Second, it allows for a better distribution of the reinforcement by providing more space for the concentrated reinforcement at the wall ends. This ensures a large moment arm which enhances the flexural capacity for the wall section. Third, it allows for the use of a minimal thickness for the concrete wall as well as minimum reinforcement in regions other than the boundary elements. This results in a more economic use of the reinforced concrete building materials.

Since the load demand for the wall reduces with height above the ground surface, the width of the boundary elements (b) shall be reduced accordingly. For regions of the wall, other than the boundary elements, a constant thickness of 150 mm is specified which allows for placement of two meshes of light reinforcement, one at each face of the wall.

In uncoupled flexural walls, the commonly adopted hierarchy for energy dissipation during seismic response is the development of a plastic hinge at the base of the wall. In addition, the flexural capacity of the wall at sections above the base should be large enough to prevent the formation of plastic hinges elsewhere (Blakeley et al., 1975). An approach to maintain this hierarchy is presented in Figure 3.5. In this figure, the probable moment of resistance refers to the computed moment resistance of the section using $1.25f_y$ as the factored stress in the reinforcement and f_c' as the factored strength of the concrete. This probable moment of resistance is obviously larger than the moment resistance used in design and which is based on a $.85f_y$ factored stress in the reinforcement and a $.6f_c'$ factored concrete strength. The probable moment of resistance represents, approximately, the maximum resistance of the section when material overstrength is taken into consideration.

With reference to Figure 3.4, the reinforcement ratios for the wall sections are defined in Equations 3.9a and 3.9b for the web and boundary elements respectively:

$$\rho_w = \frac{A_{sw}}{b_w L_w} \qquad (3.9a)$$

ρ_w = reinforcement ratio for the web

A_{sw}= total area of longitudinal reinforcement in the web (mm^2)

$$\rho_b = \frac{A_{sb}}{bL_b} \qquad (3.9b)$$

ρ_b = reinforcement ratio for the boundary element

A_{sb} = total area of longitudinal reinforcement in the boundary element (mm^2)

For the boundary elements, ρ_b is maintained at .01. This value is reached based on trial calculations using several values and studying the influence of ρ_b on the dimensions of the boundary elements. Larger values of ρ_b result in dimensions for the boundary element in the compression zone that are larger than those for the boundary element in the tension zone, the opposite being true for ρ_b<.01. Due to seismic load reversal effects, it is essential to maintain the dimensions of both boundary elements identical. Based on the trial calculations, this is achieved using ρ_b=.01. For the web, the minimum value of ρ_w=.0025, stipulated in CAN3-A23.3-M84, is maintained. As seen from Figure 3.5, the plastic hinge region, for the wall models, should extend a distance of 12 m above the ground surface. For practical purposes, this distance is taken as 14.4 m (i.e. four storeys).

The dimensions of the boundary elements are based on the computed axial forces and bending moments. The probable moment of resistance is also computed at different sections along the wall height. The dimensions of the boundary elements are sometimes increased to ensure that at any section above the plastic hinge region, the computed probable moment of resistance exceeds the moment expected at this section after the development of the plastic hinge (see Figure 3.5). The corresponding shear forces are found to be significantly lower than the shear capacity of the

selected wall cross-sections. The final dimensions for the boundary elements for the three wall models are given in Table 3.10. Similar to the case of the frame models, the boundary element width is changed, if required by design, only every other storey.

3.5.4 Dynamic Analyses of the Walls.

FLUSH is used to compute T for the three wall models, based on the gross concrete sections. The effective shear area (A_r) is specified according to Equation 3.6a. A viscous damping of 5 percent is assumed and the dynamic analyses are carried out using the unfactored dead loads only. The computed T values, listed in Table 3.11, are significantly lower than the value estimated using Equation 3.8. The main reason for this is that the length of the structural wall, rather than the building dimension in the direction of analysis, is used in NBCC 90 to estimate T as given in Equation 3.8. This change was introduced in the 1985 edition of NBCC. It is worth noting that Equation 3.8 was originally derived, based on a large number of vibration observations, using the building dimension, rather than the length of the structural system, in Equation 3.8.

3.6 FOUNDATIONS FOR THE STRUCTURAL MODELS.

3.6.1 Foundation Models.

Binney and Paulay (1980) assert that for earthquake resistant structures, the criterion for the design of the foundations should be the ability of these foundations to support the design gravity loads while maintaining the desired hierarchy for energy dissipation during transient seismic excitations. Since the energy dissipation mechanisms, adopted in

the current study, are restricted to the superstructure, the foundations are designed to respond elastically during the seismic excitations.

In the current study, the foundations are assumed to be reinforced concrete walls with a bearing mat as shown in Figure 3.6 for two main reasons. First, this type of foundation realizes the desired energy dissipation mechanism for the wall models by allowing for adequate fixity of the walls at the base which is a necessary condition for the development of a plastic hinge at the wall base. Second, these foundations inhibit the development of undesirable differential settlements between the frame columns. In addition, this foundation model is consistent with the common practice of incorporating a basement in high-rise buildings.

A foundation model is developed for each of the three sites included in the current study. As outlined earlier, the lateral earthquake loads associated with the wall models are larger than those associated with the respective frame models. As a result, the loads transmitted from the wall models to their foundations are chosen as the design loads for the foundation models.

3.6.2 Design of the Reinforced Concrete Foundations.

For each of the three sites, the thickness of the foundation wall (t_f) is specified as the larger of b for the base column of the respective frame or b for the boundary element at the base of the respective wall. The design of the foundation models is based on the sand soil model S1 which represents reasonably average soil properties, measured in terms of G_o, for the soil models developed in the current study.

The Meyerhof bearing capacity relation for vertical loads (Bowles,

1988) is used to determine the bearing capacity of the S1 soil model at the foundation level. For this soil model, the angle of internal friction (ϕ) is specified as 30°, determined as the average value of the typical range for loose sands (Bowles, 1988). The height (h_f) for the three foundation models is maintained at 5 m, considered appropriate for incorporation of a basement in the building. Based on tentative values for the width of the bearing mat (B_m), a width of 3 m is chosen and maintained for the three foundation models. A smaller value for B_m results in soil bearing stresses exceeding the allowable soil capacity. On the other hand, a larger value for B_m is uneconomical because the allowable soil bearing stress is not fully utilized. The thickness of the bearing mat (t_m) is specified based on the local transverse bending moment arising from the soil bearing stresses (see Figure 3.6). t_m is determined using Table 2.3 from the Canadian Portland Cement Association (1985) for the material properties listed in Table 3.1 and ρ=.01. The low specified value of ρ results in a relatively large t_m which is desirable to maintain the assumed uniform distribution of the soil bearing stress in the transverse direction as shown in Figure 3.6.

The length of the foundation model (L_f) is based on the load demand on the foundations, for the different sites. A factor of safety of 2 is used to derive the allowable soil bearing pressure from the ultimate value derived according to the Meyerhof bearing capacity relation. This value of the safety factor is recommended in the case of transient earthquake design loads (Bowles, 1988). The concrete dimensions for the three foundation models are listed in Table 3.12. These dimensions can be interpreted with reference to Figure 3.6.

Due to the large overturning moments associated with the transient earthquake loads, it may not be possible, nor feasible, to maintain contact between the bearing mat and the underlying soil all along the foundation length. In this case, the distribution of the soil bearing stress takes the form shown in Figure 3.6. The final values of L_f, listed in Table 3.12, are achieved through a process of iterations with the objective of maintaining contact between the bearing mat and the underlying soil along at least half the foundation model length. This is necessary to avoid rocking of the foundation, due to the soil deformations, under the seismic ground motion excitations. A rocking foundation mechanism would obviously inhibit the development of the desired energy dissipation mechanisms in the superstructure. In any case, L_f must not be less than 10 m to accommodate the structural models.

A check for safety of the foundation models against sliding and overturning is also performed. Significant passive soil pressures, acting against the basement walls, resist both sliding and overturning of the foundations. These are, however, not included in the computations, but are recognized by applying a low factor of safety of 1.5 against sliding and overturning of the foundations.

Table 3.1 Reinforced concrete material properties

Concrete	
Unit weight, γ_c	24 kN/m^3
Compressive strength, f_c'	30 MPa
Modulus of elasticity, E_c	27386 MPa
Poisson's ratio, ν_c	.2
Shear modulus, G_c	11411 MPa
Reinforcement	
Yield strength, f_y	400 MPa
Modulus of elasticity, E_s	200000 MPa

Table 3.2 Specified gravity loads

Dead load	(kN/m^2)
12 cm slab	2.88
floor beams	1.72
partitions	1.00
mechanical and electrical fixtures	0.50
finishes	0.25
total distributed dead load	6.35
Live load	
residential	1.90

Table 3.3 Definition of the seismic zones

Z_a, Z_v	PHA, PHV	a, v
0	<.04	.0
1	.04 to <.08	.05
2	.08 to <.11	.10
3	.11 to <.16	.15
4	.16 to <.23	.20
5	.23 to <.32	.30
6	.32 and larger	.40

Table 3.4 Design base shear parameters for the frame models

Frame model	v	W (kN)	BSC	V (kN)
Ottawa	.10	9200	.0318	290
Vancouver	.20	9720	.0636	620
Prince Rupert	.30	10140	.0955	970

Table 3.5 Distribution of the seismic lateral loads for the frame models

Storey number	Lateral load (kN)		
	Ottawa	Vancouver	Prince Rupert
20	63.5	137.7	215.4
19	22.6	48.2	75.5
18	21.4	45.7	71.5
17	20.3	43.2	67.6
16	19.1	40.6	63.6
15	17.9	38.1	59.5
14	16.7	35.6	55.6
13	15.5	33.0	51.6
12	14.3	30.4	47.6
11	13.1	27.9	43.7
10	11.9	25.4	39.7
9	10.7	22.9	35.8
8	9.5	20.3	31.8
7	8.3	17.7	27.8
6	7.2	15.2	23.9
5	6.0	12.7	19.8
4	4.8	10.1	15.8
3	3.6	7.6	11.9
2	2.4	5.1	7.9
1	1.2	2.6	4.0
Total	290.0	620.0	970.0

Table 3.6 Tables from the Canadian Portland Cement Association (1985)

Structural members	Table
Girders (flange in tension)	2.3
Girders (flange in compression)	2.17
Columns (350≥h>250)	7.10.1
Columns (500≥h>350)	7.10.4
Columns (h>500)	7.10.6

Table 3.7 Fundamental periods for the frame models

Frame model	T (sec)
Ottawa	3.46
Vancouver	2.74
Prince Rupert	2.34

Table 3.8 Design base shear parameters for the wall models

Wall model	v	W (kN)	BSC	V (kN)
Ottawa	.10	11330	.0359	410
Vancouver	.20	11640	.0719	840
Prince Rupert	.30	12050	.1078	1300

Table 3.9 Distribution of the seismic lateral loads for the wall models

Storey number	Lateral load (kN)		
	Ottawa	Vancouver	Prince Rupert
20	90.6	186.7	288.4
19	31.9	65.3	101.2
18	30.3	61.9	95.8
17	28.6	58.5	90.6
16	26.9	55.0	85.2
15	25.2	51.6	79.8
14	23.5	48.2	74.6
13	21.9	44.7	69.2
12	20.2	41.2	63.8
11	18.5	37.8	58.6
10	16.8	34.4	53.2
9	15.1	31.0	48.0
8	13.4	27.5	42.6
7	11.8	24.0	37.2
6	10.1	20.6	32.0
5	8.4	17.2	26.6
4	6.7	13.7	21.2
3	5.0	10.3	16.0
2	3.4	6.9	10.6
1	1.7	3.5	5.4
Total	410.0	840.0	1300.0

Table 3.10 Concrete dimensions for the boundary elements

Storey number	(bxL_b) in mm		
	Ottawa	Vancouver	Prince Rupert
19,20	150x1900	150x1650	150x1500
17,18	150x1900	150x1650	300x1500
15,16	300x1900	300x1650	300x1500
13,14	300x1900	300x1650	400x1500
11,12	300x1900	400x1650	500x1500
9,10	400x1900	400x1650	600x1500
7,8	400x1900	500x1650	700x1500
5,6	400x1900	500x1650	700x1500
3,4	400x1900	500x1650	700x1500
1,2	400x1900	500x1650	700x1500

Table 3.11 Fundamental periods for the wall models

Wall model	T (sec)
Ottawa	1.37
Vancouver	1.28
Prince Rupert	1.14

Table 3.12 Concrete dimensions for the foundation models

Foundation model	L_f (m)	h_f (m)	B_m (m)	t_f (mm)	t_m (mm)
Ottawa	10	5	3	400	600
Vancouver	12	5	3	500	600
Prince Rupert	15	5	3	700	600

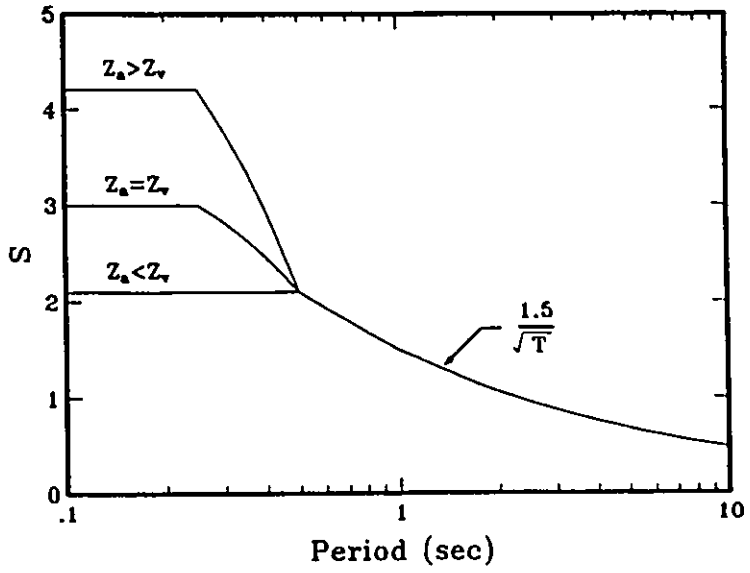

Figure 3.1 Seismic response factor

ω_d=distributed dead load
ω_l=distributed live load
P_d=concentrated dead load
P_l=concentrated live load

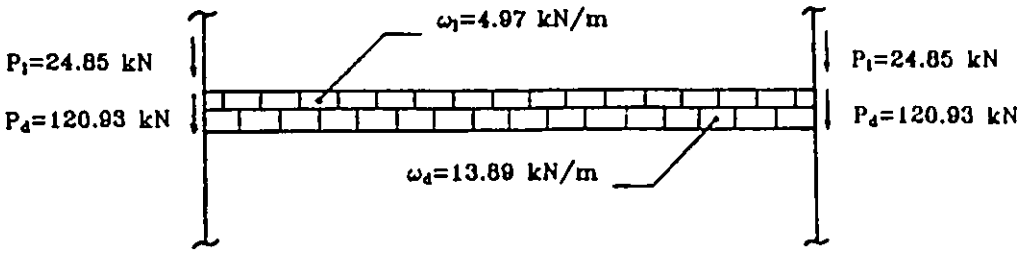

Figure 3.2 Unfactored dead and live loads from a single storey for a typical frame

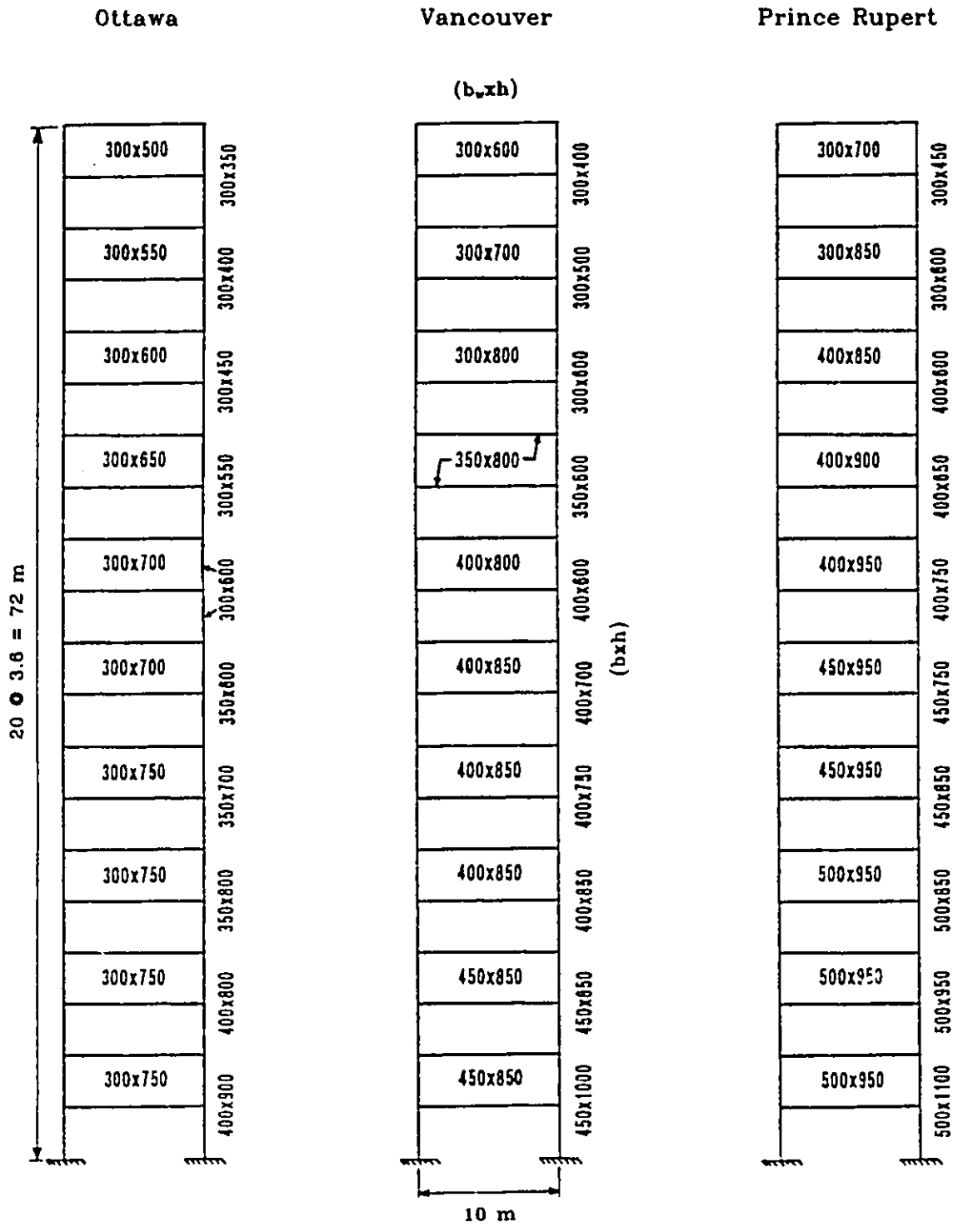

Figure 3.3 Concrete dimensions for the frame models

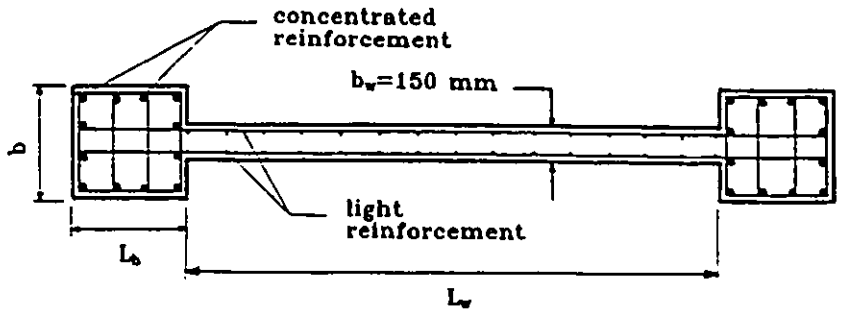

Figure 3.4 Schematic diagram for a wall cross-section (not to scale)

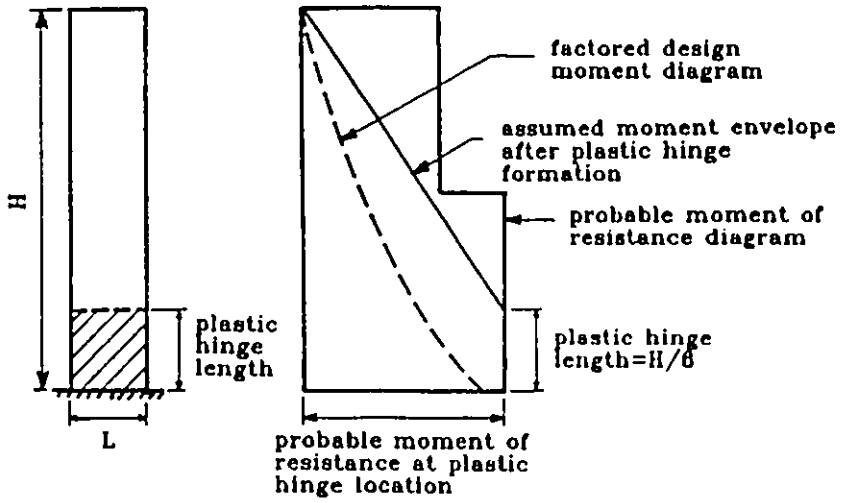

Figure 3.5 Approach to restrict plastic hinge formation to the base of the wall (after Canadian Portland Cement Association, 1985)

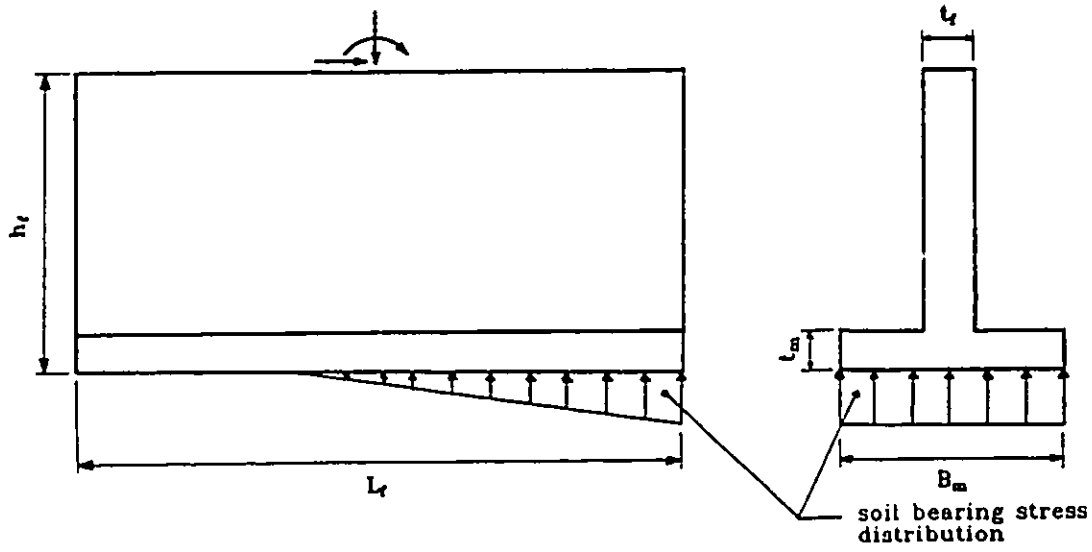

Figure 3.6 Schematic diagram for the foundation model (not to scale)

CHAPTER 4

SITE-SPECIFIC INPUT GROUND MOTIONS

4.1 INTRODUCTION.

Seismic hazards mapping, based on the model for seismicity of Canada proposed by Basham et al. (1982), at the probability of exceedence of 10 percent in 50 years, resulted in the seismic zoning maps of PHA and PHV incorporated in the NBCC provisions since 1985. For site-specific dynamic analyses, it is customary practice to use either of these two peak ground motion parameters to scale a single time history, or preferably a set of time histories, so as to be consistent with the ground motion intensity assigned to that site according to the appropriate seismic zoning map.

Ground motion scaling based solely on peak ground motion parameters is a practice flawed by several drawbacks. First, recorded peak ground motion parameters are associated with high variability, especially so for PHA. As a result, scaling of seismic ground motions using these parameters usually results in a wide scatter in the computed dynamic response. Second, ground motion scaling using solely PHA or PHV corresponds to the erroneous assumption that all recorded ground motions are similar in frequency content and strong motion duration. Third, Nau and Hall (1984) demonstrated that using scaling factors based on response quantities results in significantly less scatter in the computed dynamic response than using scaling factors based on recorded ground motion

parameters.

An abundance of ground motion data recorded in Western North America (WNA), especially in California, has facilitated the development of relations to predict the PHA, PHV or response spectral ordinates corresponding to a specified magnitude and source-distance combination in WNA (Joyner and Boore, 1988). These prediction relations, essentially developed for Western United States, are also used for Western Canada because the magnitude and distance dependence of strong ground motions observed in the Western United States are assumed to apply to the similar geologic and tectonic environment of Western Canada (Hasegawa et al., 1981). Due to the scarcity of recorded seismic ground motions in Eastern North America (ENA), similar relations have been developed for ENA based on a theoretical stochastic model which has been well matched by existing data from small to moderate earthquakes (Atkinson and Boore, 1990).

Prediction relations for response spectra are of special importance since these spectra provide a better description of the ground motion than do PHA or PHV. Since response spectra actually represent the response of simple sdof systems to the ground motion, these become more relevant for use in dynamic analyses than PHA or PHV.

In the current study, a scheme is proposed for implementing spectral prediction relations in ground motion scaling. This scheme has been verified using ground motions recorded in the San Francisco area during the October 1989 Loma Prieta earthquake (Hosni and Heidebrecht, 1992). An important feature of this scheme is that it can be easily adapted to any region for which spectral prediction relations exist. For Ottawa and Prince Rupert, this scheme is adopted for the development of

the seismic bedrock motions used as the input ground motions for the soil-structure models. It is not used for the development of the input ground motions for Vancouver due to the lack of spectral prediction relations for subduction events off the west coast.

Hasegawa et al. (1981), whose prediction relations for PHA and PHV were adopted in the development of the seismic zoning maps in NBCC, did not develop corresponding prediction relations for the spectral ordinates. As a result, in the development of the input ground motions for this study, it is necessary to resort to spectral prediction relations established by others. Two relations for prediction of response spectra in North America are included in the current study. The spectral prediction relation proposed by Atkinson and Boore (1990) for shallow intraplate faulting in ENA is used to develop the input ground motions for Ottawa. The spectral prediction relation proposed by Sadigh et al. for shallow interplate faulting in WNA, and presented in Joyner and Boore (1988), is used to develop the input ground motions for Prince Rupert.

4.2 SPECTRAL PREDICTION RELATIONS.

The potential for soil deposits to amplify underlying bedrock motions has been well established in the literature. In view of the fact that even shallow dense deposits exhibit this amplification potential (Henderson et al., 1990), development of the site-specific input ground motions is restricted to rock sites. This is quite appropriate given the fact that these represent the bedrock motions for the analytical soil-structure models. As a result, the spectral prediction relations adopted in the current study are restricted to those developed for rock sites.

4.2.1 Spectral Prediction Relation for ENA.

Atkinson and Boore (1990) developed a stochastic model to generate synthetic time histories, corresponding to a specified earthquake magnitude and source-distance combination, for rock sites in ENA. The parameters used to define this model were based on seismological studies of earthquake source and attenuation processes. Ground motion predictions, based on this stochastic model, were shown to match available recorded ground motions from small to moderate earthquakes in ENA.

Atkinson and Boore used a simple functional form to fit the predictions, based on their model, for the randomly oriented horizontal component of pseudovelocity response at 5 percent damping (PSV). They used the definition of the source-distance (r_{AB}) as being the hypocentral or closest distance to the ruptured area. The resulting spectral prediction relation takes the form:

$$\log(PSV(T)) = a+b(M-6)+c(M-6)^2-\log(r_{AB})+kr_{AB} \qquad (4.1)$$

PSV = pseudovelocity response (cm/s)

T = period (sec)

M = moment magnitude

r_{AB} = source-distance (km)

Coefficients a, b, c and k are listed in Table 4.1 for different periods. This spectral prediction relation is valid for making predictions in the moment magnitude range of 4.5-7.5 and the source-distance range of 10-400 km.

4.2.2 Spectral Prediction Relation for WNA.

Sadigh et al. developed a prediction relation for the randomly

oriented horizontal component of pseudoacceleration response at 5 percent damping (PSA). This relation, presented in Joyner and Boore (1988), is based on a regression analysis of a ground motion data set comprising shallow events from Western United States supplemented by other shallow events from other parts of the world. This data set comprised records from earthquakes of moment magnitudes in the range of 4-6.9 and corresponding to source-distances in the range of 1-113 km (Sadigh, 1992). Both horizontal components from each recording station were included in the regression analysis. Sadigh et al. used the definition of the source-distance (r_S) as being the closest distance from the site to the rupture surface.

In the current study, this spectral prediction relation is preferred to the widely published prediction relation, for PSV response in WNA, proposed by Joyner and Boore (1988). This is because in compiling the data set used for the development of their prediction relation, Joyner and Boore classified ground motion records obtained on shallow soil deposits as being obtained at rock sites. In a study investigating the role of site effects on the response of soil-structure systems, incorporation of the Joyner and Boore prediction relation is not considered appropriate. Furthermore, for the same magnitude and source-distance combination, Hosni and Heidebrecht (1992) have shown the Sadigh et al. relation to predict more reasonable spectral shapes than the Joyner and Boore relation.

Sadigh et al. distinguished between strike-slip and reverse earthquakes in developing their prediction relation. Since the ground motion data used in the development of the input ground motions for Prince Rupert are mostly associated with strike-slip faulting, the spectral

prediction relation of Sadigh et al. used herein is that developed for strike-slip earthquakes. For rock sites, their spectral prediction relation takes the form:

$$\ln(PSA(T)) = a+1.1M+c_1(8.5-M)^{2.5}-2.05\ln(r_s+h_1\exp(h_2M)) \quad (4.2)$$

PSA = pseudoacceleration response (g)

r_s = source-distance (km)

Coefficients a, c_1, h_1 and h_2 are listed in Table 4.2 for different periods. In both the spectral prediction relations included in the current study, the moment magnitude is preferred to other magnitude scales because it corresponds to a well-defined physical property of the source (Campbell, 1985).

Throughout this study, PSV response is preferred to other spectral response parameters in describing the ground motions for two main reasons. First, for undamped sdof oscillators, there exists a close resemblance between the Fourier amplitude ordinates and the corresponding spectral velocity response ordinates (Hudson, 1979). As a result, spectral velocity response ordinates are better able to simultaneously describe both the intensity and frequency content of the ground motion as compared to spectral acceleration or spectral displacement. Second, PSV response resembles, to an acceptable degree, the exact velocity response while allowing the use of tripartite plots. These plots provide a comprehensive description of the ground motion as measures of the spectral acceleration, spectral velocity and spectral displacement can be simultaneously shown on a single plot using a single curve.

4.3 GROUND MOTION SCALING.

In spite of the existence of a large data base of recorded seismic ground motions from around the world, refined site-specific analyses, in most cases, require some form of ground motion scaling. This is necessarily so if the ground motion records are to be representative of the focal mechanism, regional geological conditions, magnitude and source-distance characterizing the seismic hazard at the specified site.

Guzman and Jennings (1976) proposed a method for ground motion scaling to develop design spectra for nuclear power plants. Their method was based on deriving a single scaling factor based on a PHA prediction relation. This scaling factor (S_{PHA}) was then used to modify an initial time history recorded during a magnitude M_I event at a source-distance r_I to correspond to a postulated magnitude M_O event at a source-distance r_O. This scaling factor was derived as follows:

$$S_{PHA} = \frac{PHA(M_O, r_O)}{PHA(M_I, r_I)} \tag{4.3}$$

PHA(M,r) is the predicted value corresponding to an earthquake of magnitude M at a source-distance r according to the selected PHA prediction relation. S_{PHA} was then used to scale the initial time history to represent the design ground motion. The final PHA for the postulated ground motion would, as a result, be the product of S_{PHA} and the recorded PHA for the initial time history. This approach has a distinct advantage over directly scaling the recorded PHA to $PHA(M_O, r_O)$. This advantage lies in the fact that ground motion prediction relations are usually based on a multitude of ground motion records covering a wide range of the magnitude and source-distance. Using S_{PHA} to scale an initial set of time histories, selected to correspond as closely as possible to the postulated

M_0 and r_0 combination, will inevitably lead to more reliable predictions of the postulated ground motions due to a stronger bias towards the M_0 and r_0 combination in the results.

The proposed scheme for ground motion scaling, while adopting this same principle, is a more elaborate variation of the approach used by Guzman and Jennings. The general applicability of the approach used by Guzman and Jennings to engineering structures is hampered by the fact that it is based on scaling to PHA, a parameter that does not correlate well with the seismic response of buildings having fundamental periods in excess of 0.5 sec (Heidebrecht and Tso, 1983). The proposed scheme aims at alleviating this drawback, thus offering a broader range of applicability in engineering practice.

4.4 DEVELOPMENT OF THE INPUT GROUND MOTIONS.

A flow chart outlining the different steps involved in the development of the site-specific ground motions, in the current study, is shown in Figure 4.1. For each of the three sites, a set of artificial time histories are developed by scaling an initially selected set of recorded ground motions according to the following process for ground motion scaling:

First: the initial recorded ground motions are scaled according to the proposed scheme, which is described in Subsection 4.4.2, to account for the magnitude and source-distance dependence of the frequency content for earthquake ground motions.

Second: the resulting time histories are scaled, as described in Subsection 4.4.3, to match the ground motion intensities,

specified in NBCC 90, for the respective sites.

For each of the three sites, the artificial time histories, developed using this scaling process, represent the bedrock motions for the respective soil-structure models. The adopted process for ground motion scaling is superior to just scaling using a single peak ground motion parameter in that it takes the frequency content of the ground motion into consideration. In addition, the criteria set forth for the selection of the initial time histories to be scaled allow for consideration of the underlying tectonic process, regional geological conditions and strong motion duration characterizing the specified site.

Although the uniform hazard spectrum (UHS) approach (Atkinson, 1991a) is a viable alternative to the proposed process for ground motion scaling, UHS are not, at the present time, generally available throughout Canada.

4.4.1 Selection of the Initial Ground Motion Data Sets.

As outlined earlier, all ground motion records included in this study are restricted to those obtained at rock sites. Atkinson (1988) has demonstrated that crustal conditions in ENA are more competent than those in WNA. This results in a slower attenuation of the ground motions, especially the higher frequency components, in ENA. This significance of the regional geological formations is taken into consideration in the selection of the initial data sets.

Another factor to be considered in making the selection is the faulting mechanism expected to dominate the seismic hazard at the site for which predictions are made. Guzman and Jennings (1976) maintain that, if

the available data base is large enough, the faulting mechanism should be taken into consideration.

The seismic zoning maps of Canada, currently incorporated in the NBCC provisions, are developed using the Cornell-McGuire seismic risk estimation method, applied to the seismological model for Canada proposed by Basham et al. (1982). This model divides Canada into 32 earthquake source zones based on the distribution of past and recent earthquakes as well as any geological or tectonic evidence that can be used to predict future earthquake activity. Each of these source zones was associated with a cumulative magnitude recurrence relation that is applied uniformly within that zone. The attenuation of PHA and PHV was determined using the prediction relations of Hasegawa et al. (1981). Based on this information, seismic risk computations resulted in site-specific values for PHA and PHV corresponding to the probability of exceedence, of 10 percent in 50 years, currently adopted in NBCC 90. These PHA and PHV data, herein referred to as the code values, were then contoured to develop the seismic zoning maps of Canada (Basham et al., 1982).

Information on the seismic risk computations specific to Ottawa, Vancouver and Prince Rupert is provided by Basham (1990). Based on this information, the M_0 and r_0 combinations dominating the seismic hazard, at the three sites, are listed in Table 4.3. These M_0 and r_0 combinations are to be maintained in the development of the respective input ground motion sets. In many cases, the available ground motion data base did not include records that directly correspond to these M_0 and r_0 combinations. As a result, selected sets of records are scaled to correspond to these M_0 and r_0 combinations. Nonetheless, every effort is exerted to select initial

data sets that resemble as closely as possible these M_0 and r_0 combinations to achieve more reliable results.

In recognition of the stochastic nature of earthquakes, the initial data set, for each of the three sites, is not restricted to a single event. Since the input ground motions are to represent the randomly oriented horizontal component of the ground motion, both horizontal components for each record, selected in the initial data sets, are included.

Since the initial ground motion records are selected to correspond as closely as possible to the seismo-tectonic environment characterizing the specified sites, the strong motion duration for these initial records is expected to be close to that for the postulated ground motions at these sites. In the current study, it is considered sufficient to limit the initial set of recorded ground motions, for each site, to 5 records (10 horizontal ground motion components).

4.4.2 Scaling for the Frequency Content.

The scheme for ground motion scaling, described subsequently, is used to modify the pseudovelocity spectra, and hence the frequency content, for the initially selected sets of ground motion records to match the M_0 and r_0 combinations postulated for the respective sites.

4.4.2.1 Scaling of the Initial Pseudovelocity Spectra.

The spectral prediction relations, presented in Equations 4.1 and 4.2, are used to derive scaling factors for the pseudovelocity spectra, corresponding to the initial sets of ground motion records, in a way

analogous to that employed by Guzman and Jennings and presented in Equation 4.3. The improvement provided herein is that instead of using a single scaling factor for the whole range of periods, scaling factors derived using the proposed scheme are period-dependent. The use of period-dependent scaling factors is recommended because the shape of ground motion spectra varies with both earthquake magnitude and source-distance. The spectral shape varies with earthquake magnitude because larger events are associated with ground motions rich in low frequencies while smaller events are associated with ground motions rich in high frequencies (Dunbar and Charlwood, 1991). The spectral shape varies with source-distance because anelastic attenuation and wave scattering alter the spectral shape by reducing high frequencies more rapidly with source-distance than low frequencies (Atkinson and Boore, 1990). Using the prediction relation of Atkinson and Boore, derivation of the period-dependent scaling factors takes the form:

$$S_{AB}(T) = \frac{PSV(T,M_0,r_0)}{PSV(T,M_1,r_1)} \tag{4.4}$$

Using the prediction relation of Sadigh et al., derivation of the scaling factors takes the form:

$$S_S(T) = \frac{PSA(T,M_0,r_0)}{PSA(T,M_1,r_1)} \tag{4.5}$$

The scaling factors, S_{AB} and S_S, are determined for each record in the initial data sets for Ottawa and Prince Rupert respectively. These are then used to scale the pseudovelocity spectra for both horizontal components of the respective records, resulting in the PSV_{AB} and PSV_S spectra for Ottawa and Prince Rupert respectively.

4.4.2.2 Spectrum-Compatible Ground Motions.

Since the developed ground motions are to be used for dynamic analyses, the time histories for the records in the initial data sets for Ottawa and Prince Rupert should also be modified to be compatible with the target spectra (PSV_{AB} and PSV_S for Ottawa and Prince Rupert respectively). This is achieved using the computer program SYNTH (Naumoski, 1985). For each time history to be modified, the program iteratively modifies the Fourier coefficients for the initial time history. The iteration process is terminated when a suitable match between the spectrum for the modified time history and the corresponding target spectrum is achieved. These resulting time histories have thus been modified to account for differences in the frequency content between the initially selected records, associated with M_I events at r_I source-distances, and the M_0 and r_0 combinations postulated for the respective sites.

4.4.3 Scaling for the Ground Motion Intensity.

Since all the structural models and most of the soil models, developed in the current study, have fundamental periods in excess of .5 sec, PHV is preferred to PHA as a measure of the ground motion intensity (Heidebrecht and Tso, 1983) as it is expected to correlate better with the seismic response of the different soil-structure systems. Since the proposed scheme for ground motion scaling does not ensure that the PHV values for the modified time histories match the respective code values, it is considered essential to further scale these time histories to achieve input ground motions having PHV values that match the code values. This is necessarily so because results from the current study are compared

to the NBCC 90 design base shear (V). As indicated by Equation 3.4 and Figure 3.1, for fundamental periods in excess of .5 sec, V is proportional to v which closely matches the corresponding PHV values for the three sites as indicated by Table 4.4. In this table, the seismic hazard parameters are listed as specified in NBCC 90 for the three sites.

For Vancouver, due to the lack of appropriate spectral prediction relations, the initial set of ground motion records cannot be scaled for the frequency content and scaling for the ground motion intensity is the only form of scaling used to develop the input ground motions for this site.

4.5 CHARACTERISTICS OF THE INPUT GROUND MOTIONS.

The initial sets of ground motion records, for the three sites, are selected. These are then scaled, according to the adopted scaling process, to develop the input ground motions used in the computations.

4.5.1 Ottawa.

Seismic hazard, for Ottawa, is dominated by shallow intraplate faulting within the American plate (Weichert, 1990). The initial set of records, selected for Ottawa, are described in Table 4.5. The selection is restricted to the Nahanni and Saguenay earthquakes in recognition of the influence of the regional crustal conditions on earthquake source parameters and ground motion attenuation characteristics in ENA. Information on the horizontal ground motion components for the selected records is provided in Table 4.6.

According to Weichert (1989), the Nahanni earthquake occurred

within a geological structure and a contemporary stress field that extend throughout most of ENA and, therefore, must be considered as a representative design earthquake for engineered structures in the active seismic zones of ENA. In the initial data set for Ottawa, two records are selected from this earthquake and one record from an aftershock that was associated with significant ground motions (Weichert et al., 1986). The Saguenay earthquake is the most significant, and widely recorded, event in ENA in over fifty years (Munro and Weichert, 1989). Two records from this earthquake are included in the initial data set.

Information on the records from the Nahanni earthquake are obtained from Weichert et al. (1986), while information on the records from the Saguenay earthquake are obtained from Munro and Weichert (1989). According to this information, the initial set of records, listed in Table 4.5, are all obtained at rock sites. The r_{AB} values, given in this table, are obtained from Atkinson (1991b). According to this table, there exist significant differences between the M_I and r_I combinations, associated with the initial set of records, and the M_O and r_O combination postulated for Ottawa. When such significant differences exist, scaling the initial records for the frequency content is essential to safeguard the reliability of the results.

The scaling factors, S_{AB}, are derived according to Equation 4.4 and are shown in Figure 4.2, for the 5 records in the initial data set. S_{AB} are derived for the periods given in Table 4.1. For intermediate periods, the scaling factors are interpolated as a linear function of the logarithm, to the base 10, of the period. In this chapter, the scaling factors as well as the pseudovelocity spectra are shown only corresponding to the period

range of .1-4 sec.

S_{AB} are then used to scale the pseudovelocity spectra for the initial records to achieve the corresponding PSV_{AB} spectra shown in Figure 4.3. According to this figure, the PSV_{AB} spectra for the records from the Saguenay earthquake are significantly higher than those for the records from the Nahanni earthquake. This is expected given the fact that the spectral prediction relation of Atkinson and Boore overpredicted the ground motions recorded during the Nahanni earthquake, but underpredicted the ground motions recorded during the Saguenay earthquake (Atkinson, 1991b).

The computer program SYNTH is used to modify the initial time histories to match the corresponding PSV_{AB} spectra. For the purpose of the current study, 10 iterations are found to be sufficient to achieve a close match between the pseudovelocity spectra for the modified time histories and the corresponding target spectra.

These modified time histories are then scaled, for the ground motion intensity, to correspond to PHV=.1 m/s, specified in NBCC 90 for Ottawa. The resulting ground motions are the input motions used in all computations specific to Ottawa in the current study. The horizontal ground motion components for these input motions are described in Table 4.7. Furthermore, the spectra corresponding to these input ground motions, referred to as PSV_f, are statistically analyzed to yield the mean and M+SD (mean plus one standard deviation) curves, which are shown in Figure 4.4.

4.5.2 Vancouver.

Seismic hazard, for Vancouver, is associated with the subduction

of the Juna de Fuca plate beneath the American plate (Milne et al., 1978). Focal depths, associated with these subduction earthquakes, are expected to be in the range of 40-70 km (Basham et al., 1982) in contrast to the shallower seismicity, with focal depths usually not exceeding 20 km, prevailing elsewhere in Canada.

Due to a lack of spectral prediction relations for subduction events off the west coast, the initial set of records selected for Vancouver cannot be scaled for the frequency content. As a result, the initial records are selected such that the associated M_I and r_I combinations bracket the M_0 and r_0 combination postulated for Vancouver. Due to a lack of ground motion records from large events associated with the subduction zone off the west coast, the initial records are selected from other subduction events around the world. The initial set of records, selected for Vancouver, are described in Table 4.8. The source-distances (r), listed in this table, are the epicentral distances associated with the different records.

The Alaskan subduction earthquakes are associated with the subduction of the Pacific plate beneath the American plate. Information on the records selected from the Alaskan subduction earthquakes is obtained from Friberg and Jacob (1990), based on a strong motion data base which includes the catalog of Alaskan subduction earthquakes that occurred from 1960 to the present time. Three records, from three different events that occurred in the Alaskan subduction zone, are included in the initial data set. Owing to its proximity to the subduction zone dominating the seismic hazard for Vancouver, more weight is given to the Alaskan subduction zone in recognition of the influence of regional geological conditions on

seismic ground motion characteristics.

The three records, from the Alaskan subduction zone, all correspond to M_I values lower than M_0. The two other records in the initial data set are selected to correspond to M_I values larger than M_0. One record is selected from the June 1978 Miyagi-Ken-Oki earthquake in Japan. This earthquake was associated with the slow subduction of the Pacific plate beneath Japan (Yanev, 1978). The other record is selected from the September 1985 Mexican earthquake. This earthquake was associated with the subduction of the Cocos plate beneath the American plate (Mitchell et al., 1986). Information on both these records is obtained from MUSE (1988). The initial set of records, listed in Table 4.8, are all obtained at rock sites (Switzer et al., 1981; MUSE, 1988).

Information on the horizontal ground motion components for the selected records is provided in Table 4.9. The pseudovelocity spectra, corresponding to these initial time histories, are shown in Figure 4.5. The spectra corresponding to the larger events, from Japan and Mexico, are understandably higher than those corresponding to the events from Alaska. The initial time histories are then scaled, for the ground motion intensity, to correspond to PHV=.21 m/s, specified in NBCC 90 for Vancouver. The resulting ground motions are the input motions used in all computations specific to Vancouver in the current study. The horizontal ground motion components for these input motions are described in Table 4.10. The mean and M+SD PSV, spectra, corresponding to these input motions, are shown in Figure 4.6.

4.5.3 Prince Rupert.

Seismic hazard, for Prince Rupert, is dominated by shallow interplate faulting between the Pacific and American plates along the Queen Charlotte Transform (Milne et al., 1978). Milne et al. also state that fault plane solutions along the transform show almost pure strike-slip motion on two vertical planes oriented approximately parallel and perpendicular to the fault strike. As a result, the Queen Charlotte Transform is considered tectonically similar to the San Andreas fault system, the dominant source of seismic hazard for California.

Owing to a lack of recorded ground motion data from events associated with the Queen Charlotte Transform, the initial data set for Prince Rupert is selected from available ground motion data that were recorded in California, and are associated with the San Andreas fault system. This initial set of records, obtained at rock sites (Switzer et al., 1981), are described in Table 4.11. The significant differences between the M_I and r_I combinations, associated with these records, and the M_0 and r_0 combination postulated for Prince Rupert are due to the limitations of the available ground motion data base. Available ground motion records from California are associated with relatively short source-distances and lack recordings at rock sites for moment magnitudes in excess of 6.9. In the selection of the initial records, more weight is given to the Loma Prieta earthquake as it is the largest event for which records at rock sites are available. Information on the horizontal ground motion components for these records is provided in Table 4.12.

Information on the first three records in Table 4.11 is obtained from Hudson et al. (1971), while information on the records from the Loma Prieta earthquake is obtained from Shakal et al. (1989). Source-distances,

according to the definition adopted by Sadigh et al., are not readily available for the first three records in Table 4.11. For the first two of these records, r_S values are assumed identical to the corresponding source-distance values given in Joyner and Boore (1981). This assumption is quite reasonable for the range of source-distances associated with both these records. Joyner and Boore used the definition of source-distance as being the shortest distance from the recording station to the vertical projection of the earth fault rupture on the earth surface. For the third record, r_S is assumed identical to the epicentral distance. The station associated with this record is located far enough from the fault to justify such an assumption. According to Campbell (1985), there is little difference between various measures of the source-distance for sites located several source dimensions from the fault.

The scaling factors, S_S, are derived according to Equation 4.5 and shown in Figure 4.7, for the 5 records in the initial data set. S_S are derived for the periods given in Table 4.2. For intermediate periods, the scaling factors are interpolated as a linear function of the logarithm, to the base 10, of the period.

The derived S_S are used to scale the pseudovelocity spectra for the initial records to achieve the corresponding PSV_S spectra shown in Figure 4.8. As seen from this figure, the PSV_S spectra for the records associated with the smaller differences between r_I and r_0 are significantly higher than those for the records associated with the larger differences. This implies that the rate of source-distance attenuation, corresponding to the source-distance range involved in developing the ground motions for Prince Rupert, is overestimated by Equation 4.2. This is expected to be a result

of developing a single spectral prediction relation corresponding to a wide range of the source-distances. This is especially true if the records in the data set used in developing the prediction relation are not uniformly distributed over this source-distance range. Body-waves usually dominate the seismic ground motions close to the fault. These body-waves are associated with larger geometric spreading factors than surface-waves that tend to dominate the seismic motions farther from the fault. As a result, recorded ground motions usually show a faster attenuation with source-distance close to the fault. It is thus desirable, in the development of ground motion prediction relations, to recognize this effect by subdividing the whole data set into ranges of the source-distance and performing the regression analyses over each range individually.

Sadigh et al. (Sadigh, 1992) have also developed another more recent prediction relation for the randomly oriented horizontal component of spectral acceleration, at 5 percent damping, for rock sites in WNA. This prediction relation is based on a more expanded data set than that used in developing Equation 4.2. This expanded data set includes records from earthquakes of moment magnitudes in the range of 4.6-7.4 and corresponding to source-distances in the range of 1-261 km. S_S values derived on the basis of this more recent prediction relation are found to be practically identical to those derived based on Equation 4.2., with the differences generally not exceeding 5 percent for the five records in the initial data set. Consequently, there is expected to be no significant difference between the PSV_S spectra, shown in Figure 4.8, and those based on this more recent prediction relation.

The computer program SYNTH is used to modify the initial time histories to match the corresponding PSV_S spectra. These modified time histories are then scaled, for the ground motion intensity, to correspond to PHV=.27 m/s, specified in NBCC 90 for Prince Rupert. The resulting ground motions are the input motions used in all computations specific to Prince Rupert in the current study. The horizontal ground motion components for these input motions are described in Table 4.13. The mean and M+SD PSV_F spectra, corresponding to these input ground motions, are shown in Figure 4.9. The high content of low frequencies, observed in this figure, are characteristic of ground motions at such long distances from the fault.

Table 4.1 Coefficients in the Atkinson and Boore prediction relation

T (sec)	a	b	c	k
0.05	1.97	.41	-.03	-.00350
0.10	2.11	.42	-.03	-.00250
0.20	2.21	.44	-.04	-.00170
0.50	2.30	.53	-.09	-.00102
1.00	2.30	.67	-.15	-.00064
2.00	2.16	.85	-.18	-.00037
5.00	1.73	.96	-.03	-.00034

Table 4.2 Coefficients in the Sadigh et al. prediction relation

T (sec)	a	c_1	M<6.5 h_1	M<6.5 h_2	M≥6.5 h_1	M≥6.5 h_2
0.1	-0.688	.007	1.353	.406	.579	.537
0.2	-0.479	-.008	1.353	.406	.579	.537
0.3	-0.543	-.018	1.353	.406	.579	.537
0.5	-0.793	-.036	1.353	.406	.579	.537
1.0	-1.376	-.065	1.353	.406	.579	.537
2.0	-2.142	-.100	1.353	.406	.579	.537
4.0	-3.177	-.150	1.353	.406	.579	.537

Table 4.3 Dominant sources of seismic hazard for the three sites

Site	M_0	r_0 (km)
Ottawa	6.6	65
Vancouver	7.0	60
Prince Rupert	7.9	200

Table 4.4 Seismic hazard parameters for the three sites

Site	Z_a	Z_v	PHA (g)	PHV (m/s)	ν
Ottawa	4	2	.20	.10	.10
Vancouver	4	4	.21	.21	.20
Prince Rupert	3	5	.13	.27	.30

Table 4.5 Description of the records in the initial data set for Ottawa

Rec.	Earthquake	M	Station	r_{AB} (km)
1	Nahanni 23 Dec., 1985	6.8	Iverson	8
2	Nahanni 23 Dec., 1985	6.8	Battlement Creek	23
3	Nahanni (aftershock) 23 Dec., 1985	5.2	Iverson	8
4	Saguenay 25 Nov., 1988	6.0	Riviere-Ouelle	118
5	Saguenay 25 Nov., 1988	6.0	St-Pascal	126

Table 4.6 Description of the horizontal ground motion components in the initial data set for Ottawa

Rec.	Earthquake	Comp.	PHA (g)	PHV (m/s)
1	Nahanni (Iverson)	N10E	1.101	.461
		N80W	1.345	.448
2	Nahanni (Battlement Creek)	N00W	.194	.034
		N90W	.186	.063
3	Nahanni aftershock	N10E	.228	.068
		N80W	.089	.032
4	Saguenay (Riviere-Ouelle)	N00W	.040	.022
		N90W	.057	.035
5	Saguenay (St-Pascal)	N00W	.046	.026
		N90W	.056	.026

Table 4.7 Description of the horizontal ground motion components developed for Ottawa

Rec.	Earthquake	Comp.	PHA (g)	PHV (m/s)
1	Nahanni (Iverson)	N10E	.208	.100
		N80W	.238	.100
2	Nahanni (Battlement Creek)	N00W	.569	.100
		N90W	.379	.100
3	Nahanni aftershock	N10E	.166	.100
		N80W	.089	.100
4	Saguenay (Riviere-Ouelle)	N00W	.194	.100
		N90W	.174	.100
5	Saguenay (St-Pascal)	N00W	.195	.100
		N90W	.242	.100

Table 4.8 Description of the records in the initial data set for Vancouver

Rec.	Earthquake	M	Station	r (km)
1	Alaskan Subduction 4 Sept., 1965	6.8	Kodiak, U.S. Naval Station	60
2	Alaskan Subduction 22 Dec., 1965	6.8	Kodiak, U.S. Naval Station	77
3	Miyagi-Ken-Oki 12 June, 1978	7.4	TH019, East Coast of Honshu	116
4	Alaskan Subduction 14 Feb., 1983	6.3	Chernabura Island	46
5	Mexican 19 Sept., 1985	8.1	La Union, Guerro Array	84

Table 4.9 Description of the horizontal ground motion components in the initial data set for Vancouver

Rec.	Earthquake	Comp.	PHA (g)	PHV (m/s)
1	Alaskan Subduction (Sept., 1965)	N10W	.017	.019
		S80W	.022	.033
2	Alaskan Subduction (Dec., 1965)	N10W	.037	.042
		S80W	.039	.043
3	Miyagi-Ken-Oki	N41E	.211	.127
		S49E	.226	.141
4	Alaskan Subduction (Feb., 1983)	N20W	.041	.030
		N70E	.048	.031
5	Mexican	N00W	.166	.203
		N90E	.150	.117

Table 4.10 Description of the horizontal ground motion components developed for Vancouver

Rec.	Earthquake	Comp.	PHA (g)	PHV (m/s)
1	Alaskan Subduction (Sept., 1965)	N10W	.193	.210
		S80W	.139	.210
2	Alaskan Subduction (Dec., 1965)	N10W	.184	.210
		S80W	.189	.210
3	Miyagi-Ken-Oki	N41E	.347	.210
		S49E	.336	.210
4	Alaskan Subduction (Feb., 1983)	N20W	.294	.210
		N70E	.323	.210
5	Mexican	N00W	.172	.210
		N90E	.270	.210

Table 4.11 Description of the records in the initial data set for Prince Rupert

Rec.	Earthquake	M	Station	r_S (km)
1	Parkfield 28 June, 1966	6.1	San Luis Obispo Recreation Building	64
2	Borrego Mountain 9 April, 1968	6.6	San Onofre SCE Power Plant	122
3	San Fernando 9 Feb., 1971	6.6	San Onofre SCE Power Plant	135
4	Loma Prieta 17 Oct., 1989	6.9	Rincon Hill	76
5	Loma Prieta 17 Oct., 1989	6.9	Yerba Buena Island	77

Table 4.12 Description of the horizontal ground motion components in the initial data set for Prince Rupert

Rec.	Earthquake	Comp.	PHA (g)	PHV (m/s)
1	Parkfield	N36W	.015	.007
		S54W	.011	.008
2	Borrego Mountain	N33E	.041	.037
		N57W	.046	.042
3	San Fernando	N33E	.012	.015
		N57W	.017	.017
4	Loma Prieta (Rincon Hill)	N00W	.080	.073
		N90E	.090	.115
5	Loma Prieta (Yerba Buena Isl.)	N00W	.029	.046
		N90E	.067	.147

Table 4.13 Description of the horizontal ground motion components developed for Prince Rupert

Rec.	Earthquake	Comp.	PHA (g)	PHV (m/s)
1	Parkfield	N36W	.306	.270
		S54W	.268	.270
2	Borrego Mountain	N33E	.230	.270
		N57W	.227	.270
3	San Fernando	N33E	.154	.270
		N57W	.183	.270
4	Loma Prieta (Rincon Hill)	N00W	.255	.270
		N90E	.175	.270
5	Loma Prieta (Yerba Buena Isl.)	N00W	.175	.270
		N90E	.109	.270

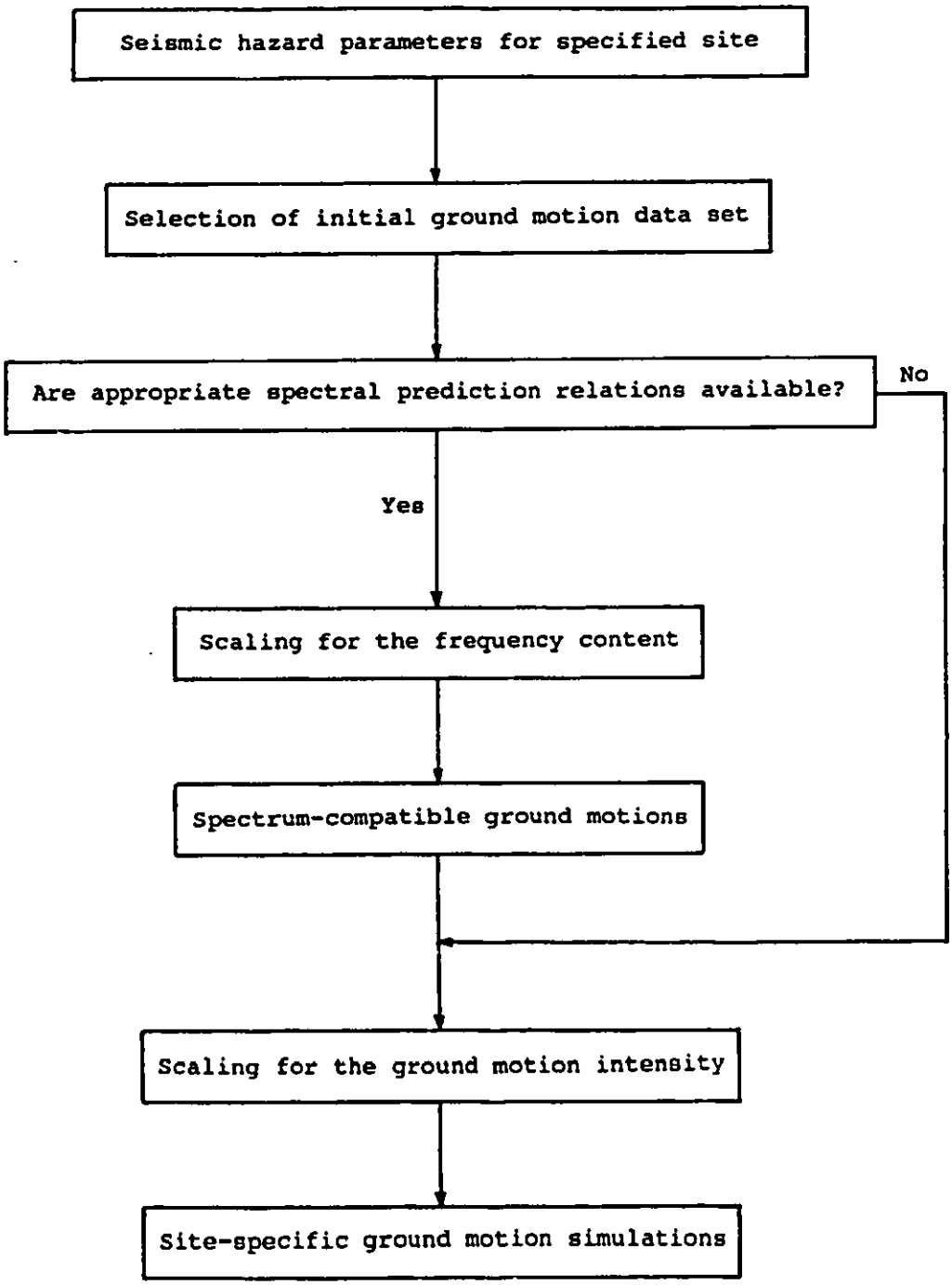

Figure 4.1 Flow chart for the development of the site-specific ground motion simulations

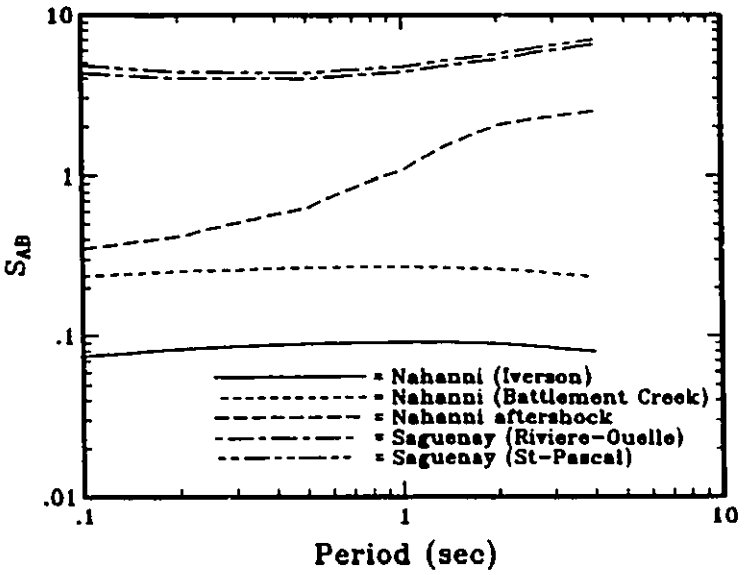

Figure 4.2 Scaling factors based on the spectral prediction relation of Atkinson and Boore

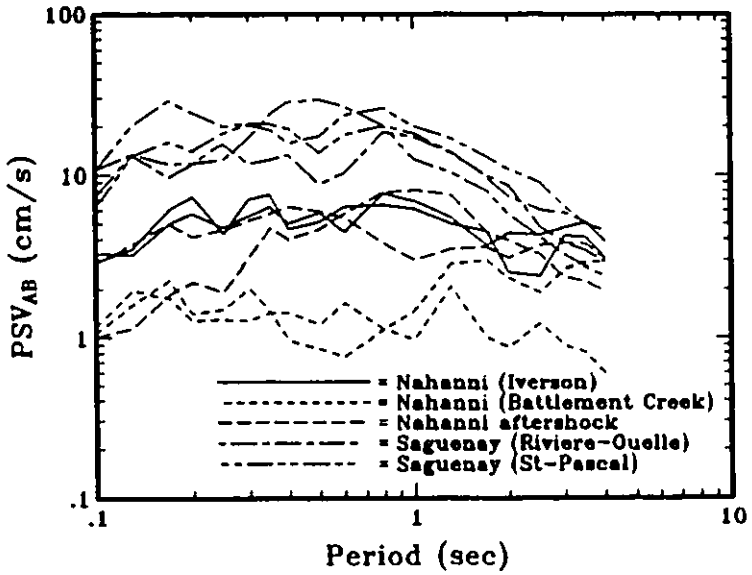

Figure 4.3 Pseudovelocity spectra scaled using the spectral prediction relation of Atkinson and Boore

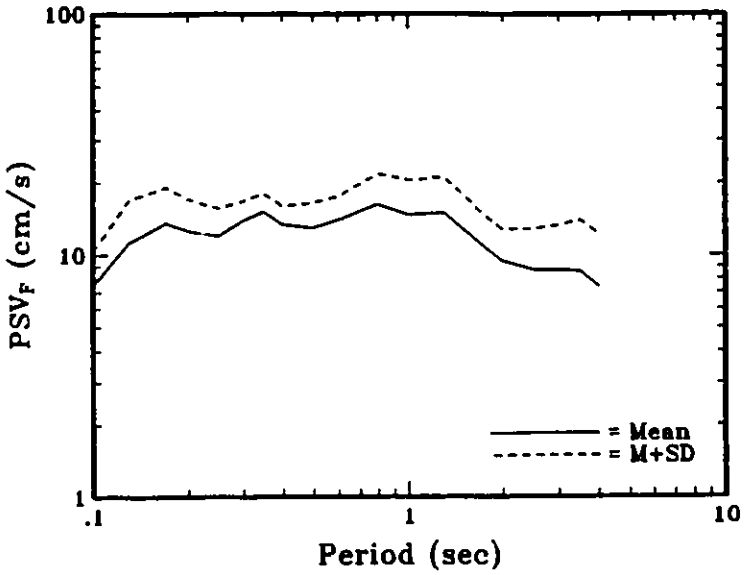

Figure 4.4 Pseudovelocity spectra based on the ground motions developed for Ottawa

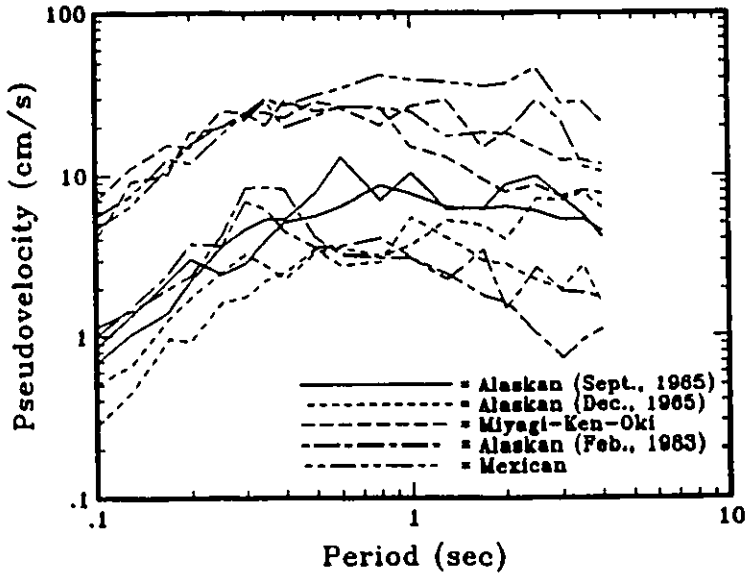

Figure 4.5 Pseudovelocity spectra based on the initial ground motion data set for Vancouver

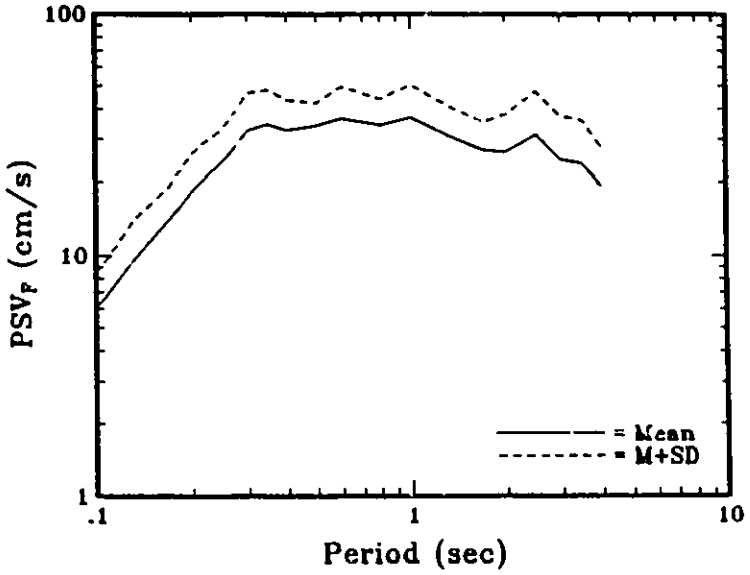

Figure 4.6 Pseudovelocity spectra based on the ground motions developed for Vancouver

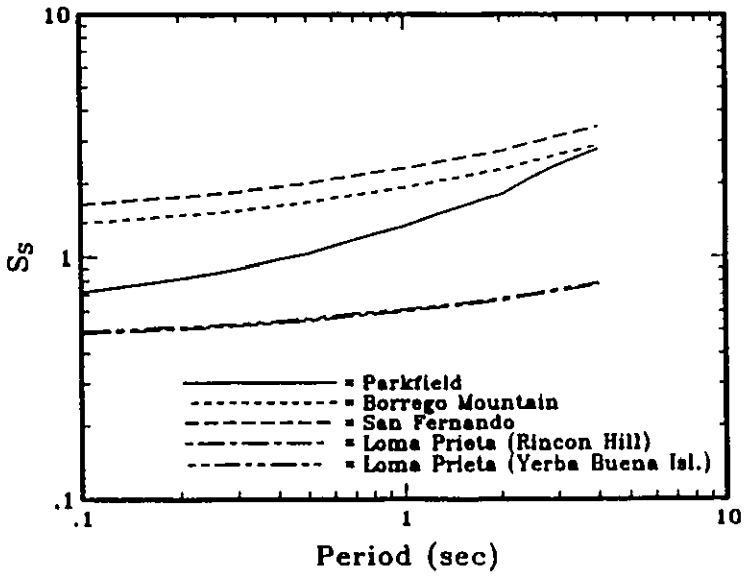

Figure 4.7 Scaling factors based on the spectral prediction relation of Sadigh et al.

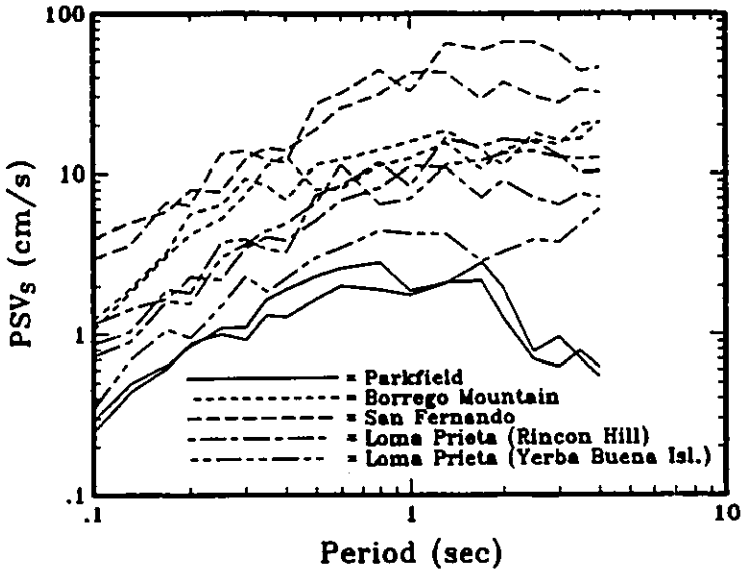

Figure 4.8 Pseudovelocity spectra scaled using the spectral prediction relation of Sadigh et al.

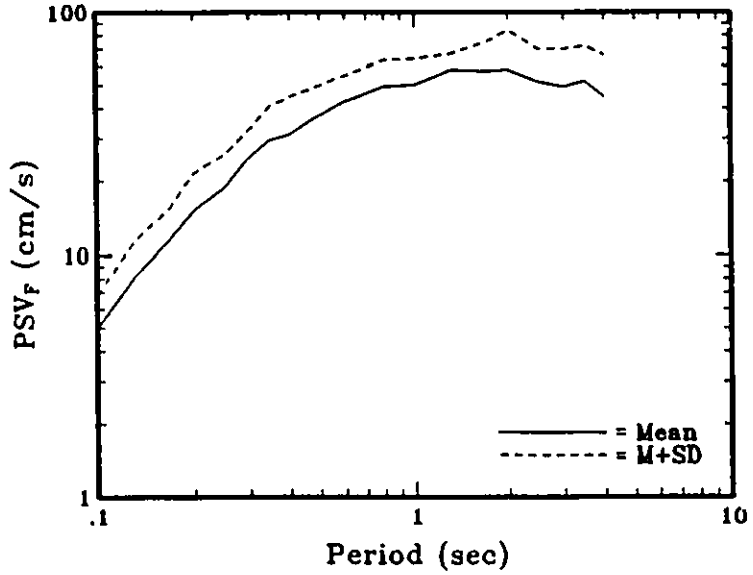

Figure 4.9 Pseudovelocity spectra based on the ground motions developed for Prince Rupert

CHAPTER 5

ANALYTICAL SOIL-STRUCTURE MODELS

5.1 INTRODUCTION.

In spite of the fact that earthquake ground motions are multi-directional, NBCC provisions, for normal buildings, allow for independent design about each of the horizontal axes of the building as this is expected to provide adequate resistance against earthquake motions occurring in any other direction. In addition, NBCC provisions maintain that there is usually adequate reserve capacity in vertical load-carrying members such that vertical accelerations can be safely ignored. As a result, analyses in the current study are restricted to the vertical plane of the frame (or wall) structural models, using the horizontal ground motions developed for the respective sites.

Geophysical models of the source dislocation are occasionally used to predict the spatial and temporal variations of the ground motions during earthquakes (e.g. Bouchon, 1980). These models are usually developed for a number of source-medium configurations to account for uncertainties in the assumptions of the dislocation characteristics. These models cannot, however, predict the associated complex wave radiation patterns with sufficient accuracy for engineering applications. As a result, simple wave patterns, validated by past research, are customarily adopted in the analyses of soil-structure interaction problems.

5.2 THE COMPUTER PROGRAM 'FLUSH'.

In FLUSH, the input ground motions are assumed to consist entirely of vertically propagating body-waves, with the shear body-waves being used to model the horizontal components of the ground motions. Gómez-Massó et al. (1983) presented an analytical approach that is very similar to that adopted in FLUSH, but which can also incorporate surface-waves in the specification of the seismic environment. They have shown that, corresponding to some specified free field motion, the seismic environment produced by vertically propagating body-waves is very similar to that produced by the more realistic combination of slightly inclined body-waves and higher-mode surface waves. Consequently, they concluded that soil-structure interaction analyses based on the assumption of vertically propagating body-waves are quite appropriate for most practical purposes.

Seed et al. (1975) carried out a comparison of the strengths and limitations of the most widely used methods for performing soil-structure interaction analyses, namely the finite element and the half-space methods. They concluded that the finite element method (e.g. FLUSH) offers the better prospect for estimating the probable behaviour of soil-structure systems, especially in the case of embedded structures.

Valera et al. (1977) used the seismic motions recorded at the Humboldt Bay Power Plant, located in California, during the Ferndale earthquake of June 1975 to investigate the potential for FLUSH to provide reliable predictions of the motions recorded within a building located at the ground surface as well as at the base of a massive concrete caisson embedded to a depth of 26 m below the ground surface. Based on knowledge of the free field motions recorded at that site, the ground motions

computed using FLUSH, for both the building and the concrete caisson, were shown to be in reasonably good agreement with the recorded motions.

In FLUSH, computations are performed in the frequency domain, with the nonlinear response of the soil deposit being modelled using an equivalent linear (iterative) approach, namely the method of complex response.

Constantopoulos et al. (1973) compared an equivalent linear approach to the more rigorous direct numerical integration in the time domain, for the dynamic analyses of nonlinear soil models. The nonlinear soil behaviour was assumed to be defined by the Ramberg-Osgood model. They found results based on both methods to be quite similar for the range of natural periods, of the soil deposits, that are of engineering interest. Similarly, Henderson et al. (1989a) found close agreement between the response of a nonlinear soil deposit, computed using the method of complex response, and that computed using nonlinear time domain analyses for different intensity levels of the ground motion excitation.

Taniguchi et al. (1988) computed the seismic response of a deeply embedded building using both an equivalent linear analysis and a nonlinear time domain analysis. They found good agreement between results from both methods. Some local geometrical nonlinearities (separation between building and soil), which cannot be accurately accounted for using an equivalent linear analysis, did occur in the nonlinear time domain analysis. These, however, had little effect on the overall response of the soil-structure system.

Based on the above-mentioned studies, it is decided to employ the computer program FLUSH for the analyses of the various soil-structure

systems developed in the current study.

5.3 THE ANALYTICAL SOIL-STRUCTURE MODELS.

The computational method, employed in FLUSH, is described in Lysmer et al. (1975). Herein, only the main characteristics of the analytical models are discussed. Schematic diagrams of the analytical models, for both a frame and a wall structure situated on a 40 m soil deposit, are shown in Figure 5.1.

5.3.1 Viscous Boundaries.

In FLUSH, viscous boundaries are used along the planar surfaces of the slice of soil on which the building is located. These viscous boundaries simulate the actual 3-D nature of the soil-structure interaction problem and are necessary to model the radiation of seismic energy, away from the structure, in the third dimension. According to Hwang et al. (1975), the computational time and computer core requirements for this simplified 3-D analysis remain essentially the same as for the 2-D analysis, while being significantly lower than those for an exact 3-D analysis. Hwang et al. found reasonable agreement between seismic response results using this simplified approach and those using an exact 3-D analysis, for a containment structure embedded to a depth of 24 m in a soil deposit. According to this simplified approach, the thickness of the slice of soil, to which these viscous boundaries are applied, is basically the length of the building in the third dimension. For all the soil-structure interaction analyses carried out in the current study, the building length in the third dimension is specified as 30 m, a reasonable

value for normal high-rise residential buildings.

In FLUSH, the Lysmer-Waas transmitting boundaries are specified at the vertical edges of the finite element mesh, as shown in Figure 5.1. Employment of these boundaries, necessary to model the exact dynamic effects of the semi-infinite soil deposit beyond the finite element mesh, has two distinct advantages. First, this allows for a drastic reduction of the size of the finite element mesh without any appreciable loss in accuracy. Lysmer et al. (1975) compared seismic response results using FLUSH, with the aforementioned viscous boundaries being used to model the 3-D effects and the Lysmer-Waas transmitting boundaries at the vertical edges of the finite element mesh, to results using an exact 3-D analysis for the same containment structure analyzed by Hwang et al. (1975). They found the differences in the response computed using both methods to be negligible for practical purposes. Second, these Lysmer-Waas boundaries are capable of transmitting any incident waves, no matter how close they are placed to the structure (Gómez-Massó et al., 1983).

Hwang et al. (1975), in their analyses of the embedded containment structure, found that the soil response became essentially identical to the free field motions, with no appreciable influence from the structure, at a distance of one length of the structural model from its centreline. Consequently, for the purpose of the current study, the Lysmer-Waas transmitting boundaries are specified at a distance of 10 m (length of the frame and wall models) from the centreline of the analytical model, as shown in Figure 5.1.

5.3.2 The Finite Element Mesh.

Similar to the approach adopted by Hwang et al. (1975) in modelling soil-structure interaction problems, plane strain conditions are assumed below the ground surface, while plane stress conditions are assumed above the ground surface. For this purpose, 2-D plane strain finite elements are used to model the soil deposits and foundations, while 2-D plane stress finite elements are used to model the structural walls. Beam elements are used to model the girders and columns of the structural frames. The soil deposit is assumed to be semi-infinite and horizontally layered. In FLUSH, the bedrock is modelled as a rigid base that does not allow the transmission of seismic waves from the soil deposit back into the bedrock.

FLUSH does not account for any nonlinearities in the superstructure during the seismic response. Due to the influence of the proximity of the fundamental periods of the structural and soil models (soil-structure resonance) on the seismic response of the soil-structure systems, it is necessary to make allowance, in the specification of the structural member properties, for the stiffness degradation associated with the development of the energy dissipation mechanisms adopted in the design of the frame and wall models. This is accomplished by applying stiffness reduction factors to both the gross concrete area (A_g) and the gross concrete moment of inertia (I_g) specified for the soil-structure interaction analyses. For this purpose, the reduction factors proposed by Goodsir et al. (1983), to reflect the expected state of cracking of different structural members during seismic response, are adopted herein. These reduction factors are listed in Table 5.1. Incorporation of these reduction factors results in an increase in the fundamental periods of the

'modified' frame and wall structural models from the values given in Tables 3.7 and 3.11, respectively, to the corresponding values given in Tables 5.2 and 5.3. Henceforth, the terms frame and wall models are used to refer to the structural models after incorporation of the stiffness reduction factors listed in Table 5.1.

Kuhlemeyer and Lysmer (1973) noted that a finite element model behaves like a low-pass filter having a definite cutoff frequency, and that waves propagating at higher frequencies cannot propagate through this finite element mesh. This 'virtual' cutoff frequency decreases with the increase of the size of the finite elements in relation to the wavelengths of the propagating waves. To avoid artificially filtering out frequency components of the input ground motions that are significant to the response of the soil-structure systems, Lysmer et al. (1975) recommend that the height of each soil layer be chosen no larger than h_{max}, which is determined as follows:

$$h_{max} = \frac{1}{5} \frac{v_s}{f_{max}} \tag{5.1}$$

h_{max} = maximum height of the soil layer (m)

v_s = shear wave velocity for the soil layer (m/s)

f_{max} = cutoff frequency (Hz)

Equation 5.1, in effect, limits h_{max} to one fifth of the wavelength of a shear body-wave propagating vertically at the cutoff frequency. For the purpose of the current study, association of h_{max} with shear body-waves is quite appropriate given the fact that only horizontal ground motions, which are modelled in FLUSH using shear body-waves, are propagated from the bedrock. For any single layer, v_s is determined from the corresponding

values of the shear modulus (G) and the soil unit weight (γ_s) according to:

$$G = \frac{\gamma_s v_s^2}{g} \qquad (5.2)$$

g = acceleration due to gravity (m/s^2)

As outlined earlier, the sand soil model S1 represents reasonably average soil properties, measured in terms of the low-strain shear modulus (G_o), among the soil models included in the current study. As a result, this soil model is used to determine the height of the different soil layers (h_s) in the analytical soil-structure models. The computed h_s values are then maintained for the other soil models included in this study. h_s are determined using f_{max}=10 Hz and assuming a shear strain amplitude (γ) of .1 percent for all the soil layers. This value of γ is a reasonable estimate of average shear strain conditions for soil deposits subjected to strong ground motion excitations (Hardin and Drnevich, 1972). Corresponding to this value of γ, the G/G_o ratio for soil model S1, according to Figure 2.5, is .342. Using this ratio and the G_o profile for this soil model, shown in Figure 2.3, the G profile corresponding to γ=.1 percent for soil model S1 is derived. Based on this G profile, Equations 5.1 and 5.2 are used to derive the h_s values listed in Table 5.4. In this table, the soil layers are numbered sequentially from the ground surface downwards. h_s values are observed to increase with depth below the ground surface by virtue of the corresponding increase in G. According to Table 5.4, the 15 m deep deposits are modelled using only the first 9 soil layers, while the 40 m deep deposits are modelled using all the 19 soil layers.

Valera et al. (1977) used a cutoff frequency of 10 Hz in their

analyses of the embedded concrete caisson. For this type of massive (short period) structure, the higher frequency components of the ground motion are expected to assume a stronger influence on the seismic response than in the case of the long period structures analyzed in the current study. As a result, the f_{max} value specified by Valera et al. is expected to be quite adequate for the analyses of the soil-structure systems included in this study. It is worth noting that the computation time, in FLUSH, is proportional to the fourth power of f_{max} and that unnecessarily large values of f_{max} should be avoided.

Due to the symmetry of the soil-structure models in the current study, only one half of the analytical model is used in the computations, with the appropriate boundary conditions being enforced at the centreline nodes.

5.3.3 The Number of Iterations.

In FLUSH, as outlined earlier, the nonlinear soil response is modelled using an iterative approach. For each soil element in the analytical model, the soil properties used within any single iteration are based on the maximum shear strain amplitude (γ_{max}) computed, for that element, from the previous iteration. A reduction factor of .65 is applied to γ_{max} to determine the effective shear strain amplitude (γ_{eff}) which represents a reasonable estimate of average shear strain conditions, for that soil element, during the whole duration of the ground motion excitation. This value of the reduction factor, though largely based on experience (Lysmer et al., 1975), is validated by the close agreement obtained between seismic response analyses based on this equivalent linear

approach and those based on the more rigorous nonlinear time domain analyses (Constantopoulos et al., 1973; Henderson et al., 1989a). In addition, predictions using FLUSH were shown to reasonably match recorded ground motions (Valera et al., 1977). For each soil element, γ_{eff} is used to derive new values for the shear modulus (G) and the hysteretic damping ratio (λ), in accordance with the respective material curves defined in Chapter 2, to be used for the next iteration.

For each soil-structure model, FLUSH performs both free field and complete interaction (coupled) analyses. In the free field analyses, the soil layers are analyzed independently from the structure. The coupled analyses, on the other hand, refer to the analyses of the complete soil-structure model, with displacement compatibility being maintained at the soil-structure interface. In FLUSH, free field analyses are carried out iteratively using closed-form relations, rather than the finite element method, for a vertically propagating shear body-wave in a linear 1-D viscoelastic medium. As a result, the free field analyses do not pose significant demands in terms of computation time or computer core requirements. For this reason, no limit is set on the number of iterations involved in the free field analyses, with iterations being terminated once the difference between the shear strain amplitudes, based on two consecutive iterations, are within 5 percent for each of the soil layers.

The coupled analyses, on the other hand, are performed using the finite element method and are quite time-consuming. Lysmer et al. (1975) expect that if the iterated (final) soil properties, based on the free field analysis, are specified as the initial soil properties for the analytical soil-structure model, it is often unnecessary to perform

iterations in the coupled analysis. This approach, for specification of the initial soil properties for the coupled analyses, is adopted in the current study.

Since the shear strain distribution, based on a coupled analysis, is expected to be significantly different from the strain distribution based on the corresponding free field analysis in the neighbourhood of the structure, it is decided to incorporate a limited number of iterations on the soil properties in the coupled analyses. For each site, ten time histories, representing the input ground motions, are used in the coupled analyses. For the purpose of the current study, two iterations are specified for the first of these time histories, with only one iteration being specified for each of the remaining nine time histories. Only a single iteration is specified for each of these nine time histories because, in each case, the specified initial soil properties are the iterated soil properties based on the coupled analysis results for the previous time history. Since the specified initial soil properties, in the case of the first time history, are the iterated soil properties based on the free field analysis, an additional iteration is warranted for this time history to ensure a reasonable convergence in the results.

Table 5.1 Stiffness reduction factors for the structural members

Structural member	Reduction factor
Frame girders	0.5
Frame columns	0.8
Walls	0.6

Table 5.2 Fundamental periods for the modified frame models

Frame model	T (sec)
Ottawa	4.55
Vancouver	3.41
Prince Rupert	2.93

Table 5.3 Fundamental periods for the modified wall models

Wall model	T (sec)
Ottawa	1.78
Vancouver	1.64
Prince Rupert	1.46

Table 5.4 Soil layer heights

Layer number	h_s (m)
1	1.15
2	1.30
3	1.50
4	1.65
5	1.80
6	1.90
7	2.00
8	2.10
9	2.20
10	2.25
11	2.35
12	2.40
13	2.45
14	2.55
15	2.60
16	2.65
17	2.70
18	2.75
19	2.80

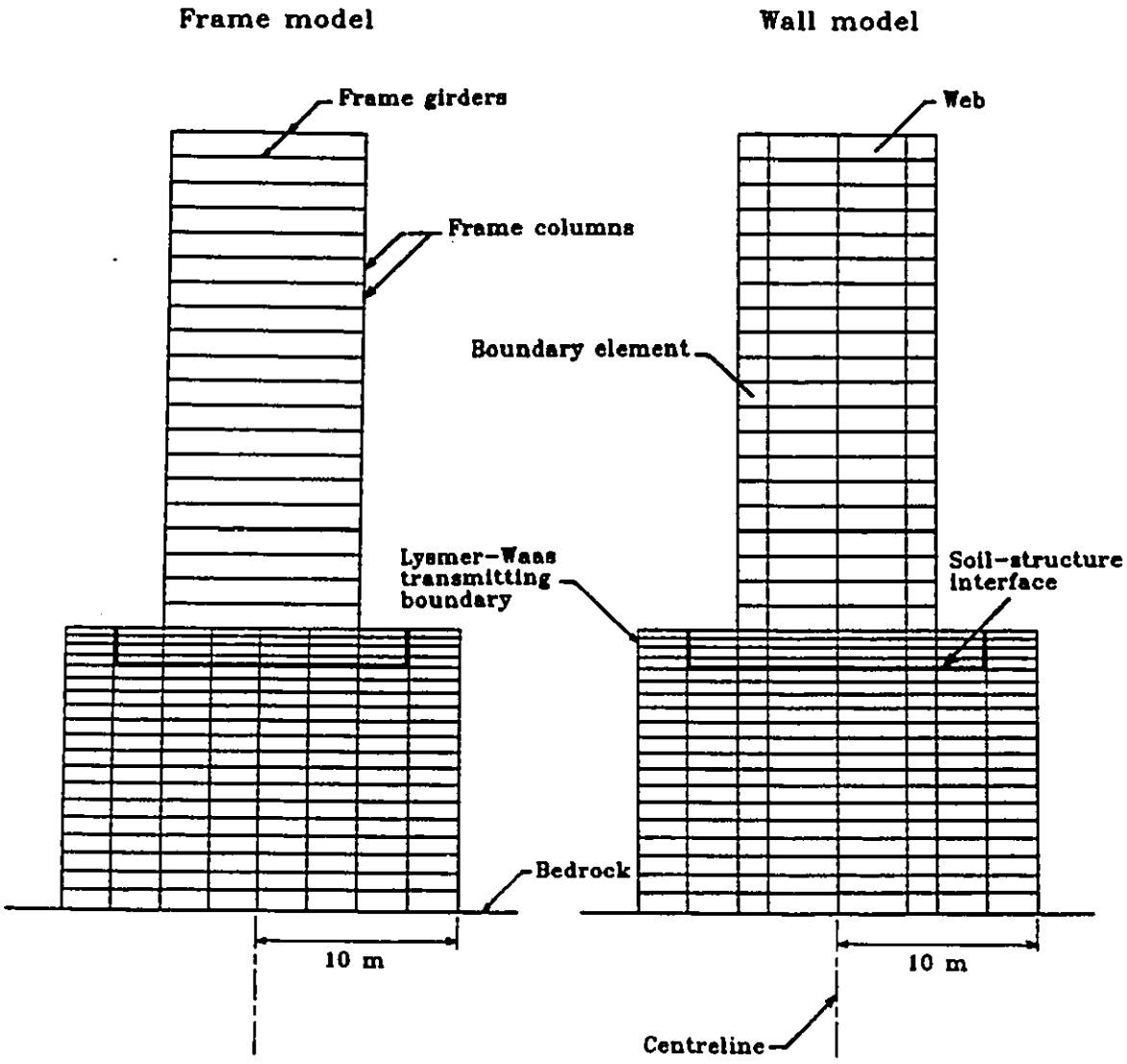

Figure 5.1 Schematic diagrams of the soil–structure analytical models for the case of a 40 m soil deposit (not to scale)

CHAPTER 6

DISCUSSION OF RESULTS

6.1 INTRODUCTION.

In both the free field and coupled analyses, Fourier amplification functions (A_f), representing the amplification of the bedrock accelerations to the nodal displacements, are computed using FLUSH. A_f curves are characterized by a dominant peak corresponding to the natural frequency of the soil model, in the case of a free field analysis, and corresponding to the fundamental frequency of the soil-structure model, in the case of a coupled analysis. A_f are consequently used to determine the fundamental periods for the different soil models and soil-structure models. For both the free field and coupled analyses, A_f are a function of the iterated soil properties. As a result, the fundamental periods determined using A_f, for a soil (or soil-structure) model, are expected to vary for the different input time histories, even if these correspond to the same input ground motion data set, due to variations in the respective iterated soil properties.

A_f, based on the free field analyses, are used to determine the natural periods (T_s) for the different soil models. For a given site, T_s values are determined for the ten time histories representing the input ground motions for that site. The T_s values, corresponding to each soil model, are then statistically analyzed to yield the mean, M+SD and M-SD (mean minus one standard deviation) T_s values for that soil model. These

results are presented in Figures 6.1 to 6.3, for the three sites included in the current study. For each soil model, the maximum and minimum T_s values, based on the ten input time histories for the specified site, are superimposed on these figures. In addition, the low strain T_s values are also shown. These low strain values correspond to shear strains (γ) smaller than .0001 percent, and represent the natural periods associated with a linear response of the soil deposits. Being associated with linear response, these low strain T_s values are independent of the input ground motions. Henceforth, these low strain T_s values are distinguished from the other T_s values, determined using the input ground motions developed in the current study, by being invariably associated with the term 'low strain'.

Figures 6.1 to 6.3 indicate only small scatter in T_s about the corresponding mean values. The mean T_s values as well as the low strain T_s values are also conveniently listed, for easier reference, in Table 6.1. Most of these mean T_s values are associated with coefficients of variation that are lower than 10 percent. The coefficient of variation (COV) is a statistical measure of the dispersion of a set of data, and is numerically equal to the standard deviation for that set of data, expressed as a percentage of the mean.

According to Table 6.1, the mean T_s values, for a given soil model, are larger for the sites associated with higher intensities of the ground motion, measured in terms of PHV. This is by virtue of the lower shear modulus (G) and larger hysteretic damping ratio (λ) values, associated with the larger induced shear strains. For a given soil model, the largest T_s values are associated with Prince Rupert, and are about twice the corresponding low strain T_s values.

In spite of the significant difference in the ground motion intensity associated with the input ground motions developed for Vancouver and Prince Rupert, the computed T_s values for the 15 m sand soil models are quite similar, based on the input ground motions for either site. This is on account of the input ground motions for Vancouver being characterized by a more significant content of seismic energy associated with the natural frequencies of these 15 m sand soil models. On the other hand, the input ground motions for Prince Rupert, being associated with a long source-distance, have most of their seismic energy associated with long periods. As a result, the input ground motions for Prince Rupert have a more significant content of seismic energy associated with the fundamental frequencies for all the other soil models, as compared to the input ground motions for Vancouver. This fact, combined with the higher ground motion intensity associated with Prince Rupert, result in T_s values that are larger, for these other soil models, than those based on the input ground motions for Vancouver.

According to Figures 6.1 to 6.3, there exists a significant difference between T_s, based on the input ground motions for the different sites, and the corresponding low strain T_s values. This fact was acknowledged by Finn (1991) who advocated caution when using T_s values, determined on the basis of low amplitude events such as microtremors, in relation to postulated main events. Elton and Martin (1989) were able to explain the damage pattern observed in Charleston, South Carolina, during an historic body-wave magnitude 6.8 earthquake using the T_s values based on nonlinear analyses of the soil deposits, rather than the low strain T_s values. Accordingly, they expect that governing building construction

within a certain city, in accordance with mapped T_s values, can greatly reduce the threat of damage during earthquakes. They used an analytical approach, quite similar to that adopted in FLUSH for the free field analyses, to develop such a T_s map for Charleston.

A_f, based on the coupled analyses, are used to determine the fundamental periods ($\bar{T}$) for the different soil-structure models. The $\bar{T}$ values, for each soil-structure model, are statistically analyzed to yield the mean $\bar{T}$ values listed in Tables 6.2 and 6.3, corresponding to the frame and wall models respectively. These tables indicate that for the same site and structural model, the mean $\bar{T}$ values are larger for the softer soil deposits. This is in agreement with the results presented by Merritt and Housner (1954), who found inertial interaction effects to be more pronounced for softer soils.

For the same site and structural model, the coupled analyses result in iterated G values for the C3 soil models that are, in general, slightly lower than those for the corresponding S1 soil models. However, Tables 6.2 and 6.3 indicate that the mean $\bar{T}$ values associated with the S1 soil models are unexpectedly equal to, or larger than the corresponding values for the softer C3 soil models. This is primarily due to the significantly larger iterated λ values associated with the S1 soil models. Although the iterated γ values are quite similar for both soil models, the more pronounced nonlinear behaviour in the case of the S1 soil models, indicated by the shear modulus ratio and λ curves presented in Chapter 2, is the reason for the higher λ values in the case of the S1 soil models.

A comparison of the mean $\bar{T}$ values, listed in Tables 6.2 and 6.3, to the corresponding T values, listed in Tables 5.2 and 5.3, indicates

that inertial interaction effects are more pronounced for the wall structural models. Table 6.2 indicates that, for the frame models, the period shifts (from T to $\tilde{T}$) are within 41 percent of T, with the larger values corresponding to the soft clay soil models. Seed (1986) has shown that frame structures situated on extremely soft soil deposits can experience period shifts, due to the inertial interaction effects, of up to 50 percent of T. On the other hand, for the wall models, Table 6.3 indicates that the period shifts, in some cases corresponding to the softer soil deposits, exceed 100 percent of T. Merritt and Housner (1954) have shown that the period shift, expressed as a ratio of T, is an increasing function of the ratio of soil to building compliancies. For the same soil model, this compliance ratio is larger for the 'stiffer' wall models, as compared to the corresponding frame models. Thus, it is not surprising to observe more significant period shifts in the case of the wall models.

Tables 6.2 and 6.3 indicate that the mean $\tilde{T}$ values associated with the 40 m deposits are equal to, or larger than the mean $\tilde{T}$ values associated with the corresponding 15 m deposits. The coupled analysis results indicate only small differences, in the iterated soil properties, between the 15 m deposits and the uppermost 15 m of the corresponding 40 m deposits, with the 15 m deposits being associated with slightly larger G and slightly lower λ values in the vicinity of the foundation. The differences in the mean $\tilde{T}$ values, associated with the 15 m and the corresponding 40 m soil deposits, are partly attributed to this difference in the iterated soil properties, but are mainly due to the contrast between the flexibility of the soil layers underlying the uppermost 15 m

of the 40 m deposits and the rigidity of the bedrock underlying the corresponding 15 m deposits.

In FLUSH, computations are carried out at a discrete number of frequencies covering the range of 0-f_{max} Hz. These frequencies are equally spaced with a frequency interval (Δf), determined as follows:

$$\Delta f = \frac{1}{T_d} \tag{6.1}$$

Δf = frequency interval for computations (Hz)

T_d = total duration of input time history (sec)

The resulting set of frequencies, used in the computations, correspond to periods that are not equally spaced. In the current study, the spacing between these periods is larger in the range of the computed $\bar{T}$ values than in the range of the computed T_s values. Since A_f are only computed at this discrete number of periods, the small period shifts associated with the input ground motions for Ottawa and the frame structural model, in the case of the stiffer soil models, are masked. This results in $\bar{T}$ values, as listed in Table 6.2 for Ottawa, that are identical to T, erroneously implying no inertial interaction effects at all. This is a minor inconvenience of frequency domain analyses that can only be circumvented by artificially increasing T_d at substantial costs in terms of computation time and computer core requirements. This measure is not considered necessary for the purpose of the current study since only a very small part of the results are affected.

The following discussion of the base shear results is conveniently divided into five sections addressing the five objectives of the current study, outlined in Chapter 1.

6.2 UNCOUPLED BASE SHEAR RATIO RESULTS.

NBCC 90 provisions account for site effects through the incorporation of the foundation factor (F) in the design base shear (V) formula, given by Equations 3.3 and 3.4. F is specified in NBCC 90 as a function of both soil type and depth. The F values, corresponding to the different soil models developed in the current study, are listed in Table 2.1.

The code F values are based on uncoupled analyses of soil-structure systems. According to the NBCC provisions, neglecting soil-structure interaction effects leads to a more conservative design, for most of the buildings addressed in the code. To assess the adequacy of the code F values in accounting for site effects, these are compared to the base shear ratio (BSR) results, based on the uncoupled analyses of the soil-structure systems included in the current study. Uncoupled analyses, by definition, do not account for soil-structure interaction effects, and thus provide a direct measure of the site effects. The mean, M+SD and M-SD values as well as the maxima and minima of the uncoupled BSR results are compared to the respective F values in Figures 6.4 to 6.6 for the frame models, and in Figures 6.7 to 6.9 for the wall models.

For the frame models, Figures 6.4 to 6.6 indicate that the code F values underestimate the amplification potential, measured in terms of the mean BSR values, of all the soil models included in the current study, with the exception of the C140 soil model, in the case of the Prince Rupert frame model. It is important to note that this soil model is associated with the largest code value of F=2. This value of F, associated only with deep soft clay deposits, was introduced in the 1990 edition of

NBCC to replace the previous value of 1.5, and is based on the observed substantial amplification effects in the soft clay deposits of Mexico City during the 1985 Mexican earthquake.

BSR results, for the frame models, also indicate that the site effects generally decrease for the higher intensities of the input ground motions. This is due to a more pronounced nonlinear soil behaviour associated with the larger induced shear strains. The only exceptions to this trend are some cases for which the mean BSR values for Prince Rupert exceed the corresponding mean BSR values for Vancouver. This is due to the fact that T for the Vancouver frame model is more shifted away from T_s, as compared to T for the Prince Rupert frame model. The resulting increase in BSR values, in the case of Prince Rupert, masks the decrease in site effects associated with the higher intensity ground motions. Dobry and Vucetic (1987) carried out uncoupled analyses for clay soil models, developed to represent the extremes of the dynamic properties for normal clay soils. In their study, they used the ground motions recorded in Mexico City during the 1985 earthquake as the input ground motions. Their results have shown that the bedrock motions while being significantly amplified in the case of the clay soil model representing the extreme linear behaviour (i.e. slower degradation of G and slower increase in λ with the increase in γ), were actually deamplified in the case of the clay soil model representing the extreme nonlinear behaviour. Based on their results, they have concluded that the degree of soil nonlinearity plays a significant role in the soil amplification of the bedrock motions.

For many of the cases presented in Figures 6.4 to 6.6, the code F values not only underestimate the mean BSR results, but are even lower

than the computed minima. This is especially true for the stiffer soil deposits, associated with F=1 in NBCC. Results indicate that F=1 underestimates the amplification potential of dense sand deposits. Henderson et al. (1990) have reached a similar conclusion based on uncoupled analyses for a 7 m dense sand deposit located in the United Kingdom. It is apparent that a specified value of F=1, while being appropriate for structures situated directly on bedrock, cannot account for the site effects associated with other soil conditions.

For the wall models, Figures 6.7 to 6.9 indicate that, similar to the results for the frame models, the code F values underestimate the amplification potential of most of the soil models developed in the current study. The relatively large amplifications associated with the S215 and S315 soil models, in the case of the Ottawa wall model, are mainly due to the proximity of T_s and the period of .35 sec, associated with the second mode of vibration for that wall model.

The observation, based on the mean BSR results for the frame models, that site effects decrease for higher intensities of the input ground motions does not hold for the wall models. This is due to the fact that, in the case of the wall models, T is closer to T_s and thus soil-structure resonance effects assume a far more significant role than in the case of the frame models, and practically mask the influence of the degree of soil nonlinearity on site effects. A noticeable example of the significance of the soil-structure resonance effects is observed in Figure 6.9 for the Prince Rupert wall model. This figure indicates that BSR results are significantly larger in the case of the 40 m clay soil deposits than in the case of the 15 m clay soil deposits. According to

Table 6.1, the 40 m clay soil deposits, in the case of Prince Rupert, are associated with mean T_s values in the range of 1.48-1.82 sec. The value of T=1.46 sec, associated with the Prince Rupert wall model, is closer to this range of mean T_s values than the range of mean T_s associated with the 15 m clay soil deposits, namely 0.78-0.99 sec. Another example of the significance of the soil-structure resonance effects is the large BSR values for the C140 soil model (mean T_s=1.55 sec), in the case of the Vancouver wall model (T=1.64 sec). The observed significance of the soil-structure resonance effects, based on the results from the current study, offers strong support to the approach proposed by Elhmadi and Heidebrecht (1991) for defining F as a function of the T/T_s ratio.

Figures 6.7 to 6.9 indicate that, similar to the results for the frame models, F=1 cannot account for the site effects associated with structures that are situated on soil deposits. The wide scatter, in the BSR results, observed in some cases and most notably for the case of the C140 soil deposit and the Vancouver wall model, provides a strong argument in favour of the adopted approach of specifying a set of time histories, rather than a single time history, to represent the input ground motions for a given site.

6.3 UNCOUPLED ANALYSES OF SOIL-STRUCTURE SYSTEMS.

In engineering practice, uncoupled analyses are usually preferred to the more rigorous, but time-consuming coupled analyses. The premise, underlying the current NBCC provisions, that neglecting soil-structure interaction effects leads to a more conservative design seems to support this approach. To assess the reliability of using uncoupled analyses in

aseismic design, it is important to ensure that these do indeed provide a conservative estimate of the base shear demand, based on the more rigorous coupled analyses. For this purpose, the 'uncoupled' base shear coefficient (BSC) results are compared to the corresponding 'coupled' BSC results. For the purpose of this comparison, linear regression analyses, universally preferred to the use of regression curves (Weinberg and Schumaker, 1969), are performed using both sets of results.

The linear regression analyses are performed, separately, for each of the six structural models, included in the current study. The best-fit straight line is assumed to take the form:

$$Y = CX \qquad (6.2)$$

Y = dependent variable

X = independent variable

C = regression coefficient

The coupled BSC results are designated the independent variables, while the uncoupled BSC results are designated the dependent variables. The use of best-fit lines having a zero constant term, as shown in Equation 6.2, provides for a convenient expression of Y as a ratio of X. For each soil-structure system, the BSC results corresponding to the 10 input time histories for a given site are treated as individual data points in the regression analyses.

Regression analysis results, along with the data points, are presented in Figures 6.10 to 6.12, corresponding to the three sites included in the current study. In these figures, the best-fit line is represented by the solid line, with its equation shown alongside. The relation X=Y is represented in these figures by the dashed line. As the

best-fit line approaches this dashed line, the adequacy of using uncoupled analyses, in lieu of the more rigorous coupled analyses, is further established.

In agreement with the assumption underlying the current NBCC provisions, Figures 6.10 to 6.12 indicate that uncoupled analyses, for practically all the cases analyzed in the current study, provide conservative estimates of the coupled base shear demand. Using the best-fit lines to indicate the average trends, the uncoupled analyses, for the frame models, overestimate the coupled base shear demand by 30-45 percent. On the other hand, uncoupled analyses for the wall models, which are associated with more pronounced soil-structure interaction effects, overestimate the coupled base shear demand by 99-164 percent.

As discussed earlier, the inertial interaction effects are expected to be more pronounced for the wall models, as compared to the corresponding frame models developed in the current study. This is also true in the case of the kinematic interaction effects. Kinematic interaction, referring to the integration of the temporal and spatial variations of the ground motion, at the different points of the foundation, into a common average motion, are more significant for the incident seismic waves associated with the shorter wavelengths (i.e. lower periods). As a result, kinematic interaction effects are more pronounced in the response of shorter period structures. For the wall models, associated with shorter fundamental periods than the corresponding frame models, kinematic interaction effects result in a more significant reduction in the base shear demands, as compared to those based on the uncoupled analyses.

According to Figures 6.10 to 6.12, the larger discrepancies, between the coupled and uncoupled BSC results, are associated with the clay soil deposits. This is by virtue of the more pronounced soil-structure interaction effects associated with these softer soil deposits. This trend is less obvious in the case of the Ottawa wall model, due to the aforementioned resonance effects associated with the proximity of T_s, for the 15 m sand soil models, and the period of the second mode of vibration for this wall model. While these resonance effects are pronounced in the uncoupled analysis results, as indicated by Figure 6.7, these diminish in the case of the coupled analysis results due to the period shift associated with the inertial interaction effects, resulting in the large discrepancies associated with these sand soil models, in the case of the Ottawa wall model.

Aside from the significant overestimate of the coupled base shear demand, obtained using the uncoupled analyses, large scatter in the data points is observed in Figures 6.10 to 6.12. In the extreme, uncoupled BSC results, for the frame models, are larger than the corresponding coupled BSC results by as much as a factor of 5. For the wall models, the uncoupled BSC results are larger than the corresponding coupled BSC results by as much as a factor of 11.

6.4 COUPLED BASE SHEAR RESULTS.

Based on the uncoupled BSR results from this study, as well as results from other studies of the NBCC provisions for site effects (Heidebrecht et al., 1990; Henderson et al., 1990; Elhmadi et al., 1990; Hosni and Heidebrecht, 1991; Elhmadi and Heidebrecht; 1991), there appears

to be a need for increasing the code F values. On account of the fact that the coupled BSR results are shown to be, almost always, lower than the corresponding uncoupled BSR results, the code F values may prove adequate if these are compared to the coupled BSR results, for which the soil-structure interaction effects are appropriately considered. In other words, recommendations for increasing the code F values would seem unjustified, if these are shown to adequately account for the combined influence of site effects and soil-structure interaction. For this purpose, the coupled BSR results are compared to the respective F values in Figures 6.13 to 6.15 for the frame models, and in Figures 6.16 to 6.18 for the wall models.

The mean coupled BSR results, shown in Figures 6.13 to 6.18, are found to be consistently lower than the corresponding uncoupled BSR results, shown in Figures 6.4 to 6.9. This is expected to be generally true for long period structures as those included in the current study. This is mainly due to the period shift away from T_s, associated with the inertial interaction effects, and to a lesser degree due to the reduction in structural response associated with the kinematic interaction effects, which are expected to be more pronounced for short period structures. The coupled BSR results are associated with a larger scatter about the mean, measured in terms of the COV, than the corresponding uncoupled BSR values. While the coupled BSR results are associated with COV values in the range of 17-36 percent, the uncoupled BSR results are associated with COV values in the range of 6-32 percent. This is mainly due to the additional variability introduced to the computations, when the soil-structure interaction effects are accounted for in the coupled analyses.

The mean coupled BSR results for the frame models, although lower than the corresponding mean uncoupled BSR results, still exceed the code F values for the stiffer soil deposits. This is due to the fact that soil-structure interaction effects are less significant for stiff soil deposits, resulting in coupled BSR results that approach the corresponding values based on the uncoupled analyses. The inertial interaction effects are less pronounced, for stiff soil deposits, as indicated by the smaller period shifts. The kinematic interaction effects are also less pronounced for stiff soil deposits as these soil deposits are associated with larger iterated G values, and consequently larger shear wave velocities (v_s). Since these larger v_s values result in longer wavelengths of the shear body-waves, the kinematic interaction effects become less pronounced.

Based on the coupled BSR results for the frame models, it appears that the approach, adopted in NBCC, of assigning a value of F=1 to stiff soil deposits is not appropriate. In the case of the frame models, the code F values appear adequate for the soft clay (C1) and loose sand (S1) models. However, in the case of the wall models, the code F values appear to be reasonably adequate for all the soil models, as a result of the more significant interaction effects. In fact, the coupled BSR results for the wall models, in many cases, indicate a deamplification, rather than an amplification, of the base shear demand associated with the bedrock motions, as indicated by BSR values lower than 1. For all the structural models, the F=2 value, introduced in NBCC 90 for deep soft clay soils, appears to be too conservative when the soil-structure interaction effects are taken into consideration.

In spite of the significant scatter associated with the computed

BSR results, it is quite reasonable to evaluate F on the basis of the mean BSR values. In fact, associating F with a higher probability level would imply a higher level of protection for structures situated on soil deposits as compared to identical structures situated directly on bedrock, which is inconsistent with the primary code objective of establishing uniform standards for building safety throughout Canada.

The fact that the coupled BSR results are shown to exceed the code F values, in some cases, casts a doubt on the level of protection provided, in NBCC 90, for the structures included in the current study. A proper evaluation of this level of protection should be based on the computed BSC results. For this purpose, the M+SD coupled base shear results are compared to the corresponding NBCC 90 design base shear in Figures 6.19 to 6.21, for the three sites included in the current study. M+SD results are chosen for comparison to the code design base shear because this probability level is customarily accepted in engineering practice as the design probability level (Newmark et al., 1973). In fact, evaluation of the NBCC provisions for design base shear is customarily carried out at this probability level (Heidebrecht and Lu, 1988).

The NBCC 90 design base shear (V_e), corresponding to elastic response, is used in this comparison because, as outlined earlier, FLUSH does not allow for modelling of the hysteretic energy dissipation in the superstructure. As a result, any reduction in V_e, for the purpose of this comparison, would be both misleading and unrealistic. The M+SD coupled BSC results are shown, in Figures 6.19 to 6.21, corresponding to the fundamental periods (T) for the different structural models, as listed in Tables 5.2 and 5.3.

Figures 6.19 to 6.21 indicate that the NBCC 90 design base shear provisions are quite conservative for 20-storey frame and wall structures, situated at the three sites included in the current study. This is true even in the cases associated with coupled BSR results exceeding the code F values due to two main reasons. First, the NBCC 90 design base shear for these structures, if assumed to be situated directly on the bedrock, is higher than that based on the input ground motions developed in the current study. This is evident when comparing the M+SD BSC results for both the frame and wall models, assumed to be directly situated on bedrock, to the code BSC curve for F=1. Second, the reduction in base shear demand, associated with the soil-structure interaction effects, is not taken into consideration in the code provisions. Since the NBCC 90 design base shear provisions are shown to be conservative for frame and wall structures, which are expected to represent the extremes of the dynamic response of regular multi-storey buildings (Fenves and Newmark, 1969; Heidebrecht and Stafford Smith, 1973; Fajfar and Strojnik, 1980), NBCC 90 design base shear provisions are considered to be conservative for regular 20-storey reinforced concrete buildings, situated at the three sites included in this study.

While the NBCC 90 provisions appear to provide a good level of protection for regular 20-storey reinforced concrete structures, the large discrepancies between the code design base shear and the computed M+SD coupled base shear demand, especially for the cases involving significant interaction effects, need to be reduced through incorporation of some measure to account for the soil-structure interaction effects in the code provisions.

6.5 A MODIFIED APPROACH TO UNCOUPLED ANALYSES.

Seed (1986) has proposed an approach to account for inertial interaction effects in uncoupled analyses of soil-structure systems. He has shown that if the system period $\bar{T}$, rather than the structural period T, were used in the uncoupled analyses, the resulting base shear demand would more closely resemble that based on the more rigorous coupled analyses. Since the 'flexibly supported' structural model, in the coupled analyses, actually responds at a fundamental period of $\bar{T}$, the proposed approach appears to be quite sound. Uncoupled analyses carried out in accordance with this proposed approach are, henceforth, referred to as the 'modified' uncoupled analyses to distinguish these from the 'conventional' uncoupled analyses, discussed earlier. To evaluate the proposed approach, modified uncoupled analyses are performed to compute the uncoupled base shear coefficients (BSC_S), for the different soil-structure systems in the current study. These results are then compared to the corresponding BSC results based on the more rigorous coupled analyses.

To simulate $\bar{T}$ in the modified uncoupled analyses, simplified models of the structure need to be used. For the purpose of the current study, simple uniform shear beam and uniform flexural cantilever continuum models are used to model the flexibly supported frame and wall structures respectively. The validity of these simple linear models in representing frame and wall structures has been verified by Heidebrecht and Stafford Smith (1973). In view of the significance of the higher mode effects for long period structures, the first five modes of vibration, for these simple models, are incorporated in the computations. In the modified uncoupled analyses, the free field ground motions are used as the input

motions for the simple uniform models. The dynamic properties of these models, as well as the approach used to compute the corresponding base shear demands, are described in Lu (1984).

Linear regression analyses are performed, using the uncoupled BSC_S results and the corresponding coupled BSC results. The coupled BSC results are designated the independent variables, while the uncoupled BSC_S results are designated the dependent variables. The regression analysis results, along with the data points, are presented in Figures 6.22 to 6.24, corresponding to the three sites included in the current study. The best-fit line and the X=Y relation are shown in each of these figures, in a similar manner to that used in presenting Figures 6.10 to 6.12.

Figures 6.22 to 6.24 indicate a significant improvement in the prediction of the coupled base shear demand, when using the modified, rather than the conventional, uncoupled analyses. As indicated by the best-fit lines, the discrepancies between the uncoupled and coupled base shear coefficient results, for the frame models, reduce from 30-45 percent, when using the conventional uncoupled analyses, to 1-13 percent, when using the modified uncoupled analyses. Similarly, the discrepancies, for the wall models, reduce from 99-164 percent to 55-91 percent, when the modified uncoupled analyses are adopted. The large discrepancies that still exist in the case of the wall models, and that are mainly associated with the kinematic interaction effects, cannot be avoided since there is no simple approach to account for these effects in uncoupled analyses. These discrepancies may also be due to the additional soil damping in the vicinity of the foundation, and which is not accounted for in uncoupled analyses.

An important observation, based on Figures 6.22 to 6.24, is the significant reduction of scatter in the results as compared to the corresponding results based on the conventional uncoupled analyses, shown in Figures 6.10 to 6.12. To appreciate the significance of this reduction in scatter, one needs only recall the fact that the conventional uncoupled analyses can predict a base shear demand that is as much as 11 times larger than the respective coupled base shear demand. Figures 6.22 to 6.24 indicate that, for the frame models, the modified uncoupled analyses can sometimes significantly underpredict the coupled base shear demand. There are three possible reasons for this. First, the assumption that the dynamic properties, namely the period ratios and modal weights, characterizing the simple uniform shear beam and flexural cantilever models, are valid for the flexibly supported frame and wall structures respectively. Second, the fact that uncoupled analyses, whether conventional or modified, cannot be expected to reproduce all aspects of the complex seismic response of coupled soil-structure systems. Third, the approximations in the computed $\tilde{T}$ values due to frequency discretization in FLUSH. In spite of this observation, one must realize that all the data points, in the case of the frame models, fall within a relatively narrow band, not only about the best-fit lines, but also about the 'optimum' X=Y relation.

In recognition of the stochastic nature of earthquake ground motions, it is customary engineering practice to use a set of time histories, rather than a single time history, to represent the postulated design motions. The cases for which the modified uncoupled analyses, according to Figures 6.22 to 6.24, significantly underpredict the coupled

base shear demand, for the frame models, are expected to assume a less significant role once this practice is adhered to.

According to the results presented herein, the modified uncoupled analyses do provide a closer estimate of the coupled BSC results. In addition, the significant reduction of the scatter in the predictions affirms the reliability of the modified uncoupled analyses as a simple, yet consistent, tool to account for the combined influence of site effects and inertial interaction effects in the aseismic design of structures underlain by soil deposits.

6.6 A SIMPLIFIED APPROACH TO ESTIMATE $\bar{T}$.

The applicability of the modified uncoupled analyses, in engineering practice, is hampered by the lack of a simple means to estimate $\bar{T}$ without resorting to the time-consuming coupled analyses. The Applied Technology Council (1978) provides a simplified expression to estimate $\bar{T}$, based on the knowledge of some properties of the structure, its foundation and the underlying soil deposit. This expression is based on the work of Veletsos and Nair (1975), who carried out extensive coupled analyses for linear, viscously damped sdof systems supported at the surface of a nonlinear viscoelastic half space. This expression, for providing an estimate of $\bar{T}$, takes the form:

$$\bar{T} = T\sqrt{1 + \frac{K}{K_y}\left(1 + \frac{K_y h^2}{K_\theta}\right)} \qquad (6.3)$$

K = lateral stiffness of the structural model (kN/m)

K_y = lateral stiffness of the foundation (kN/m)

K_θ = rocking stiffness of the foundation (kN.m/rad.)

h = effective height of the structural model (m)

= 0.7H for regular buildings

Though based on analyses of simplified soil-structure models, Equation 6.3 was shown to provide close estimates of $\bar{T}$, computed using rigorous coupled analyses, for a 22-storey reinforced concrete building situated on a deep and relatively uniform soil deposit (Wallace and Moehle, 1990). The input ground motions, in that case, were those recorded during the surface-wave magnitude 7.8 Chile earthquake of March 1985. In the current study, Equation 6.3 is evaluated by comparing its predictions to the computed $\bar{T}$ values based on the coupled analyses, for a selected set of soil-structure systems.

Simple expressions are provided by the Applied Technology Council (1978) to compute K, K_y and K_θ for use in Equation 6.3. K_y and K_θ represent the resistance of the surrounding soil to the foundation motions, and are derived using an average G value for the soil deposit. This average G value should correspond to the soil response expected to develop during the postulated seismic ground motions. In the derivation of K_y and K_θ, allowance is made for the foundation embedment in the soil, and which is associated with an increased lateral and rocking stiffness of the foundation. For the purpose of the current study, the average G values, used to derive K_y and K_θ, are determined using the iterated soil properties from the free field analyses.

Based on the mean $\bar{T}$ values, listed in Tables 6.2 and 6.3, the C140 soil model is associated with the largest period shifts for both the frame and wall models. Consequently, the evaluation of Equation 6.3 is based on

its ability to provide reasonable estimates of $\bar{T}$ for this soil model, and corresponding to both the frame and wall structural models. Equation 6.3 is used to provide estimates of $\bar{T}$ associated with Prince Rupert since this site corresponds to the largest period shifts for that soil model. Estimates of $\bar{T}$ are made corresponding to the different time histories of the Prince Rupert input ground motion data set.

Based on statistical analyses of the results, the mean $\bar{T}$ values and the associated COV are listed in Table 6.4, along with the corresponding values from the coupled analyses of the respective soil-structure systems. Whether based on Equation 6.3 or coupled analyses, there is no appreciable difference in scatter of the computed $\bar{T}$ values about the mean, measured in terms of the COV. According to the mean $\bar{T}$ values listed in Table 6.4, Equation 6.3 accounts for about 80 percent of the period shifts associated with the respective coupled analyses. This is a quite satisfactory approximation, given the simplifications involved in the development of this equation. Since the derivation of $\bar{T}$ using Equation 6.3 is based on the iterated soil properties from the free field analyses, rather than the coupled analyses, errors of this magnitude, in the estimate of $\bar{T}$, are not surprising and should be expected. This is especially true for higher intensity input ground motions due to the larger discrepancies, in the shear strain distribution and consequently the iterated G values, between free field and coupled analyses.

Based on the results from the current study, it appears that the modified uncoupled analyses, when used in conjunction with Equation 6.3, provide a viable alternative to the use of the time-consuming coupled analyses in aseismic design. Even within the framework of the equivalent

static load approach, used to specify the design base shear in NBCC 90, there is still room for implementation of Equation 6.3. The estimated $\bar{T}$ value, rather than T, can be used to derive the design base shear. This is expected to reduce the large discrepancies, observed in Figures 6.19 to 6.21, between the computed M+SD coupled base shear demand and the corresponding NBCC 90 design base shear, and which are attributed to the current lack of provisions, in NBCC 90, to account for the soil-structure interaction effects. A similar approach is proposed by the Applied Technology Council (1978), with a maximum allowable reduction of 30 percent in the design base shear when $\bar{T}$, rather than T, is used. Since the NBCC 90 design base shear is a non-increasing function of the fundamental period of the structure, implementation of Equation 6.3 will be invariably associated with a reduction in the design base shear for long period structures. This is in agreement with the results from the current study, and which show that the soil-structure interaction effects are, almost always, associated with a reduction in the base shear demand for high-rise buildings. However, it must be noted that if Equation 6.3 is to be used to account for the inertial interaction effects in the specification of the NBCC 90 design base shear, the code F values need to be increased to adequately account for the significant site effects observed in the current study.

Table 6.1 Mean natural periods for the soil models

Soil model	T_s (sec)			
	Low strain	Ottawa	Vancouver	Prince Rupert
Sand soil				
S115	0.32	0.46	0.59	0.62
S140	0.65	0.94	1.17	1.31
S215	0.26	0.40	0.52	0.53
S240	0.54	0.83	1.03	1.13
S315	0.22	0.36	0.46	0.46
S340	0.46	0.73	0.91	1.00
Clay soil				
C115	0.52	0.73	0.91	0.99
C140	1.00	1.30	1.55	1.82
C215	0.41	0.59	0.77	0.91
C240	0.81	1.09	1.40	1.68
C315	0.38	0.52	0.69	0.78
C340	0.75	1.00	1.27	1.48

Table 6.2 Mean fundamental periods for the frame soil-structure models

Soil model	$\bar{T}$ (sec)		
	Ottawa	Vancouver	Prince Rupert
Sand soil			
S115	4.55	4.06	3.40
S140	5.12	4.06	3.52
S215	4.55	3.95	3.23
S240	4.55	3.95	3.27
S315	4.55	3.53	3.14
S340	4.55	3.67	3.16
Clay soil			
C115	5.12	4.23	3.83
C140	5.12	4.28	4.12
C215	4.55	4.10	3.53
C240	5.12	4.10	3.71
C315	4.55	3.98	3.36
C340	4.66	3.98	3.46

Table 6.3 Mean fundamental periods for the wall soil-structure models

Soil model	$\bar{T}$ (sec)		
	Ottawa	Vancouver	Prince Rupert
Sand soil			
S115	2.73	2.90	2.59
S140	2.87	2.90	2.75
S215	2.52	2.53	2.22
S240	2.56	2.53	2.35
S315	2.37	2.29	2.05
S340	2.41	2.35	2.15
Clay soil			
C115	3.41	3.41	3.18
C140	3.60	3.92	3.65
C215	2.85	2.93	2.80
C240	2.93	3.05	3.07
C315	2.56	2.68	2.44
C340	2.70	2.83	2.69

Table 6.4 Mean fundamental periods for the Prince Rupert structural models underlain by the C140 soil model

Structural model	$\bar{T}$ (FLUSH)		$\bar{T}$ (ATC 3-06)	
	MEAN	COV	MEAN	COV
Frame	4.12	3.7	3.90	3.1
Wall	3.65	4.4	3.12	5.5

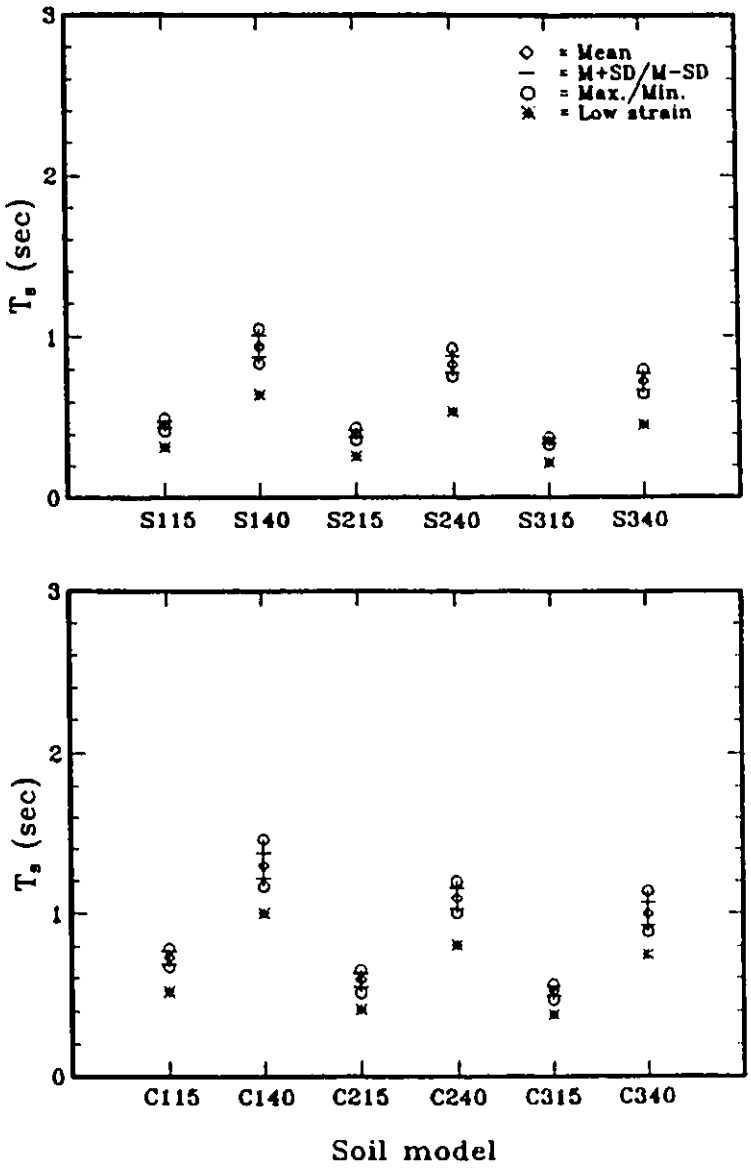

Figure 6.1 Natural periods for the soil models subjected to the input ground motions for Ottawa

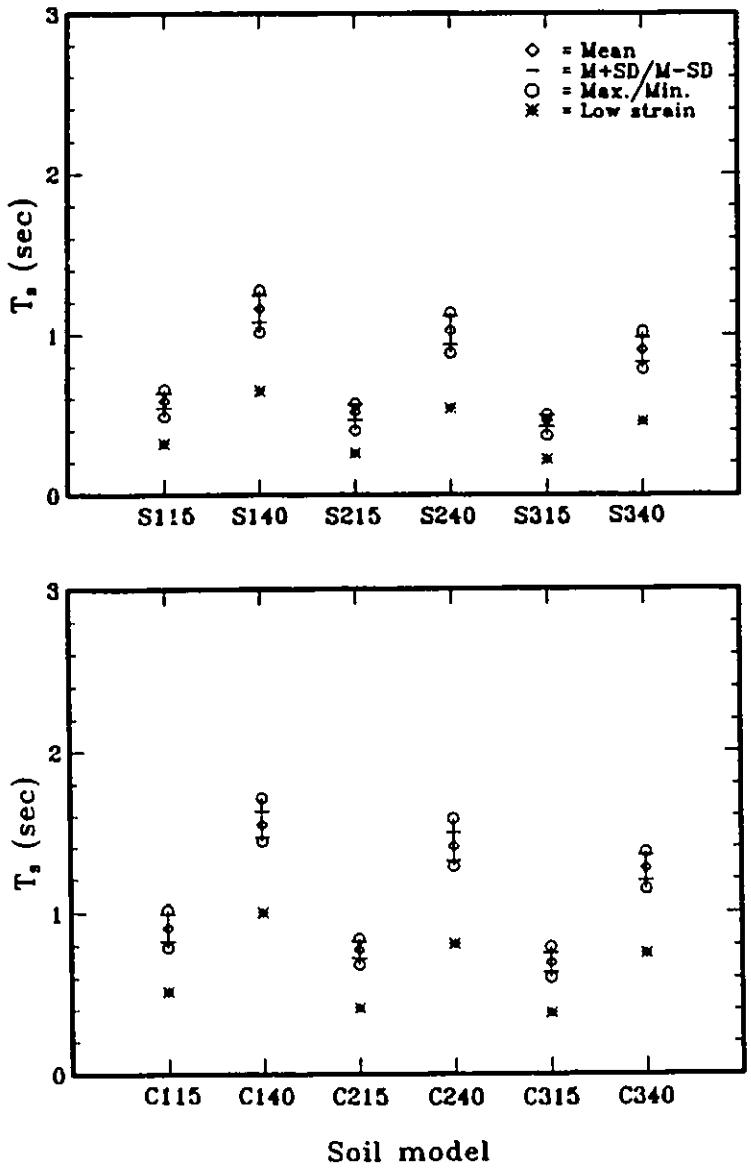

Figure 6.2 Natural periods for the soil models subjected to the input ground motions for Vancouver

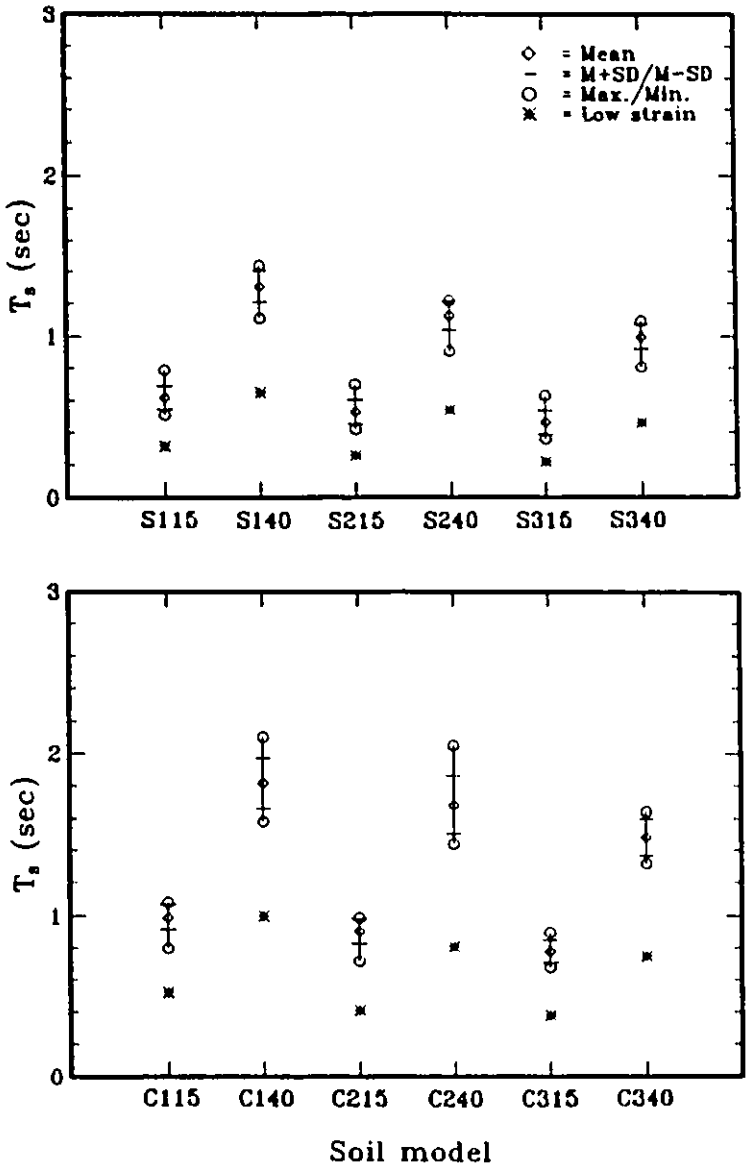

Figure 6.3 Natural periods for the soil models subjected to the input ground motions for Prince Rupert

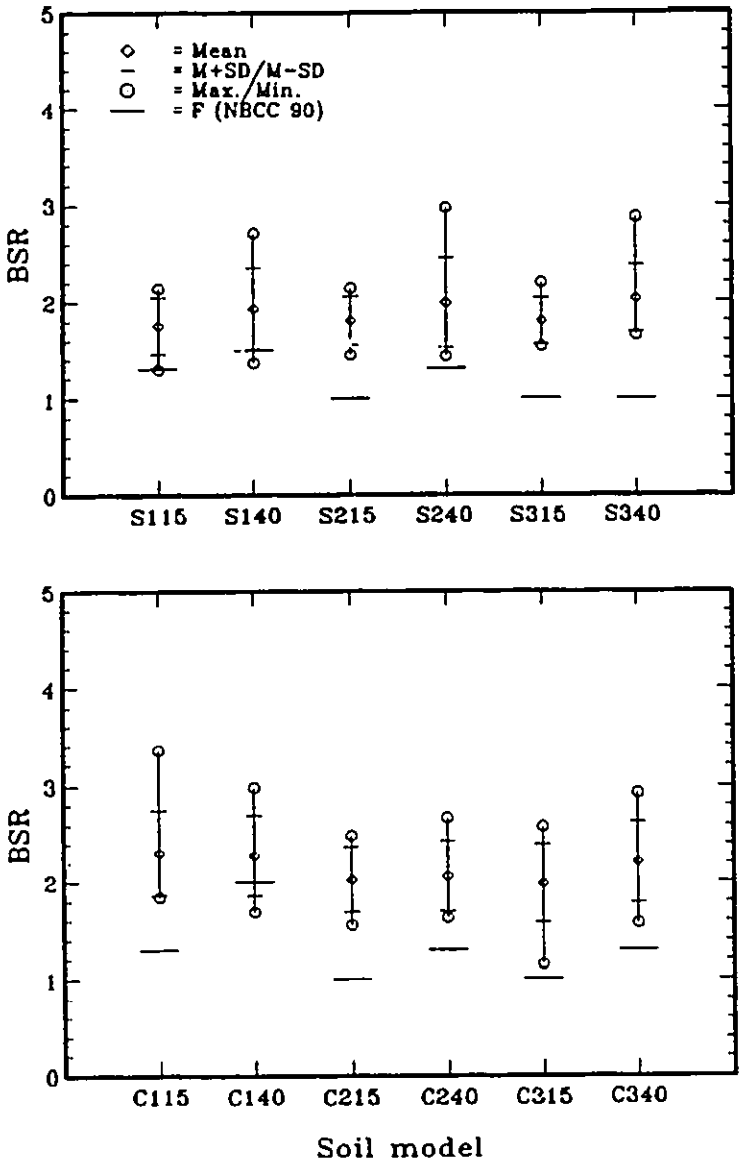

Figure 6.4 Uncoupled base shear ratio results for the Ottawa frame model

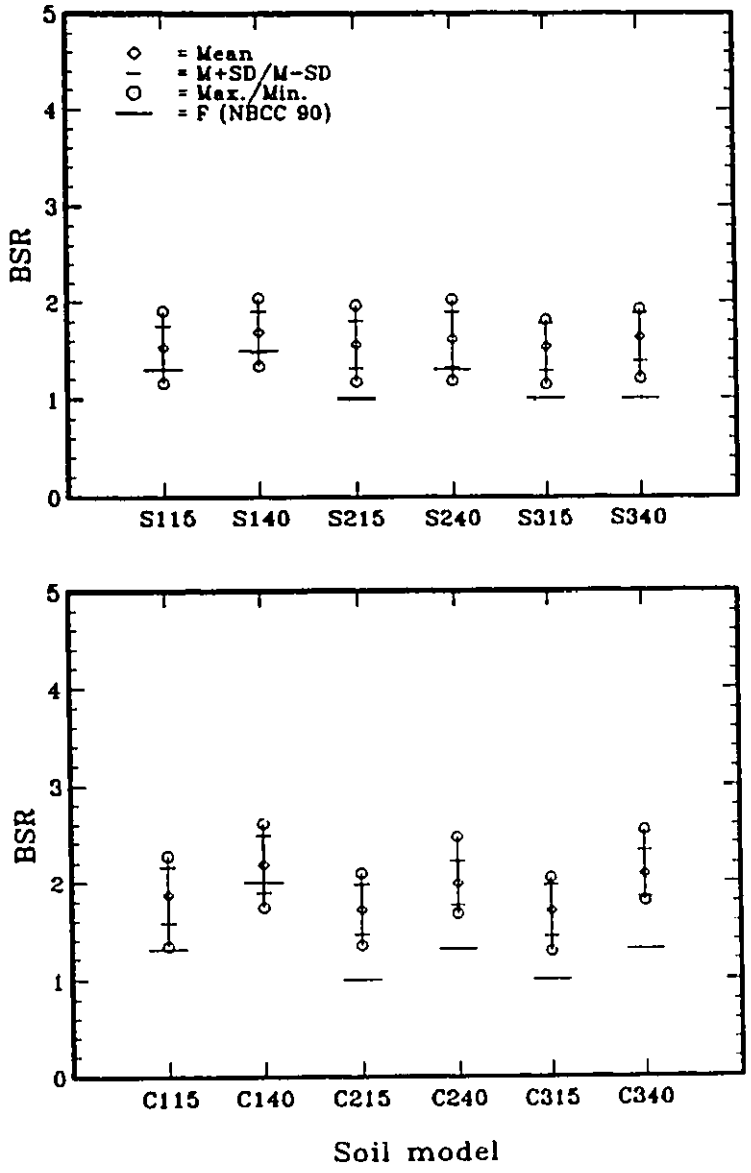

Figure 6.5 Uncoupled base shear ratio results for the Vancouver frame model

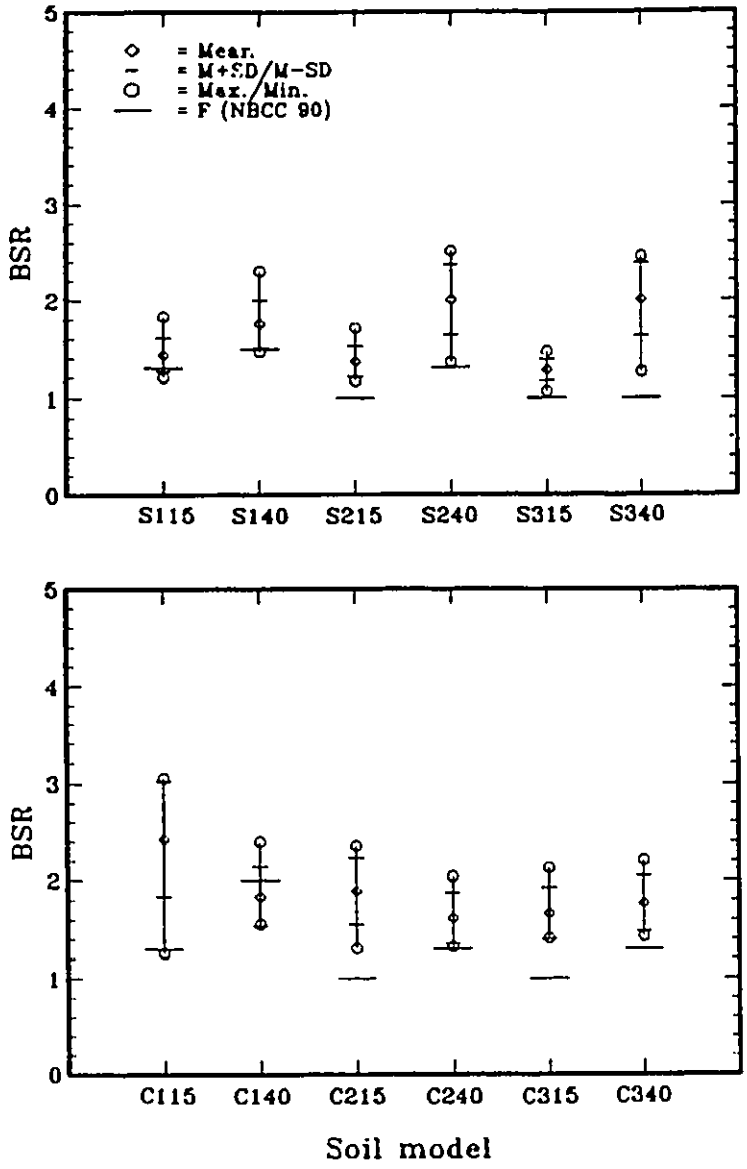

Figure 6.6 Uncoupled base shear ratio results for the Prince Rupert frame model

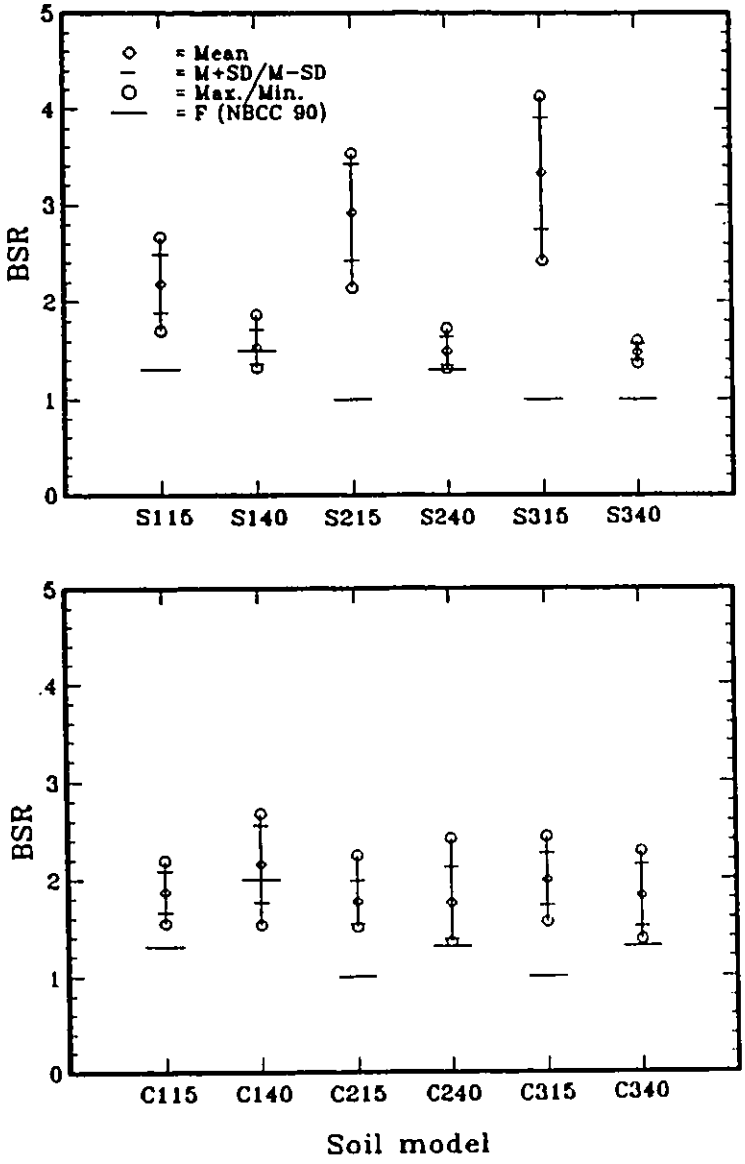

Figure 6.7 Uncoupled base shear ratio results for the Ottawa wall model

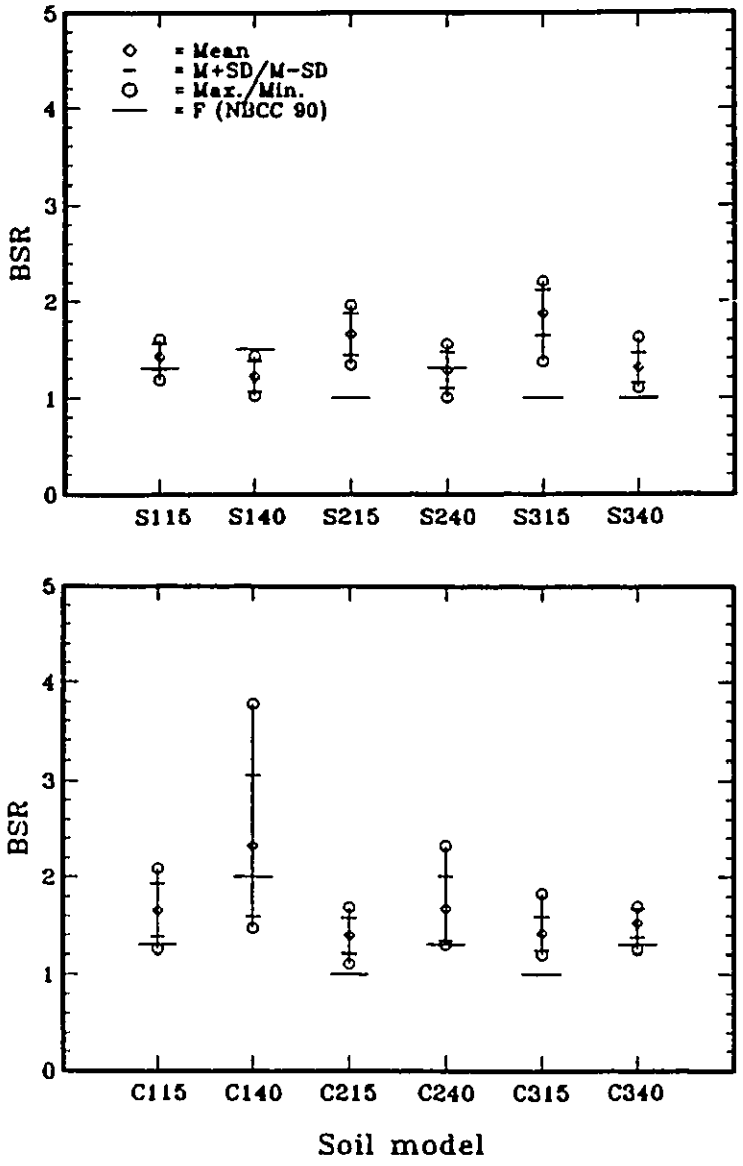

Figure 6.8 Uncoupled base shear ratio results for the Vancouver wall model

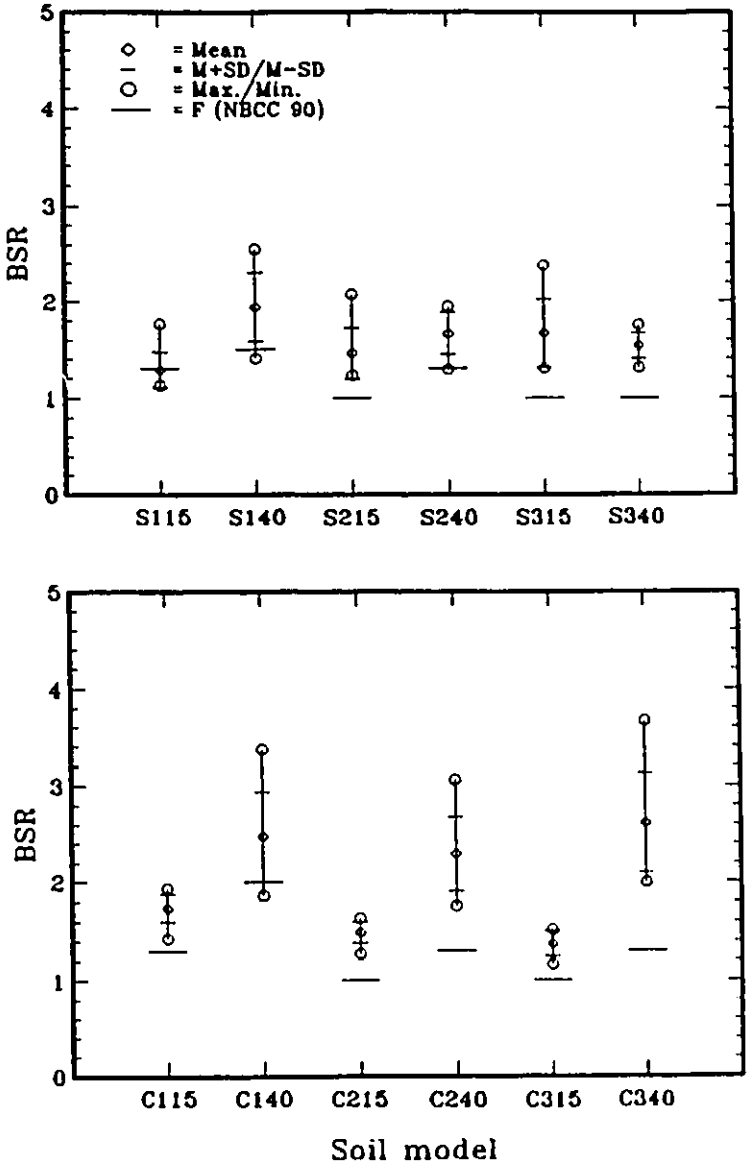

Figure 6.9 Uncoupled base shear ratio results for the Prince Rupert wall model

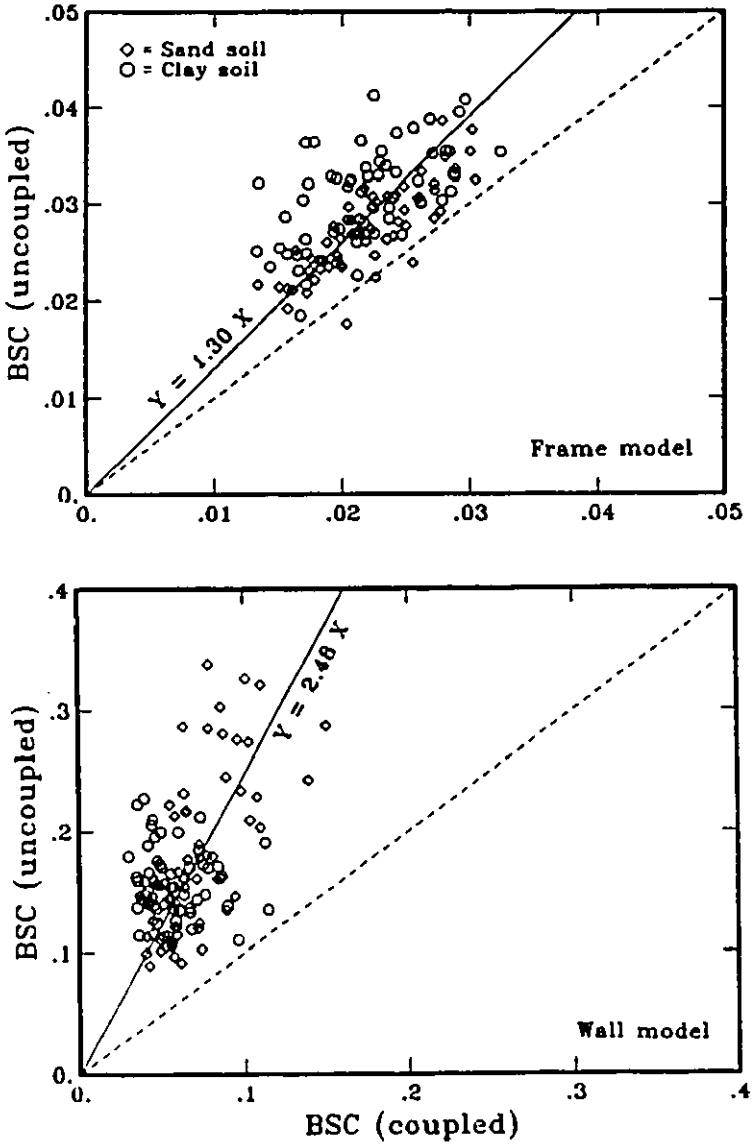

Figure 6.10 Regression analyses based on the base shear coefficient results for Ottawa

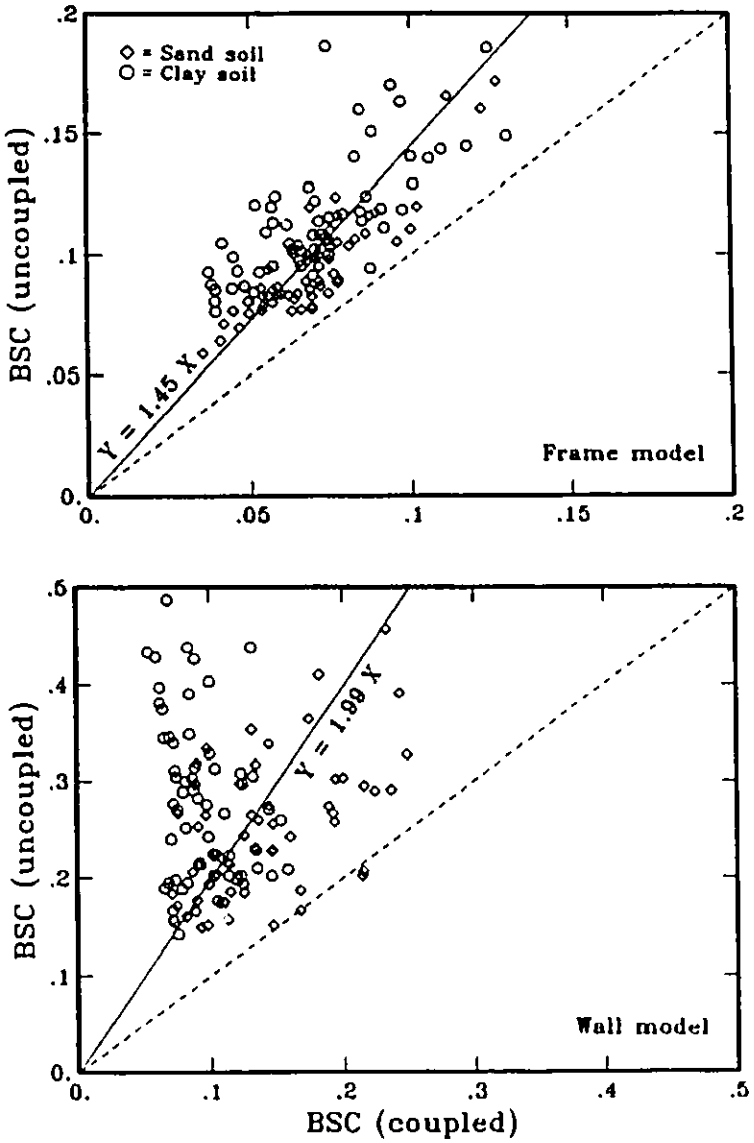

Figure 6.11 Regression analyses based on the base shear coefficient results for Vancouver

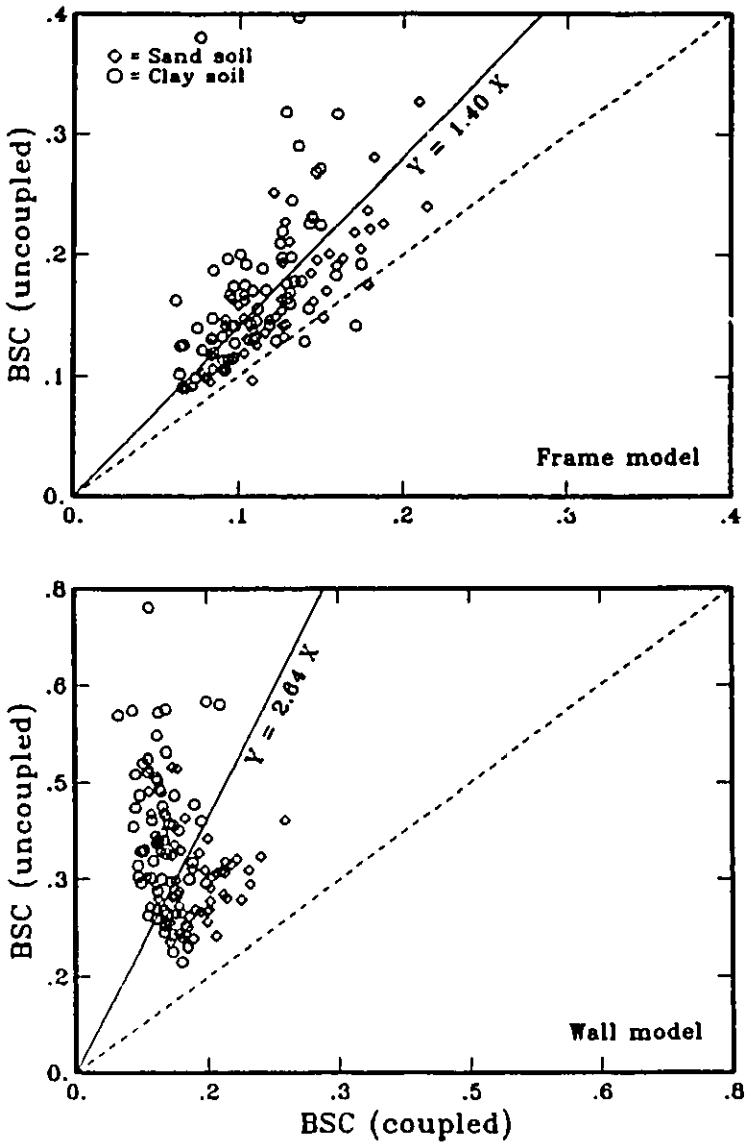

Figure 6.12 Regression analyses based on the base shear coefficient results for Prince Rupert

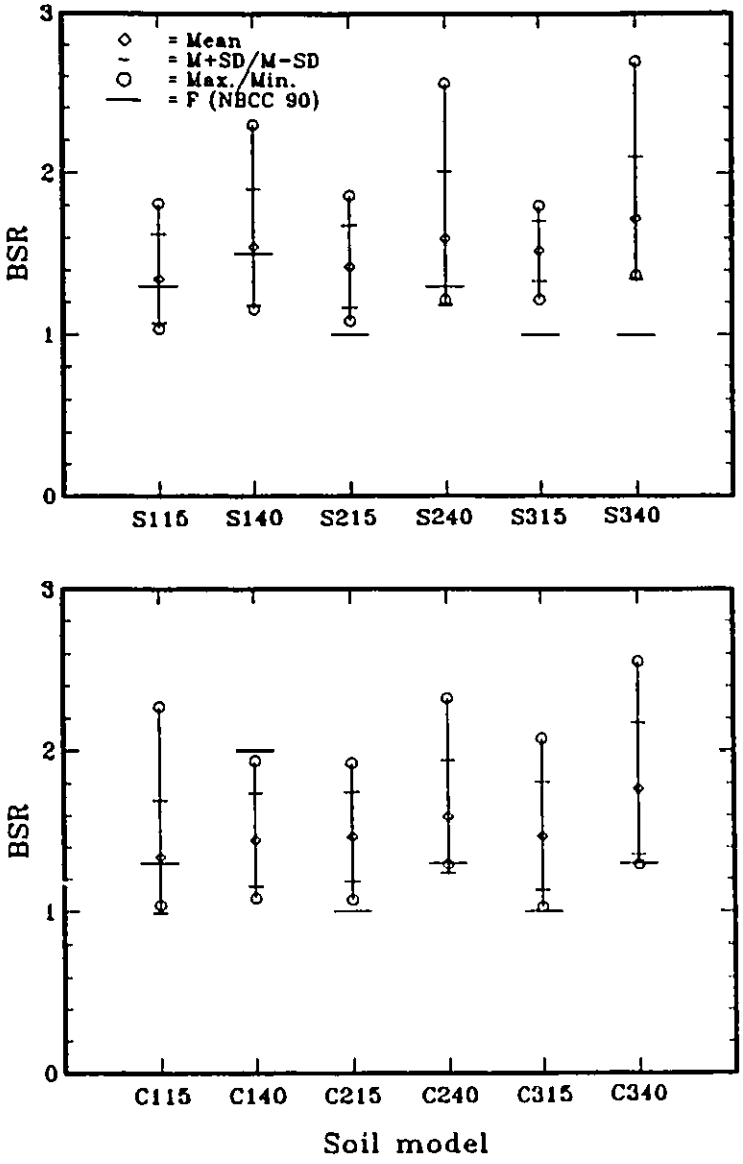

Figure 6.13 Coupled base shear ratio results for the Ottawa frame model

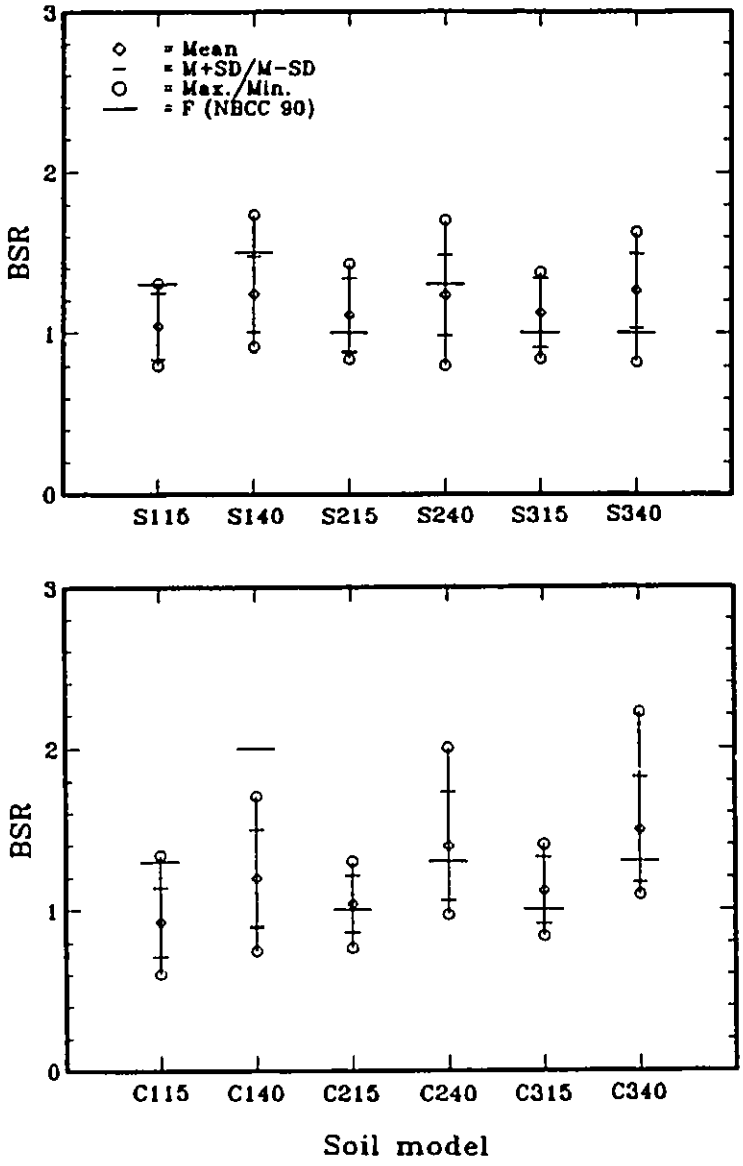

Figure 6.14 Coupled base shear ratio results for the Vancouver frame model

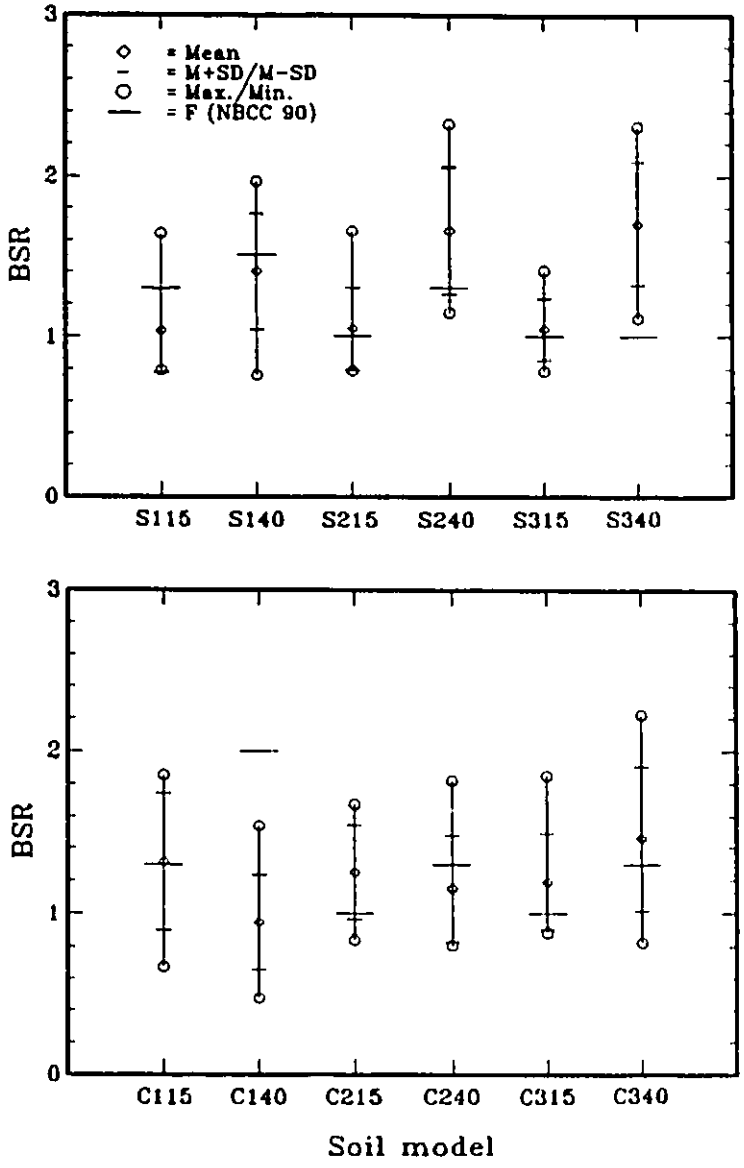

Figure 6.15 Coupled base shear ratio results for the Prince Rupert frame model

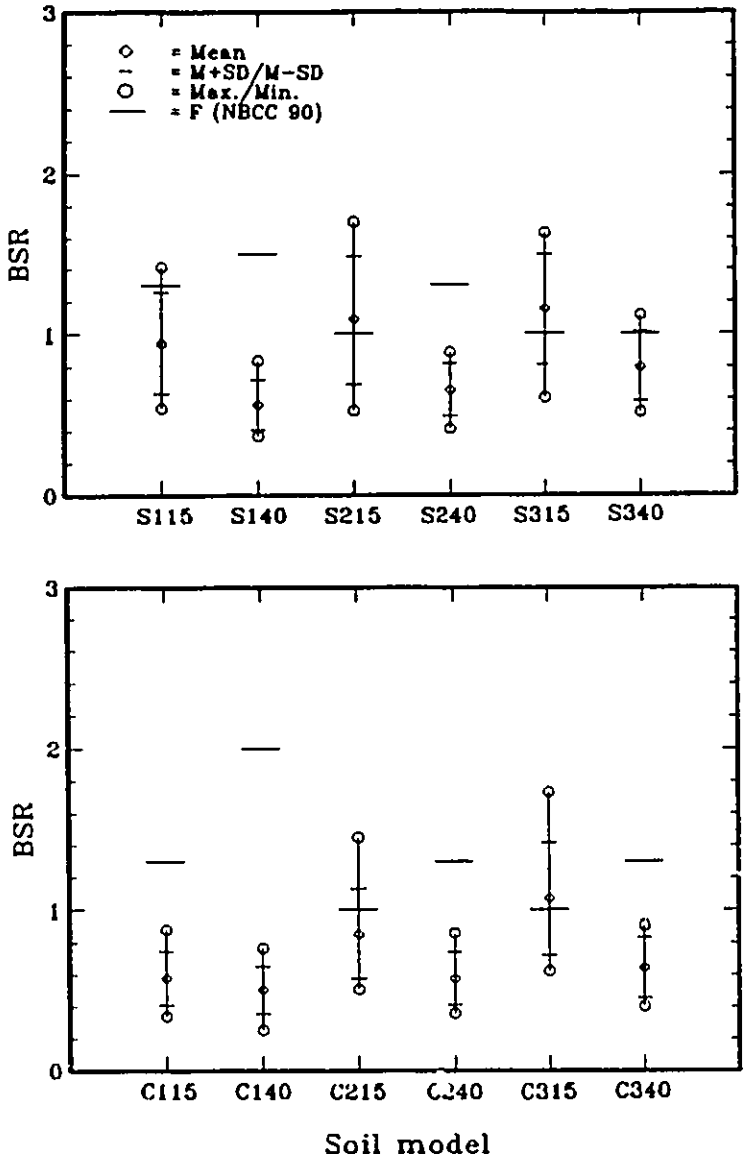

Figure 6.16 Coupled base shear ratio results for the Ottawa wall model

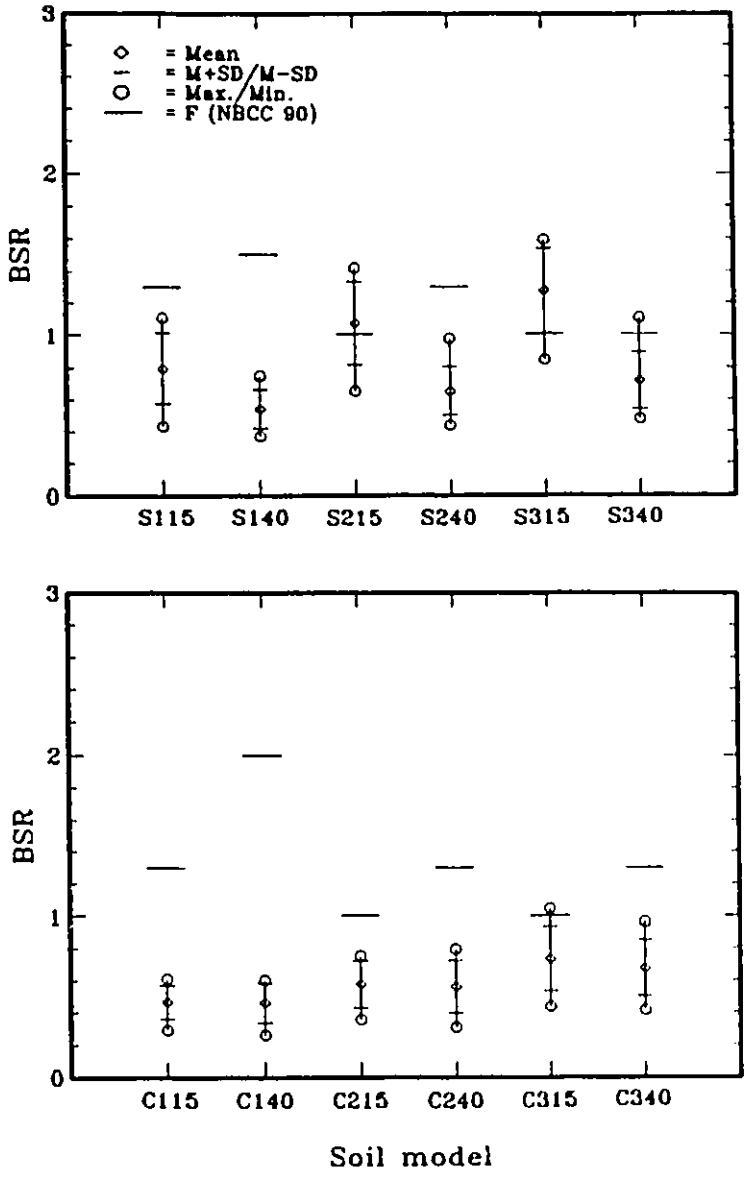

Figure 6.17 Coupled base shear ratio results for the Vancouver wall model

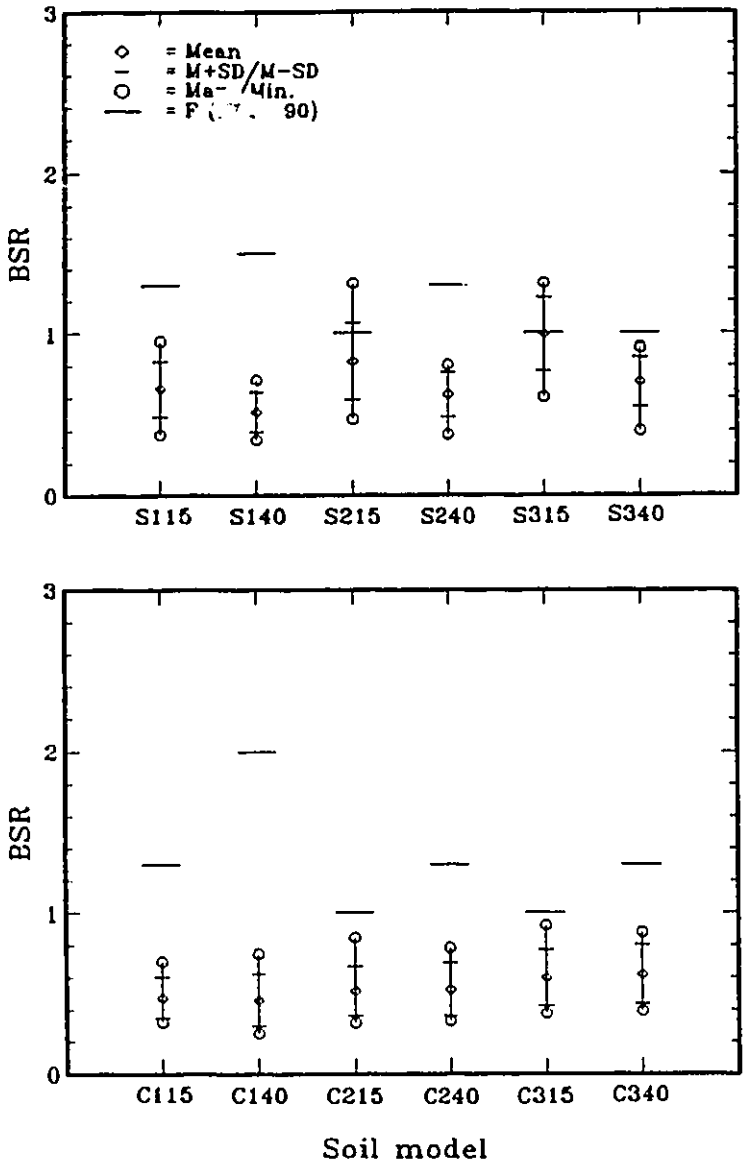

Figure 6.18 Coupled base shear ratio results for the Prince Rupert wall model

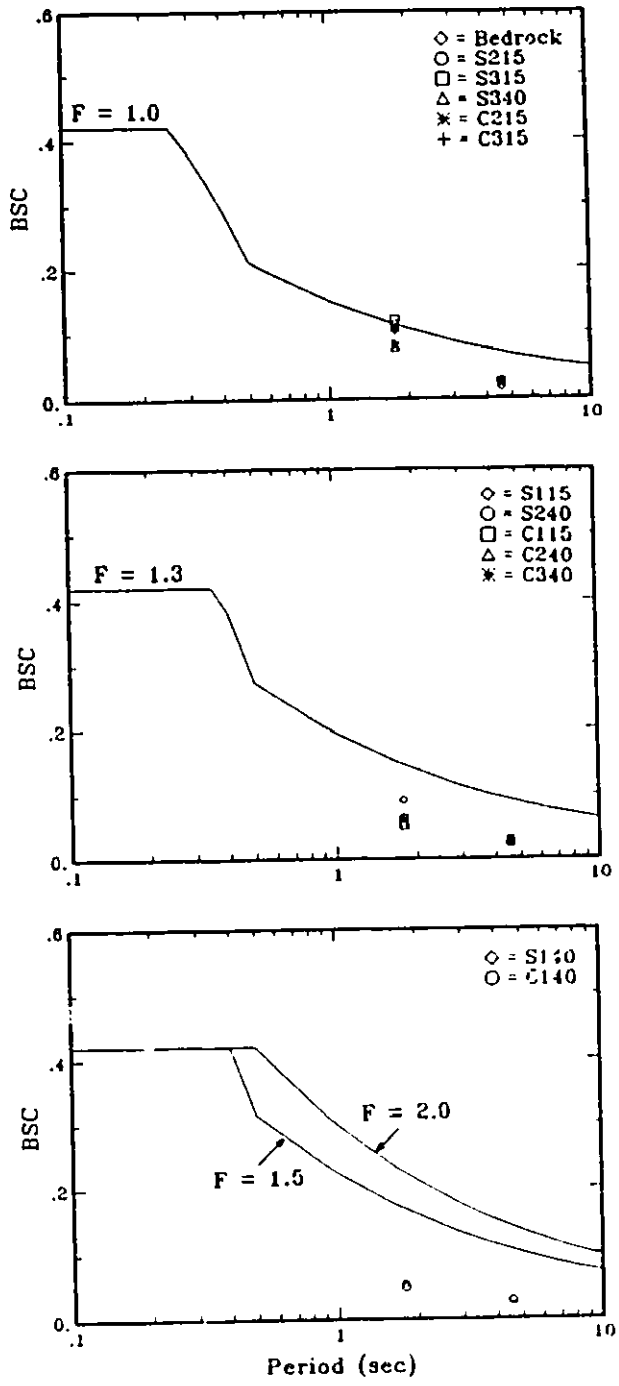

Figure 6.19 M+SD base shear coefficient results for Ottawa

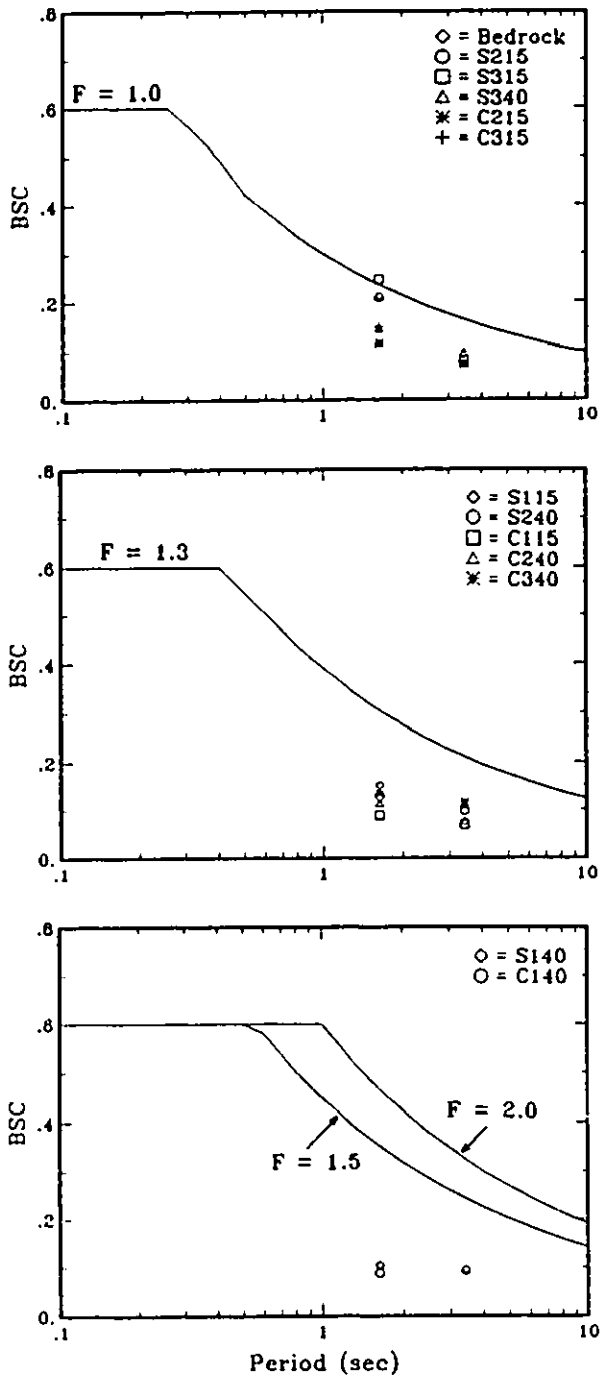

Figure 6.20 M+SD base shear coefficient results for Vancouver

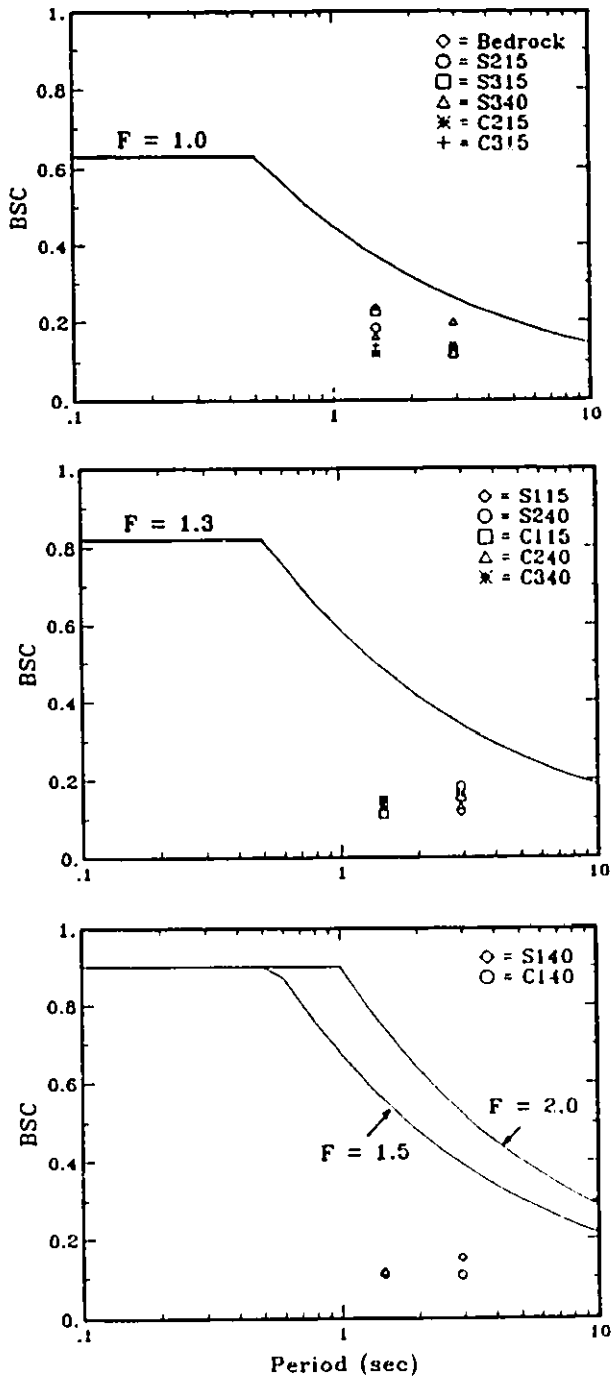

Figure 6.21 M+SD base shear coefficient results for Prince Rupert

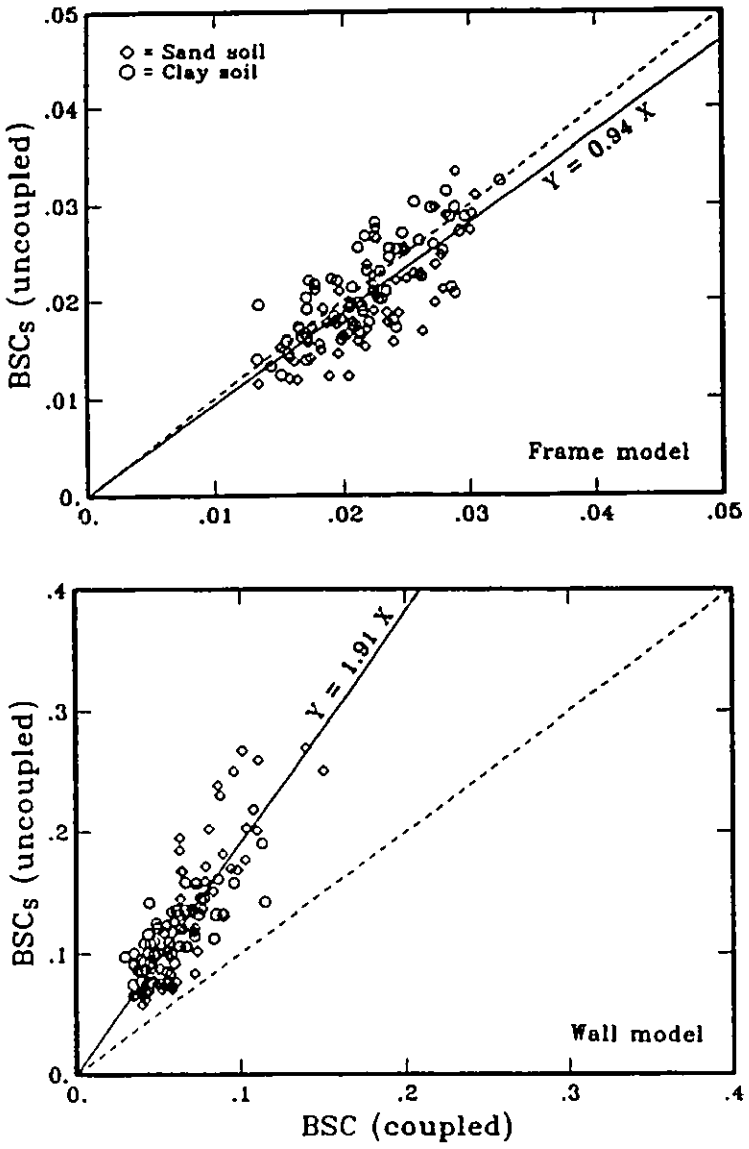

Figure 6.22 Regression analyses based on the modified uncoupled analysis results for Ottawa

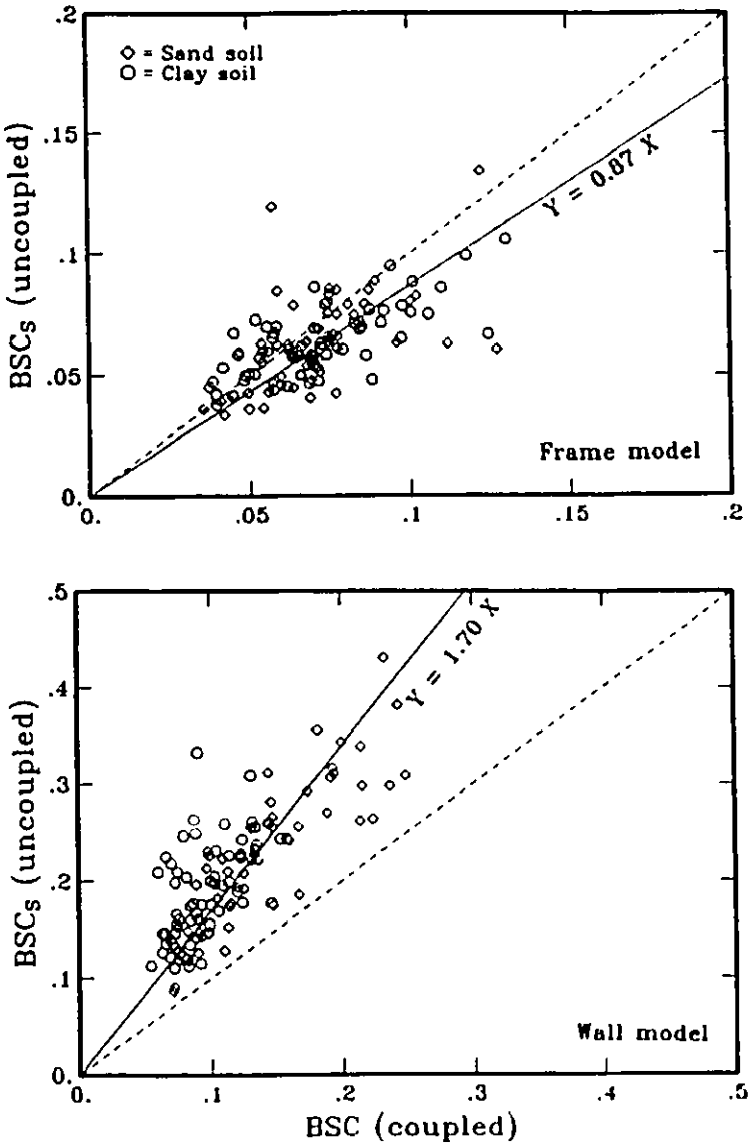

Figure 6.23 Regression analyses based on the modified uncoupled analysis results for Vancouver

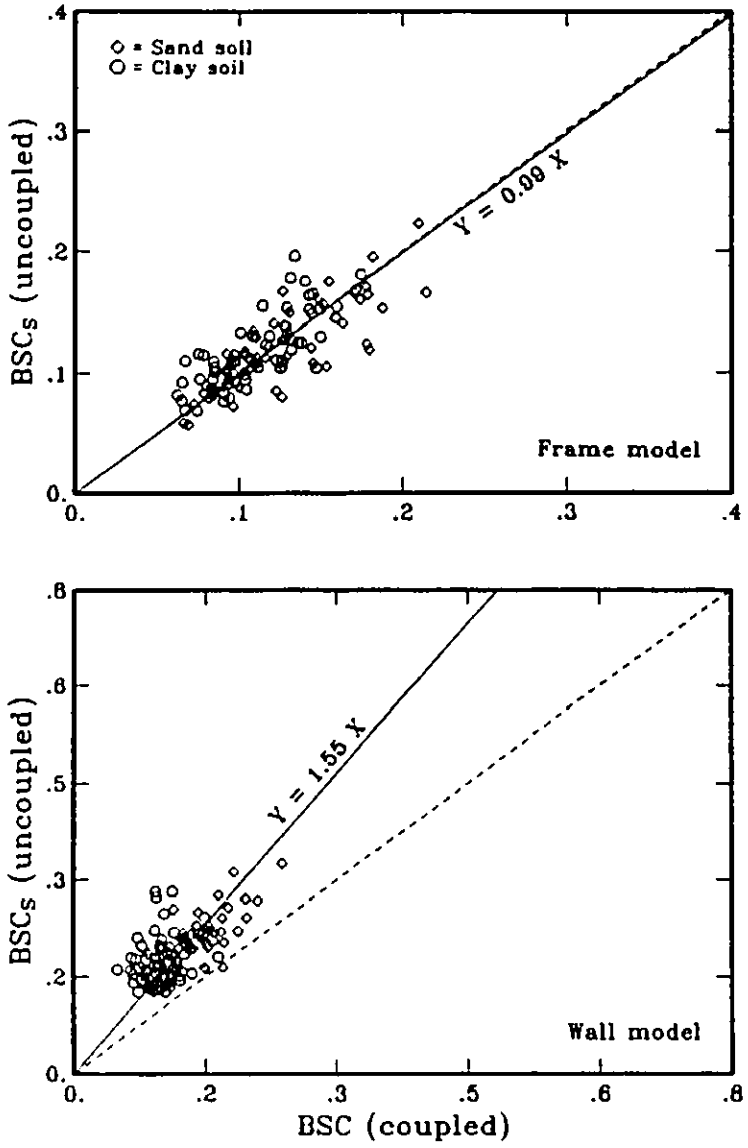

Figure 6.24 Regression analyses based on the modified uncoupled analysis results for Prince Rupert

CHAPTER 7

SUMMARY AND CONCLUSIONS

7.1 SUMMARY.

The current study of the implications of soil-structure interaction effects on the seismic response of high-rise reinforced concrete buildings has the following objectives:

First. Evaluate the NBCC 90 provisions for site effects.

Second. Assess the common practice of neglecting soil-structure interaction in aseismic design.

Third. Study the implications of soil-structure interaction effects on the NBCC 90 provisions.

Fourth. Investigate a simplified approach to account for the inertial interaction effects in uncoupled analyses of soil-structure systems.

Fifth. Evaluate a simplified approach to estimate the coupled system period.

The current study is carried out on a site-specific basis for three cities, corresponding to the three major sources of seismic hazard in Canada and the three combinations of the acceleration-related seismic zone (Z_a) and the velocity-related seismic zone (Z_v). Ottawa is chosen from Eastern Canada to represent sites where seismic hazard is associated with shallow intraplate faulting within the American plate, and for which $Z_a > Z_v$. Vancouver is chosen from Western Canada to represent sites where seismic

hazard is associated with the subduction of the Juan de Fuca plate beneath the American plate, and for which $Z_a=Z_v$. Prince Rupert is chosen from Western Canada to represent sites where seismic hazard is associated with shallow interplate faulting along the Queen Charlotte Transform, and for which $Z_a<Z_v$.

Soil models are developed to correspond to the soil classifications used to define the foundation factor (F) in NBCC 90. These soil models represent homogeneous deposits of loose, compact and dense sands. Additional soil models are also developed to represent homogeneous deposits of soft, firm and stiff clays. In the development of the soil models, a depth of 40 m is chosen to represent deep soil deposits, while a depth of 15 m is chosen to represent shallow soil deposits. Both static and dynamic soil properties for the different soil models are specified.

For the purpose of this study, 20-storey reinforced concrete buildings are chosen to represent regular high-rise (long period) buildings. Symmetrical one-bay frame models, with a span of 10 m, are developed to represent 20-storey ductile moment-resisting frames. Cantilever wall models, with a length of 10 m, are developed to represent 20-storey uncoupled ductile flexural walls. The frames (or walls) are assumed to be spaced at 6 m centre-to-centre in plan. The storey heights are assumed to be 3.6 m, with a total height of 72 m, above the ground surface, for the 20-storey structures.

Structural models are developed for each of the three sites, to represent the expected variations in stiffness characteristics between structures located at these sites. The design gravity and earthquake loads are specified in accordance with the NBCC 90 provisions for limit states

design. The design of the structural models conforms to the special provisions for seismic design in CAN3-A23.3-M84. A foundation model is developed, corresponding to each site, to support the design loads while maintaining the desired hierarchy for energy dissipation, in the superstructure, during the transient seismic excitations.

For each of the three sites, the magnitude (M_0) and source-distance (r_0) combination dominating the seismic hazard at that site is specified, based on the seismic risk computations used to develop the seismic zoning maps of Canada. For each site, 5 records (10 horizontal ground motion components) are selected from the available ground motion data base to correspond, as closely as possible, to the respective M_0 and r_0 combination and be consistent with the seismo-tectonic environment and the regional geological conditions characterizing the respective site. These initial records are then scaled for the frequency content, to account for the magnitude and source-distance dependence of the frequency content for earthquake ground motions. Scaling for the frequency content is performed using a proposed scheme for implementing spectral prediction relations in ground motion scaling. The modified time histories are then scaled for the ground motion intensity, to achieve seismic ground motions having peak horizontal ground velocity (PHV) values identical to those specified in NBCC 90 for the respective sites. For Vancouver, due to the lack of appropriate spectral prediction relations, the initial records can only be scaled for the ground motion intensity. The final ground motion records, developed according to the adopted process for ground motion scaling, represent the input (bedrock) ground motions used for the computations in the current study.

In the current study, analyses are restricted to the vertical plane of the frame (or wall) structural models. The computer program FLUSH is employed to perform the dynamic analyses for the different soil-structure models developed in the current study. The input ground motions are assumed to consist entirely of vertically propagating shear body-waves. Viscous boundaries are used along the planar surfaces of the slice of soil on which the building is located. The thickness of this slice of soil is specified as 30 m, corresponding to the assumed length of the building in the third dimension. These viscous boundaries model the radiation of seismic energy away from the structure in the third dimension. Lysmer-Waas transmitting boundaries are specified at the vertical edges of the finite element mesh, located at a distance of 10 m from the centreline of the analytical model, to model the exact dynamic effects of the semi-infinite soil deposit beyond the finite element mesh.

In developing the analytical soil-structure models, 2-D plane strain finite elements are used to model the soil deposits and foundations, while 2-D plane stress finite elements are used to model the structural walls. Beam elements are used to model the girders and columns of the structural frames. Since FLUSH does not account for any nonlinearities in the superstructure during the seismic response, stiffness reduction factors are applied, in the specification of the structural member properties, to account for the stiffness degradation associated with the development of the energy dissipation mechanisms adopted in the design of the frame and wall models. A cutoff frequency of 10 Hz is specified for the frequency domain computations in FLUSH. The size of the finite elements, used to model the soil deposits, are

specified in accordance with set criteria to avoid these artificially filtering out frequency components of the input ground motions that are significant to the response of the soil-structure systems.

In FLUSH, computations are carried out iteratively, using the equivalent linear method of complex response, to model the nonlinear response of the soil model. For each of the soil-structure models developed in the current study, FLUSH is used to perform both the free field and coupled analyses. No limit is set on the number of iterations in the case of the free field analyses, while a limited number of iterations are specified for the time-consuming coupled analyses. The natural periods for the different soil models are determined from the free field analyses, while the fundamental periods for the different soil-structure models are determined from the coupled analyses.

To evaluate the NBCC 90 provisions for site effects, the computed uncoupled base shear ratio (BSR) results are compared to the respective code F values. Assessment of the common practice of neglecting soil-structure interaction in aseismic design . hieved through a comparison of the coupled and uncoupled base shear coefficient (BSC) results. Linear regression analyses are performed, using both sets of BSC results, to reveal the general trend.

To study the implications of soil-structure interaction effects on the NBCC 90 provisions, the coupled BSR results are compared to the respective code F values. In addition, the M+SD coupled base shear results are compared to the corresponding NBCC 90 design base shear to evaluate the level of protection provided, in the NBCC 90 provisions, for the structures included in the current study.

A simplified approach to account for inertial interaction effects in uncoupled analyses is investigated through a comparison of the uncoupled BSC results, based on this simplified approach, to the corresponding coupled BSC results. Linear regression analyses are performed, using both sets of BSC results, to reveal the general trend.

Finally, a simplified approach to estimate the coupled system period ($\tilde{T}$), without need to resort to the time-consuming coupled analyses, is evaluated by comparing its predictions to the corresponding $\tilde{T}$ values based on the coupled analyses, for a selected set of soil-structure systems.

7.2 CONCLUSIONS.

Following are the most significant observations, based on results from the current study:

1. For a given soil deposit, the natural period (T_s) is larger for the sites associated with higher intensities of the seismic ground motions, measured in terms of the peak horizontal ground velocity (PHV). This is by virtue of the lower shear modulus (G) and larger hysteretic damping ratio (λ) values associated with the larger induced shear strains. These T_s values are larger than, and should be clearly distinguished from, the corresponding low strain T_s values associated with a linear response of the soil deposits.
2. Soil-structure interaction effects, measured in terms of the period shift from T to $\tilde{T}$ for the flexibly supported structure as well as the discrepancies between the coupled and uncoupled base shear demands, are more pronounced for the 'stiffer' wall structures, as compared to

the frame structures. These interaction effects are also more pronounced for the softer soil deposits, i.e. those associated with lower G and larger λ values.

3. The code F values, in most cases, underestimate the site effects associated with the respective soil deposits, for both the frame and wall structures.
4. Soil-structure resonance effects can have a significant effect on the magnitude of the site effects. The proximity of the natural period for the soil deposit (T_s) and the structural period (T) or even, in some cases, the period associated with a higher mode of vibration for the structure, can result in a significant increase in the site effects.
5. Site effects generally decrease for higher intensities of the input ground motions, as a result of the more pronounced nonlinear soil behaviour associated with the larger induced shear strains. However, in cases involving significant soil-structure resonance effects, this trend may be masked.
6. To properly account for site effects, F needs to be defined in terms of the T/T_s ratio. In addition, the influence of both the intensity and frequency content of the bedrock motions should also be incorporated in the specification of F. The foundation factors proposed by Elhmadi and Heidebrecht (1991), to replace the current code F values, are based on this sound rationale.
7. The assumption, underlying the current NBCC provisions, that neglecting soil-structure interaction results in a conservative design for most of the buildings addressed in the code is justified for high-rise (long period) buildings. In many cases, however, the degree of

conservatism appears to be excessive and not economically desirable.

8. For high-rise buildings situated on soil deposits, the base shear demand based on a conventional uncoupled analysis of the soil-structure system almost always exceeds the corresponding base shear demand based on the more rigorous coupled analysis. This is mainly due to the period shift away from T_s, associated with the inertial interaction effects, and to a lesser degree due to the reduction in structural response associated with the kinematic interaction effects.
9. The reliability of using conventional uncoupled analyses in aseismic design is hampered by the associated significant scatter in the base shear predictions, and which can result in predictions that exceed the corresponding coupled base shear by as much as a factor of 11.
10. The code F values appear to be reasonably adequate in accounting for the combined influence of site effects and soil-structure interaction. In fact, corresponding to many of the soil deposits in the case of the wall structures, the coupled analyses indicate a deamplification of the base shear demand associated with the bedrock motions.
11. In spite of some apparent deficiencies in the code F values, the NBCC 90 design base shear is conservative for regular 20-storey reinforced concrete buildings, situated in Ottawa, Vancouver or Prince Rupert.
12. To achieve an economical design, the large discrepancies between the code design base shear and the coupled base shear demand, especially for the cases involving significant interaction effects, need to be reduced through the incorporation of some measure, to account for soil-structure interaction effects, in the code provisions.
13. The approach proposed by Seed (1986), to account for inertial

interaction effects in uncoupled analyses, does provide a significant improvement in the prediction of the coupled base shear demand. The significant reduction of scatter in the base shear predictions, as compared to the conventional uncoupled analyses, establishes this approach as a simple, yet consistent, tool to replace the more rigorous, but time-consuming coupled analyses.

14. In view of the stochastic nature of earthquake ground motions, coupled (or uncoupled) analyses of soil-structure systems should be performed using a set of time histories, rather than a single time history, to represent the postulated seismic ground motions at a given site.

15. The simplified approach to estimate $\bar{T}$, proposed by the Applied Technology Council (1978), provides a satisfactory estimate of $\bar{T}$ values based on the more rigorous coupled analyses.

16. The modified approach to uncoupled analyses, proposed by Seed (1986), when used in conjunction with the simplified approach to estimate $\bar{T}$, proposed by the Applied Technology Council (1978), provides a viable alternative to the use of the time-consuming coupled analyses in aseismic design.

17. To account for the inertial interaction effects within the framework of the equivalent static load approach in NBCC, $\bar{T}$, rather than T, could be used to derive the design base shear. This is expected to reduce the large discrepancies, observed in the current study, between the computed coupled base shear demand and the code design base shear. For this purpose, the simplified approach proposed by the Applied Technology Council (1978) could be used to provide an estimate of $\bar{T}$, in lieu of resorting to the time-consuming coupled analyses.

18. If some measure is incorporated in the NBCC provisions to account for soil-structure interaction effects in the specification of the design base shear, the code F values need to be increased to adequately account for the significant site effects observed in this study.

Based on these observations, following are the main conclusions of the current study:

1. In agreement with recent studies of site effects, the code F values generally underestimate the site effects associated with the respective soil deposits.
2. The common practice of neglecting soil-structure interaction effects in aseismic design is justified for regular high-rise buildings. However, the associated degree of conservatism appears to be excessive, especially in cases involving significant soil-structure interaction effects.
3. When soil-structure interaction effects are taken into consideration, the NBCC 90 design base shear is conservative for regular high-rise buildings situated in Ottawa, Vancouver or Prince Rupert.
4. The modified approach to uncoupled analyses, proposed by Seed (1986), provides a significant improvement in the prediction of the coupled base shear demand, as compared to the conventional uncoupled analyses.
5. The simplified approach to estimate the coupled system period, proposed by the Applied Technology Council (1978), provides a satisfactory estimate of $\tilde{T}$ values based on the more rigorous coupled analyses.

REFERENCES

Applied Technology Council. 1978. Tentative provisions for the development of seismic regulations for buildings. Applied Technology Council Publication ATC 3-06, Palo Alto, California.

Associate Committee on the National Building Code. 1990. National Building Code of Canada 1990. National Research Council of Canada, Ottawa.

Atkinson, G.M. 1988. Implications of eastern ground motion characteristics for seismic hazard assessment in Eastern North America. Workshop on the Selection of Earthquake Ground Motions for Engineering Design and Analysis in Eastern Canada, Acres International Limited, Toronto.

Atkinson, G.M. and Boore, D.M. 1990. Recent trends in ground motion and spectral response relations for North America. Earthquake Spectra, Vol. 6, No. 1, 15-35.

Atkinson, G.M. 1991a. Use of the uniform hazard spectrum in characterizing expected levels of seismic ground shaking. Proceedings of the Sixth Canadian Conference on Earthquake Engineering, 469-476, Toronto.

Atkinson, G.M. 1991b. A comparison of ENA ground motion observations with theoretical predictions. Submitted to Seismological Research Letters.

Basham, P.W., Weichert, D.H., Anglin, F.M. and Berry, M.J. 1982. New probabilistic strong seismic ground motion maps of Canada: a compilation of earthquake source zones, methods and results. Earth Physics Branch Open File Report No. 82-33, Energy, Mines and Resources Canada, Ottawa.

Basham, P.W. 1990. Personal communication.

Bathe, K., Wilson, E.L. and Peterson, F.E. 1973. SAP IV - A structural analysis program for static and dynamic response of linear systems. EERC Report No. 73-11, Earthquake Engineering Research Center, University of California, Berkeley, California.

Binney, J.R. and Paulay, T. 1980. Foundations for shear wall structures. Bulletin of the New Zealand National Society for Earthquake Engineering, Vol. 13, No. 2, 171-181.

Blakeley, R.W., Cooney, R.C. and Megget, L.M. 1975. Seismic shear loading at flexural capacity in cantilever wall structures. Bulletin of the New Zealand National Society for Earthquake Engineering, Vol. 8, No. 4, 278-290.

Bouchon, M. 1980. The motion of the ground during an earthquake: 1. the

case of a strike slip fault. Journal of Geophysical Research, Vol. 85, No. B1, 356-366.

Bowles, J.E. 1988. Foundation analysis and design. Fourth Edition, McGraw-Hill Book Company.

Campbell, K.W. 1985. Strong motion attenuation relations: a ten-year perspective. Earthquake Spectra, Vol. 1, No. 4, 759-804.

Canadian Portland Cement Association. 1985. Concrete design handbook. Ottawa.

Canadian Standards Association. 1984. Design of concrete structures for buildings. CSA Standard CAN3-A23.3-M84, Toronto.

Constantopoulos, I.V., Roesset, J.M. and Christian, J.T. 1973. A comparison of linear and exact nonlinear analyses of soil amplification. Proceedings of the Fifth World Conference on Earthquake Engineering, Vol. 2, 1806-1815, Rome, Italy.

Council on Tall Buildings and Urban Habitat. 1979. Structural design of tall steel buildings. Monograph on planning and design of tall buildings, ASCE, Vol. SB, New York.

Das, B.M. 1985. Advanced soil mechanics. International Student Edition, McGraw-Hill Book Company.

Dobry, R. and Vucetic, M. 1987. Dynamic properties and seismic response of soft clay deposits. Proceedings of the International Symposium on Geotechnical Engineering of Soft Soils, Vol. 2, 51-87, Mexico City, Mexico.

Dunbar, W.S. and Charlwood, R.G. 1991. Empirical methods for the prediction of response spectra. Earthquake Spectra, Vol. 7, No. 3, 333-353.

Elhmadi, K., Heidebrecht, A.C. and Hosni, S. 1990. Parametric study of seismic site response effects. EERG Report No. 90-01, Earthquake Engineering Research Group, McMaster University, Hamilton.

Elhmadi, K. and Heidebrecht, A.C. 1991. A proposed dynamic foundation factor for the National Building Code of Canada. Canadian Journal of Civil Engineering, Vol. 18, No. 6, 974-984.

Elton, D.J. and Martin, J.R. 1989. Dynamic site periods in Charleston, SC. Earthquake Spectra, Vol. 5, No. 4, 703-734.

Fajfar, P. and Strojnik, Š. 1980. Simplified method for computation of earthquake induced shears and overturning moments in regular multistorey structures. Proceedings of the Seventh World Conference on Earthquake Engineering, Vol. 5, 561-564, Istanbul, Turkey.

Fenves, S.J. and Newmark, N.M. 1969. Seismic forces and overturning moments in buildings, towers and chimneys. Proceedings of the Fourth World Conference on Earthquake Engineering, Vol. III, B-5, 2-12, Santiago, Chile.

Finn, W.D. 1991. The effects of site conditions on ground motions. Proceedings of the Sixth Canadian Conference on Earthquake Engineering, 17-33, Toronto.

Fischinger, M. and Fajfar, P. 1990a. The role of overstrength in seismic resistance of buildings. Proceedings of the Ninth European Conference on Earthquake Engineering, Vol. 2, 329-338, Moscow, Russia.

Fischinger, M. and Fajfar, P. 1990b. On the response modification factors for reinforced concrete buildings. Proceedings of the Fourth U.S. National Conference on Earthquake Engineering, Vol. 2, 249-258, Palm Springs, California.

Friberg, P. and Jacob, K. 1990. NCEER strong-motion data base: a user manual for the Geobase release. National Center for Earthquake Engineering Research Technical Report No. NCEER-90-0005, State University of New York at Buffalo, New York.

Gómez-Massó, A., Lysmer, J., Chen, J. and Seed, H.B. 1983. Soil-structure interaction with Rayleigh waves. Earthquake Engineering and Structural Dynamics, Vol. 11, No. 4, 567-583.

Goodsir, W.J., Paulay, T. and Carr, A.J. 1983. A study of the inelastic seismic response of reinforced concrete coupled frame-shear wall structures. Bulletin of the New Zealand National Society for Earthquake Engineering, Vol. 16, No. 3, 185-200.

Guzman, R.A. and Jennings, P.C. 1976. Design spectra for nuclear power plants. Journal of the Power Division, ASCE, Vol. 102, No. PO2, 165-178.

Hardin, B.O. and Drnevich, V.P. 1972. Shear modulus and damping in soils: design equations and curves. Journal of the Soil Mechanics and Foundations Division, ASCE, Vol. 98, No. SM7, 667-692.

Hasegawa, H.S., Basham, P.W. and Berry, M.J. 1981. Attenuation relations for strong seismic ground motion in Canada. Bulletin of the Seismological Society of America, Vol. 71, No. 6, 1943-1962.

Heidebrecht, A.C. and Stafford Smith, B. 1973. Approximate analysis of tall wall-frame structures. Journal of the Structural Division, ASCE, Vol. 99, No. ST2, 199-221.

Heidebrecht, A.C. and Tso, W.K. 1983. Proposed seismic loading provisions - National Building Code of Canada 1985. Proceedings of the Fourth Canadian Conference on Earthquake Engineering, K19-K29, Vancouver.

Heidebrecht, A.C., Basham, P.W., Rainer, J.H. and Berry, M.J. 1983. Engineering applications of new probabilistic seismic ground-motion maps of Canada. Canadian Journal of Civil Engineering, Vol. 10, No. 4, 670-680.

Heidebrecht, A.C. and Lu, C.Y. 1988. Evaluation of the seismic response factor introduced in the 1985 edition of the National Building Code of Canada. Canadian Journal of Civil Engineering, Vol. 15, No. 3, 382-388.

Heidebrecht, A.C., Henderson, P., Naumoski, N. and Pappin, J.W. 1990. Seismic response and design for structures located on soft clay sites. Canadian Geotechnical Journal, Vol. 27, No. 3, 330-341.

Henderson, P., Heidebrecht, A.C., Naumoski, N. and Pappin, J.W. 1989a. Site response study - methodology, calibration and verification of computer programs. EERG Report No. 89-01, Earthquake Engineering Research Group, McMaster University, Hamilton.

Henderson, P., Heidebrecht, A.C., Naumoski, N. and Pappin, J.W. 1989b. Site response study - presentation of results. EERG Report No. 89-03, Earthquake Engineering Research Group, McMaster University, Hamilton.

Henderson, P., Heidebrecht, A.C., Naumoski, N. and Pappin, J.W. 1990. Site response effects for structures located on sand sites. Canadian Geotechnical Journal, Vol. 27, No. 3, 342-354.

Hosni, S. and Heidebrecht, A.C. 1991. Code provisions for structures on deep soft sites. Proceedings of the Sixth Canadian Conference on Earthquake Engineering, 767-774, Toronto.

Hosni, S. and Heidebrecht, A.C. 1992. Use of spectral prediction relations in ground motion scaling. Submitted to Earthquake Spectra.

Hudson, D.E., Trifunac, M.D. and Brady, A.G. 1971. Strong motion earthquake accelerograms - digitized and plotted data. Earthquake Engineering Research Laboratory, California Institute of Technology, Pasadena, California.

Hudson, D.E. 1979. Reading and interpreting strong motion accelerograms. Engineering monographs on earthquake criteria, structural design and strong motion records, Earthquake Engineering Research Institute, Berkeley, California.

Hwang, R.N., Lysmer, J. and Berger, E. 1975. A simplified three-dimensional soil-structure interaction study. Proceedings of the Second ASCE Specialty Conference on Structural Design of Nuclear Plant Facilities, Vol. I-A, 786-808, New Orleans, Louisiana.

Joyner, W.B. and Boore, D.M. 1981. Peak horizontal acceleration and velocity from strong-motion records including records from the 1979 Imperial Valley, California, earthquake. Bulletin of the

Seismological Society of America, Vol. 71, No. 6, 2011-2038.

Joyner, W.B. and Boore, D.M. 1988. Measurement, characterization, and prediction of strong ground motion. Proceedings of the Speciality Conference sponsored by the Geotechnical Engineering Division of the American Society of Civil Engineers, 43-102, Park City, Utah.

Kim, T.C. and Novak, M. 1981. Dynamic properties of some cohesive soils of Ontario. Canadian Geotechnical Journal, Vol. 18, No. 3, 371-389.

Kuhlemeyer, R.L. and Lysmer, J. 1973. Finite element method accuracy for wave propagation problems. Journal of the Soil Mechanics and Foundations Division, ASCE, Vol. 99, No. SM5, 421-427.

Lu, C.Y. 1984. An evaluation of seismic response factors to be used in seismic base shear provision of NBCC 1985. M.Eng. Thesis, McMaster University, Hamilton.

Lysmer, J., Udaka, T., Tsai, C. and Seed, H.B. 1975. FLUSH - a computer program for approximate 3-D analysis of soil-structure interaction problems. EERC Report No. 75-30, Earthquake Engineering Research Center, University of California, Berkeley, California.

Merritt, R.G. and Housner, G.W. 1954. Effect of foundation compliance on earthquake stresses in multistory buildings. Bulletin of the Seismological Society of America, Vol. 44, No. 4, 551-569.

Milne, W.G., Rogers, G.C., Riddihough, R.P., McMechan, G.A. and Hyndman, R.D. 1978. Seismicity of Western Canada. Canadian Journal of Earth Sciences, Vol. 15, No. 7, 1170-1193.

Miranda, E. and Bertero, V.V. 1989. The Mexico earthquake of September 19, 1985- performance of low-rise buildings in Mexico City. Earthquake Spectra, Vol. 5, No. 1, 121-143.

Mitchell, D., Adams, J., DeVall, R.H., Lo, R.C. and Weichert, D. 1986. Lessons from the 1985 Mexican earthquake. Canadian Journal of Civil Engineering, Vol. 13, No. 5, 535-557.

Moriwaki, Y., Pyke, R., Bastick, M. and Udaka, T. 1981. Specification of input motions for seismic analyses of soil-structure systems within a nonlinear analyses framework. EPRI Report No. NP-2097, Electric Power Research Institute, Palo Alto, California.

Munro, P.S. and Weichert, D. 1989. The Saguenay earthquake of November 25, 1988 - processed strong motion records. Geological Survey of Canada Open File Report No. 1996, Ottawa.

MUSE 1988. McMaster University Seismological Executive database system. Earthquake Engineering Research Group, McMaster University, Hamilton.

Nagaraj, T.S. and Murthy, B.R. 1985. Prediction of the preconsolidation

pressure and recompression index of soils. Geotechnical Testing Journal, ASTM, Vol. 8, No. 4, 199-202.

Nakase, A., Kamei, T. and Kusakabe, O. 1988. Constitutive parameters estimated by plasticity index. Journal of Geotechnical Engineering, ASCE, Vol. 114, No. 7, 844-858.

Nau, J.M. and Hall, W.J. 1984. Scaling methods for earthquake response spectra. Journal of Structural Engineering, ASCE, Vol. 110, No. 7, 1533-1548.

Naumoski, N. 1985. SYNTH program: generation of artificial acceleration time history compatible with a target spectrum. McMaster Earthquake Engineering Software Library, Department of Civil Engineering and Engineering Mechanics, McMaster University, Hamilton.

Newmark, N.M., Blume, J.A. and Kapur, K.K. 1973. Seismic design spectra for nuclear power plants. Journal of the Power Division, ASCE, Vol. 99, No. PO2, 287-303.

Osteraas, J. and Krawinkler, H. 1989. The Mexico earthquake of September 19, 1985- behaviour of steel buildings. Earthquake Spectra, Vol. 5, No. 1, 51-88.

Pappin, J.W., Heidebrecht, A.C., Henderson, P. and Naumoski, N. 1989. Site response study - soil modelling. EERG Report No. 89-02, Earthquake Engineering Research Group, McMaster University, Hamilton.

Park, R. and Paulay, T. 1975. Reinforced concrete structures. John Wiley & Sons, Inc.

Pillai, S.U. and Kirk, D.W. 1988. Reinforced concrete design. Second Edition, McGraw-Hill Ryerson Limited.

Prakash, S. 1981. Soil dynamics. McGraw-Hill Book Company.

Sadigh, K. 1992. Personal communication.

Seed, H.B., Lysmer, J. and Hwang, R. 1975. Soil-structure interaction analyses for seismic response. Journal of the Geotechnical Engineering Division, ASCE, Vol. 101, No. GT5, 439-457.

Seed, H.B., Wong, R.T., Idriss, I.M. and Tokimatsu, K. 1984. Moduli and damping factors for dynamic analyses of cohesionless soils. EERC Report No. 84-14, Earthquake Engineering Research Center, University of California, Berkeley, California.

Seed, H.B. 1986. The eighth Nabor Carrillo lecture. Presented at the Mexican Society for Soil Mechanics XIII National Meeting, Mazatlán, Sinaloa, Mexico.

Shakal, A., Huang, M., Reichle, M., Ventura, C., Cao, T., Sherburne, R.,

Savage, M., Darragh, R. and Petersen, C. 1989. CSMIP strong-motion records from the Santa Cruz Mountains (Loma Prieta), California earthquake of 17 October 1989. CSMIP Report No. OSMS 89-06, California Strong Motion Instrumentation Program, California Department of Conservation, Sacramento, California.

Somerville, P.G., McLaren, J.P., LeFevre, L.V., Burger, R.W. and Helmberger, D.V. 1987. Comparison of source scaling relations of Eastern and Western North American earthquakes. Bulletin of the Seismological Society of America, Vol. 77, No. 2, 322-346.

Sun, J.I., Golesorkhi, R. and Seed, H.B. 1988. Dynamic moduli and damping ratios for cohesive soils. EERC Report No. 88-15, Earthquake Engineering Research Center, University of California, Berkeley, California.

Switzer, J., Johnson, D., Maley, R. and Matthiesen, R., comp. 1981. Western hemisphere strong-motion accelerograph station list - 1980. USGS Open File Report No. 81-664, United States Geological Survey, Menlo Park, California.

Taniguchi, H., Ueda, M., Sugimoto, M., Tanaka, H., Yamashita, T. and Nukui, Y. 1988. Effect of nonlinear behaviours on the earth pressure for a deeply embedded building. Proceedings of the Ninth World Conference on Earthquake Engineering, Vol. III, 647-652, Tokyo, Japan.

Valera, J.E., Seed, H.B., Tsai, C.F. and Lysmer, J. 1977. Seismic soil-structure interaction effects at Humboldt Bay Power Plant. Journal of the Geotechnical Engineering Division, ASCE, Vol. 103, No. GT10, 1143-1161.

Veletsos, A.S. and Nair, V.V. 1975. Seismic interaction of structures on hysteretic foundations. Journal of the Structural Division, ASCE, Vol. 101, No. ST1, 109-129.

Vucetic, M. and Dobry, R. 1991. Effect of soil plasticity on cyclic response. Journal of Geotechnical Engineering, ASCE, Vol. 117, No. 1, 89-107.

Wallace, J.W. and Moehle, J.P. 1990. Evaluation of ATC requirements for soil-structure interaction using data from the 3 March 1985 Chile earthquake. Earthquake Spectra, Vol. 6, No. 3, 593-611.

Weichert, D.H., Wetmiller, R.J., Horner, R.B., Munro, P.S. and Mork, P.N. 1986. Strong motion records from the 23 December 1985, M_S 6.9 Nahanni, NWT, and some associated earthquakes. Geological Survey of Canada Open File Report No. 86-1-PGC, Ottawa.

Weichert, D.H. 1989. Implications of some important strong-motion recordings of mid-plate earthquakes. Annals of the New York Academy of Sciences, Vol. 558, 95-104.

Weichert, D.H. 1990. Personal communication.

Weinberg, G.H. and Schumaker, J.A. 1969. Statistics - an intuitive approach. Second Edition, Brooks/Cole Publishing Company.

Yanev, P.I., ed. 1978. Miyagi-Ken-Oki, Japan earthquake - June 12, 1978. Reconnaissance Report, Earthquake Engineering Research Institute, Berkeley, California.

Zhu, T. 1989. Inelastic response of reinforced concrete frames to seismic ground motions having different characteristics. Ph.D. Thesis, McMaster University, Hamilton.